

From Clinical and Experimental Pathology, Research Center Borstel to Lübeck University
Head: Prof. Dr. med. Dr. med. vet. Dr. h.c. Ekkehard Vollmer

Functional studies on the initial phase of mycobacterial infections in human lung tissues

Thesis for the Acquisition of a Doctorate
at the University of Lübeck
-Section: Medicine-

Submitted by
Dariimaa Ganbat
Ulaanbaatar, Mongolia

Supervisors: Prof. Dr. rer. nat. Torsten Goldmann
PD Dr. rer. nat. Elvira Richter
Prof. Dr. med. Dr. med. vet. Dr. h.c. Ekkehard Vollmer

Lübeck University 2014

1-Referee: Prof. Dr. rer. nat. Torsten Goldmann

2-Referee: Priv.-Doz. Dr. med. Daniel Drömann

Day of oral examination: 31.03.2015

Granted for print. Lübeck,

Contents

List of tables	6
List of figures	7
List of abbreviations	9
1. Introduction	11
1.1. State of knowledge	11
1.1.1. Mycobacterium	11
1.1.2. Tuberculosis (TB)	11
1.1.3. Nontuberculous mycobacterial infection (NTM)	14
1.1.3.a. <i>Mycobacterium avium</i> complex	15
1.1.3.b. <i>Mycobacterium abscessus</i>	16
1.2. Definition of problems of mycobacterial infections	17
1.3. Aim of the study	18
2. Materials and Methods	21
2.1. Collection of samples	21
2.2. <i>Ex vivo</i> STST lung model for mycobacteria	21
2.2.a. Preparation of tissues	21
2.2.b. Preparation of suspensions	21
2.2.c. Incubation of tissue culture	22
2.2.d. CFU control of working suspensions	22
2.3. Collection of supernatants and tissue processing	23
2.4. Sectioning, deparaffinization and rehydration of HOPE-fixed, paraffin-embedded tissues	23
2.5. Histochemical stainings	24
2.6. Experiments with nucleic acids	25
2.6.1. DNA analysis	25
A. Purification of DNA from HOPE-fixed, paraffin-embedded tissue blocks	25
B. Quantification of nucleic acids	25
C. Polymerase chain reaction (PCR)	25
D. Agarose gel electrophoresis	26
E. Visualization and analysis of amplified PCR product	27
2.6.2. RNA analysis	27
A. Extraction of total RNA from HOPE-fixed, paraffin-embedded tissue blocks	27
B. RNA integrity	27
C. Transcriptome analysis	27
2.7. Investigations with primary cells	28
2.7.1. <i>In vitro</i> infection of primary cells	28

2.7.2. Vitamin stimulation to induce “self split” cell death	29
2.8. Viability tests	29
2.8.1. MTT assay	29
2.8.2. TUNEL assay	29
2.9. Software	30
2.10. Statistics	30
3. Results	32
3.1. Establishment of the STST <i>ex vivo</i> model for mycobacteria	32
3.1.1. Viability of tissues	32
3.1.1.a. Histopathological overview	32
3.1.1.b. MTT colorimetric assay	33
3.1.1.c. TUNEL assay	36
3.1.2. Infection of tissues	37
3.1.2.a. CFU determination of suspensions	37
3.1.2.b. Histopathological overview	38
3.1.2.c. Detection of mycobacterial DNA in the <i>ex vivo</i> -infected tissues	39
3.2. Findings using the <i>ex vivo</i> STST model	41
3.2.1. Infected cell types	41
3.2.2. <i>In vitro</i> infection of primary cells	47
3.2.2. a. Cellular uptake of primary cells by <i>M. tuberculosis</i> strain H37Rv	49
3.2.2. b. Replication of <i>M. tuberculosis</i> strain H37Rv within primary cells	49
3.2.2. c. Results of real-time PCR of antimycobacterial activity	51
3.2.3. Changes of cellular morphology	52
3.2.3.a. Types of cellular changes	52
3.2.3.b. Cellular measurements	58
A. Measurements of cytoplasmic and nuclear size	59
B. Measurements of cytoplasmic and nuclear light density (LD) of the atypical pyknotic cells	60
C. Relationship between cell sizes and LDs of the atypical pyknotic cells	61
3.2.4. Vitamin stimulation of “self-split” cell death	64
3.2.5. Transcriptome analysis of mycobacterial infection	66
3.2.5.a. Transcription profiling	66
3.2.5.b. Transcriptome analysis	67
3.2.6. Validation of genes	68
4. Discussion	70
4.1. Establishment of the <i>ex vivo</i> STST model for mycobacteria	70
4.2. Findings using the <i>ex vivo</i> STST model for mycobacteria	73
4.2.1. Monocytes and macrophages	75
4.2.2. Neutrophils	76
4.2.3. Pneumocytes-II	79

4.2.4. Other cell types	82
4.3. “A self-split cell death” is a potential host defense mechanism of eliminating mycobacteria	83
5. Summary	87
6. Bibliography	88
7. Appendices	98
Appendix-I	98
Appendix-II	107
8. Declaration	118
9. Acknowledgements	119
10. Curriculum vitae	120

List of tables

Table 1-1. Clinical settings for nontuberculous mycobacteria lung disease

Table 2-1. Sequences of primers

Table 2-2. PCR master reaction mixture

Table 2-3. Amplification conditions

Table 2-4. General consideration of agarose gel electrophoresis

Table 2-5. The genes list evaluated by real time PCR

Tables in Appendix

Table A.1. Reagents and tools for incubation of tissue culture

Table A.2. Reagents and tools used for collecting supernatants and tissue processing steps

Table A.3. Reagents and tools used for sectioning, deparaffinization and rehydration of HOPE-fixed, paraffin-embedded tissue

Table A.4. Histochemical stainings

Table A.4.1. Hematoxylin and Eosin staining protocol

Table A.4.2. Cold Ziehl-Neelsen technique/ Kinyoun staining:

Table A.4.3. Gram staining

Table A.4.4. Immunohistochemical staining

Table A.4.5. IHC with Auramin-Rhodamin- Fluorescence double staining

Table A.4.6. Pappenheim staining

Table A.5. Purification of DNA from formalin-fixed, paraffin-embedded tissues

Table A.6. Quantification of DNA and RNA

Table A.7. DNA agarose gel electrophoresis

Table A.8. Total RNA extraction from HOPE-fixed, paraffin-embedded tissue blocks

Table A.9. Determining RNA integrity number via bioanalyzer

Table A.10. TUNEL assay

Table 3-1. One way ANOVA associated MTT assay for tissue viability

Table 3-2. Streamline correlation matrix associated MTT assay for tissue viability

Table 3-3. Kruskal-Wallis Test for patient's comparisons among all mycobacterial strains

Table 3-4. The amount of cells and bacilli used for the study

Table 3-5. The amounts of intracellular mycobacteria

Table 3-6. Contingency table for Chi square and association tests

Table 3-7. Kruskal-Wallis tests for changes of cellular morphology

Table 3-8. Tukey's HSD tests for log transformed data of karyolysis and karyorrhexis in 3 locations

Table 3-9. Cellular measurements of infected and non-infected cells

Table 3-10. Spearman's rank correlation matrix for cellular sizes and LDs in infected and non-infected cells

List of figures

- Figure 1-1.** A diagrammatic scheme of typical development of tuberculosis.
- Figure 1-2.** Clinical relevance of pulmonary NTM isolates (Asia, 1971–2007).
- Figure 1-3.** Overview of main and sub-strategies against TB.
- Figure 2-1.** General schema of the *ex vivo* STST model and further analysis
- Figure 2-2.** Comparison between regular and optimized cold ZN stainings
- Figure 3-1.** The overview of the establishment of the *ex vivo* STST model
- Figure 3-2.** A representative mycobacteria-stimulated sample's image
- Figure 3-3.** Influence of culture conditions on tissue viability
- Figure 3-4.** No increase of DNA-double strand breaks upon tissue culture
- Figure 3-5.** Influence of the *ex vivo* culture on tissue viability
- Figure 3-6.** Successful mycobacterial infection using the *ex vivo* STST model
- Figure 3-7.** A. Observation of serial sections of the whole block
B. Photomicrograph of intra- and extra-cellular mycobacteria
- Figure 3-8.** Distribution of infected cells according to depth of tissue
- Figure 3-9.** Mycobacterial DNA can be detected in infected *ex vivo* human tissue samples
- Figure 3-10.** A. A plot of real time PCR reaction of mycobacterial DNA
B. A chromatograph of DNA sequencing of *M. abscessus*
- Figure 3-11.** Overview of findings from *ex vivo* STST model and their relationship
- Figure 3-12.** Mycobacteria invaded different cell types in the *ex vivo* human lung tissues
- Figure 3-13.** Cellular populations infected by 6 mycobacterial strains
- Figure 3-14.** Comparisons of each cell type separately among mycobacterial species
- Figure 3-15.** *Ex vivo* infected human lung tissues reveal significant differences of infected cell types regards to mycobacterial strains
- Figure 3-16.** Correspondence analysis map for mycobacterial species and cell types
- Figure 3-17.** Photomicrographs of intracellular mycobacteria detected by double staining
- Figure 3-18.** Observations of the *ex vivo* infected macrophages and pneumocytes-II by mycobacteria
- Figure 3-19.** Comparison of relative initial invasion between professional and non-professional phagocytes
- Figure 3-20.** Comparisons of bacterial growth within professional and non-professional phagocytes
- Figure 3-21.** Intracellular changes within primary cells
- Figure 3-22.** Detection and comparisons of cytokines release in the culture supernatant of human primary cells
- Figure 3-23.** Cellular changes in infected cells
- Figure 3-24.** Frequency of indicated morphological changes in the infected macrophages
- Figure 3-25.** The nonparametric Kruskal-Wallis tests for cellular changes in infected cells

- Figure 3-26.** The median tests for cellular changes
- Figure 3-27.** Correspondence analysis map for mycobacterial species and cellular changes
- Figure 3-28.** The counting analysis of TUNEL assay
- Figure 3-29.** Measuring of cellular diameters and light densities
- Figure 3-30.** Comparisons of nuclear and cytoplasmic sizes between infected and non-infected cells
- Figure 3-31.** Comparisons of nuclear and cytoplasmic LDs between infected and non-infected cells
- Figure 3-32.** Two-way grouped scatter plot of cell sizes and LDs
- Figure 3-33.** Scatter plots associated with linear regression of standardized variables
- Figure 3-34.** Dose-response curve of vitamin combination-treated alveolar macrophages
- Figure 3-35.** “Self-split” cell death of primary alveolar macrophages
- Figure 3-36.** Hierarchical clustering of the transcriptomes from *ex vivo* infected human tissues with mycobacteria
- Figure 3-37.** Venn diagram from up-regulated genes upon 3 mycobacterial strains
- Figure 3-38.** Immunohistochemical detection of some candidate genes

List of abbreviations

AEC II	Alveolar epithelial cell type 2
AFB	Acid-fast bacilli
AIDS	Acquired immunodeficiency syndrome
AM	Alveolar macrophages
BCG	Bacille Calmette-Guérin
BME	beta-Mercaptoethanol
CDC	Centers for disease control and prevention
CD ₉₀	Cytotoxic doses
CFU	Colony forming units
CGD	Chronic granulomatous disease
COPD	Chronic obstructive pulmonary disease
DAPI	4', 6-diamidino-2-phenylindole
DEPC	Diethylpyrocarbonate
DMEM	Dulbecco/Vogt Modified Eagle's minimal essential medium
DNA	Complementary DNA
DNase	Deoxyribonuclease
DTH	Delayed type hypersensitivity response
FCS	Fetal calf serum
h	hour
H&E	Hematoxilin and Eosin
HBSS	Hank's balanced salt solution
HIV	Human immunodeficiency virus
HOPE	Hepes glutamic acid buffer mediated organic solvent protection effect
IFN- γ	Interferon-gamma
IHC	Immunohistochemistry
LDH	Lactate dehydrogenase
LTBI	Latent TB infection
LJ	Löwenstein-Jensen medium
MAC	<i>Mycobacterium avium</i> complex
MAI	<i>Mycobacterium avium-intracellulare</i> infection
MDR	Multi drug-resistance
min	Minute
MOTT	Mycobacteria other than <i>M. tuberculosis</i>
MOI	Multiplicity of infection
mRNA	messenger RNA
<i>Mtb</i>	<i>Mycobacterium tuberculosis</i>
MTT	(4,5-dimethylthiazol-2-yl)-2,5-diphenyltetrazolium bromide
NK	Natural killer

NTC	no-template control
NTM	Nontuberculous mycobacteria
PBS	Phosphate buffered saline
PCR	Polymerase chain reaction
PCLS	precision-cut lung slices
RGM	Rapidly growing mycobacteria
ROS	Reactive oxygen species
RPMI	Roswell park memorial institute medium
s	second
STAT	Signal transducers and activators of transcription
STST	Short-Term Stimulation of Tissue
TB	Tuberculosis
TNF- α	Tumor necrosis factor alpha
TST	Tuberculin skin test
TUNEL	Terminal deoxynucleotidyl transferase dUTP nick end labeling
WHO	World Health Organization
ZN	Ziehl-Neelsen

1. Introduction

1.1. State of knowledge

1.1.1. Mycobacterium

Mycobacterium is a genus of bacteria. Currently more than 150 species of mycobacteria have been identified, many of which are related with human disease [1, 2]. Approximately 28 new species have been described in the last 5 years [3]. Mycobacteria cells are straight or slightly curved rods between 0.2-0.6 μm wide by 1.0-10 μm long. They are non-spore-forming, non-motile, aerobic and the rods occasionally form branched filaments, but these can be disrupted easily. All *Mycobacterium* species share a characteristic lipid-rich waxy cell wall, which is thicker than in other bacteria. The genus *Mycobacterium* usually is considered as acid-fast and weakly Gram-positive. The unique impermeable cell wall consists of a hydrophobic mycolate layer and a peptidoglycan layer held together by a polysaccharide and arabinogalactan. Their dominant mycolic acid constituents are covalently linked to arabinoglactans [2, 4]. This cell envelope is responsible for many of the characteristic properties of the bacteria, for instance acid-fastness, slow growth, resistance to detergents, common antibacterial antibiotics, their antigenicity and clumping [5]. Mycobacteria can be divided into three major groups for purpose of diagnosis and treatment: *M. tuberculosis* complex which can cause tuberculosis, *M. leprae* causes leprosy and nontuberculous mycobacteria (NTM) are all the other mycobacteria, which can cause pulmonary disease sometimes resembling tuberculosis, lymphadenitis, skin or soft tissue disease or disseminated disease [6]. NTM can be classified according to Runyon groups based on the rate of growth and production of yellow pigments [7].

1.1.2. Tuberculosis (TB)

Tuberculosis is a contagious bacterial disease primarily involving the lungs, that develops after inhalation of infected droplets released following a cough from someone infected with the *Mycobacterium tuberculosis* (Mtb) complex bacteria [8]. However, the term tuberculosis describes a broad range of clinical illnesses, since the causative agent can affect virtually every organ [9].

The World Health Organization (WHO) declared tuberculosis a global public health emergency, which is estimated to affect 1.7 billion individuals worldwide, resulting in 8-10 million new cases and 1.6 million deaths annually. It causes life-threatening disease among millions of people each year and ranks as the second leading cause of death from infectious diseases worldwide, after the human immunodeficiency virus (HIV). Most of these TB cases and deaths occur among men, but the burden of disease among women is increasing in developing countries [10-12].

Mtb complex comprises several species: *M. tuberculosis*, *M. bovis*, *M. africanum*, *M. canetti*, *M. caprae*, *M. pinnipedii*, *M. microti* and *M. bovis* BCG [11]. They share

99.9% sequence identity and likely evolved from a single clonal ancestor [13]. Therefrom, *M. tuberculosis* is responsible for the vast majority of TB cases. Mtb complex bacteria rate of growth is slow, namely at 37⁰C under optimal availability of oxygen and nutrients, the generation time is between 18-24 hours, compared with much less than 1 hour for most common bacterial pathogens; visible growth, a white to light –yellow colony, takes from 2 to 4 weeks [5].

Tuberculosis has been identified in a wide range of species ranging from birds to primates. In all cases, the disease can disseminate and be shed into the environment [14]. However, humans are the main reservoir for the species *M. tuberculosis* [15]. *M. bovis* causes disease in cattle and spreads to humans through animal contact and consumption of unpasteurized milk [16]. Almost all infections with *M. tuberculosis* are due to inhalation of droplet nuclei—infectious particles from a person with pulmonary tuberculosis aerosolized by coughing, sneezing and talking, remain suspended for long periods and reach the terminal air passages. Other modes of transmission are rather rare. For instance, large drops of respiratory secretions and fomites are unimportant in transmission, and special housekeeping measures for dishes and bed linens are unnecessary. Although, skin inoculation of *M. tuberculosis* from contamination of an abrasion occurs in pathologists and by syringes in microbiologists [17, 18].

Tuberculosis flourishes wherever there is poverty, crowded living conditions and chronic debilitating illness [11, 19]. Particularly outbreaks of TB in crowding have been documented in environments such as hospitals, schools, factories, homeless shelters, and prisons [20-24]. The often-interrelated risk factors of socioeconomic conditions are intravenous drug abuse, acquired immunodeficiency syndrome (AIDS) epidemic, poor nutrition, lack of hygiene, dearth of medical care and alcoholics [25-27]. A phenomenon link between primary immune deficiency and mycobacterial infection has been theorized after the major global challenges related to the intersection of the AIDS and TB pandemics. With the exception of primary immune deficiencies, there exists general agreement that susceptibility to tuberculosis is multifactorial. There is much knowledge obtained from epidemiological studies about which conditions predispose to suffer the disease, including malnutrition, cancer, diabetes mellitus, Hodgkin lymphoma, chronic lung disease (particularly silicosis), chronic renal failure, cirrhosis, age, stress and others [28-30]. It is important to note that infection with Mtb needs to be differentiated from disease (Figure 1-1).

- **Latent TB infection (LTBI):** It means the presence of Mtb organisms within the lungs following the first exposure to infection, when Mtb are inhaled, which may or may not cause clinically significant disease [11, 31]. At this time Mtb is persisting in a dormant stage. This nonreplicating state is characterized by low metabolic activity and drug resistance [32]. However, little is known about the physiology of the dormant tubercle bacillus and prevailing theories remain controversial [33]. There are 3 alternatives of LTBI destiny: (1) It can progress toward active disease, (2) It can be contained as latent infection and (3) It can be eradicated by the host's immune system [31, 34]. It is

impossible to predict who will contain latent infection throughout lifetime and remain healthy, and who will develop active TB at some point [10].

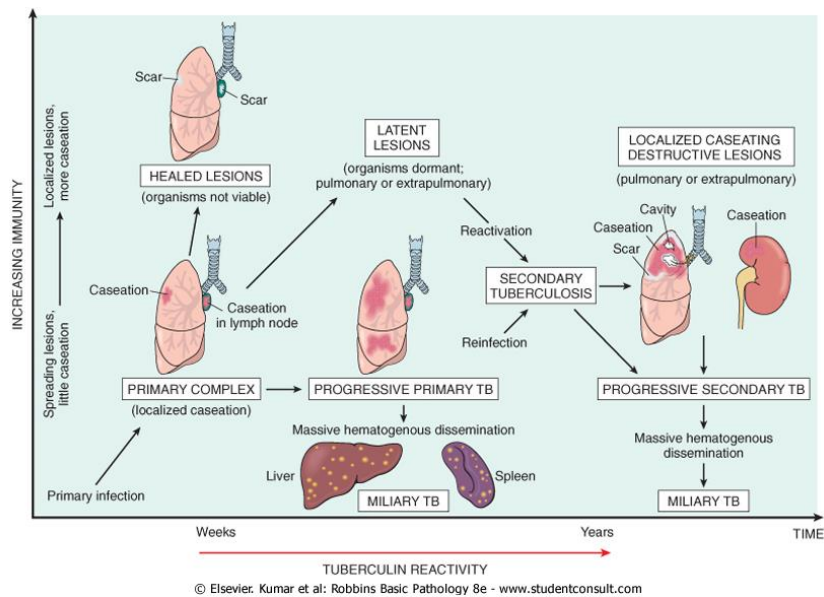


Figure 1-1. A diagrammatic scheme of typical development of tuberculosis [35].

- Primary Tuberculosis:** It indicates the form of disease that develops in a previously unexposed and unsensitized person [11]. This occurs in individuals who are immunocompromised because of a defined illness (such as AIDS) or because of nonspecific impairment of host defenses (as may occur in malnourished children, elderly), and certain racial groups (e.g., Inuit [36]). The main implications of primary tuberculosis are: (1) In most cases, the patients are asymptomatic and initial local lesions induced by mycobacteria heal within a few weeks remaining only radiologically detectable as Ranke complex, (2) a small proportion of patients fail to heal primary pulmonary lesions and thus be the nidus for reactivation at a later time when host defenses are compromised [11, 37, 38], (3) Uncommonly, the disease may develop without interruption into so-called progressive primary tuberculosis and arises when immune function is impaired, or responses are delayed [9, 39].
- Secondary or postprimary tuberculosis:** It describes the pattern of disease that arises in a previously sensitized host [11]. Secondary tuberculosis may result from reactivation of dormant Mtb, when host resistance is weakened or from exogenous reinfection with new organisms [40, 41]. Reactivation of endogenous tuberculosis is more common in low-prevalence areas, whereas reinfection plays an important role in regions of high contagion. Cavitation occurs readily in the secondary form, resulting in dissemination along the airways [9, 37].

During tuberculosis, clinical presentations include classic symptoms of cough, weight loss, fatigue, fever, night sweats, and chills. Upon continued progression, the patient will experience anorexia, hemoptysis, and pain with breathing or coughing due to pleurisy. The onset of symptoms is usually gradual. Coughing to clear cavitory secretions is usually mild and the mucopurulent sputum is nonspecific. Approximately 1% of people

affected with tuberculosis will develop associated arthritis (tuberculous arthritis, granulomatous arthritis). The joints most frequently involved are the spine, hips, knees, wrists, and ankles. Most cases involve just one joint. Tuberculosis involving the spine is often referred to as Pott’s disease. Indeed, secondary pulmonary tuberculosis develops preferentially in young immunocompetent adults aged 15–45 years. In the aged, tuberculosis typically runs a slower course with pulmonary interstitial inflammation leading to pulmonary fibrosis rather than cavities [9, 39, 42, 43].

The treatment of all forms of tuberculosis is based on the principle of drug combination and standard treatment today comprises two phases:

- (1) Intensive phase: 2 months of HRZE (H-isoniazid, R-rifampicin, Z-pyrazinamide, E-ethambutol). The combination of drugs to avoid the selection of anti-TB drug resistance.
- (2) Continuation phase: 4 months for HRE or HR. Prolonged treatment is needed in order to ensure that all bacteria in their different phases of metabolic growth are effectively killed.

With appropriate management and resources for rapid diagnosis, more than 90% of patients with TB due to pan-drug sensitive strains of Mtb can be cured [44, 45].

1.1.3. Nontuberculous mycobacterial infection (NTM)

Previous names for this group of organisms include “atypical mycobacteria” or “mycobacteria other than *M.tuberculosis* (MOTT)” and “environmental mycobacteria”; and so far more than 150 NTM different species have been detected. The NTM infections are increasing nowadays and the factors that may contribute to these increases are: (1) An increased number of clinical specimens submitted for determination of acid-fast bacilli (AFB) stains and cultures, (2) Improved laboratory techniques, (3) Higher recognition of NTM disease [46]. The NTM can cause a wide range of infections in humans and animals, but commonly they include some organ systems, which are (1) pulmonary diseases, (2) cervical and lymphadenitis, (3) skin and soft tissue disease, (4) skeletal diseases, (5) catheter-related infections, (6) disseminated infections.

Among them, the pulmonary diseases caused by non-tuberculous mycobacteria are most frequent and emerging [47, 48], in parallel to a slow decline of tuberculosis. In **Figure 1-2** clinical relevance of pulmonary nontuberculous mycobacterium is shown and clinical settings for nontuberculous mycobacterial lung disease are placed in **Table 1-1**.

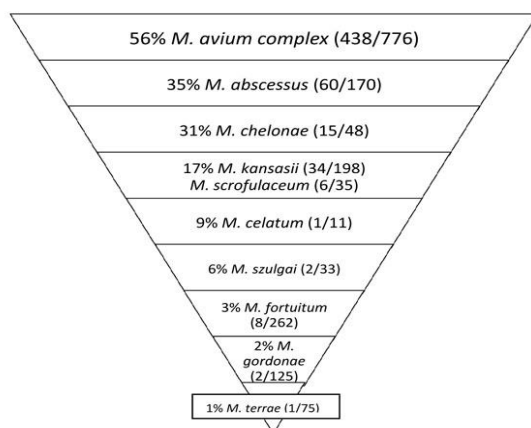


Figure 1-2. Clinical relevance of pulmonary NTM isolates (Asia, 1971–2007). Relevance per species was defined as percentage of patients with pulmonary NTM isolates meeting the American Thoracic Society criteria. Species reported infrequently, i.e., <5%, are not shown [47].

In addition, the signs and symptoms of NTM lung diseases are often variable and nonspecific, which is why disease with NTM is difficult to diagnose without multiple positive cultures from respiratory specimens.

Table 1-1. Clinical settings for nontuberculous mycobacteria lung disease [49].

Radiographic Disease	Setting	Usual Pathogen	Rare Pathogen
Upper lobe cavitory	Male smokers, often abusing alcohol, usually in their early 50s	<i>M. avium</i> complex, <i>M. kansasii</i>	
RML, lingular nodular bronchiectasis	Female nonsmokers, usually older than 60 yr	<i>M. avium</i> complex, <i>M. abscessus</i>	<i>M. kansasii</i>
Localized alveolar, cavitory disease	Prior granulomatous disease (usually tuberculosis) with bronchiectasis	<i>M. abscessus</i> , <i>M. avium</i> complex	
Not well established	Adolescents with cystic fibrosis	<i>M. avium</i> complex, <i>M. abscessus</i>	
Reticulonodular or alveolar lower lobe disease	Achalasia, chronic vomiting secondary to GI disease, exogenous lipid pneumonia (mineral oil aspiration, etc.)	<i>M. fortuitum</i>	<i>M. abscessus</i> , <i>M. avium</i> complex, <i>M. smegmatis</i>
Reticulonodular disease	HIV-positive hosts, patients with preexisting bronchiectasis, others	<i>M. avium</i> complex	

GI, gastrointestinal; HIV, human immunodeficiency virus; RML, right middle lobe.

There are some categories of pulmonary disease, that can be nosologically identified. Herein:

- The disease occurs in middle-aged or older patients, usually men with a history of lung disease.
- The disease occurs in otherwise apparently healthy persons, although some may have minor and covert immune defects.
- The disease occurs in children with more severe immune defects or predisposing pulmonary disease, notably cystic fibrosis or severe fungal infection.
- The disease occurs in very immunosuppressed patients, of which HIV infection is the prevalent cause worldwide [6, 50].

1.1.3.a. *Mycobacterium avium* complex

Mycobacterium avium is the NTM most commonly associated with human disease. It is a member of the *Mycobacterium avium-intracellulare* complex (MAI), comprising two closely related organisms: *M. avium* and *Mycobacterium intracellulare*, which are difficult to differentiate, that is why they are collectively referred to as MAI or MAC (*M. avium* complex). Four subspecies of *M. avium* have been described, of which *M. avium* subsp. *Hominissuis* is the pathogen of humans [1, 9].

NTM infections began to be reported more frequently after the incidence of tuberculosis declined in the 1950s. During 1979-80, NTM represented one third of mycobacterial isolates reported to the Centers for Disease Control and Prevention (CDC), and 61% of these were MAC. Pulmonary diseases caused by MAC are seen in most

developed countries, however *M. avium* is prevalent worldwide. In the United States [51] and in Japan [52] there are approximately 1.3/100.000 persons infected by *M. avium*, whereas in France there are 0.2/100.000 [53], Switzerland there are 0.9/100.000 [54] and MAC infection has also been reported from other parts of the world, including Australia (1.92/100.000), Tanzania, Zambia, and others [6].

This microorganisms grow slowly (10-21 days) on solid media and produce thin-translucent colonies. The nonpigmented, light tan colonies are classified as Runyon Group III, although some MAC strains produce yellow pigment that increases by aging [2, 4]. MAC is relatively avirulent in the normal host, however, it can cause diseases in AIDS patients, patients with pre-existing structural lung disease, children [55], women increasingly beyond menopause [56], and rarely in nonimmuno-compromised persons. Also the infection of MAC is highly associated with deficiency of TNF- α and IFN- γ receptor expression or IFN- γ production due to genetic defects [57, 58] and hairy cell leukemia [59]. MAC are ubiquitous in distribution and can be found in many environmental sites, including aerosolized water, piped hot water systems (e.g., including household and hospital water supplies), bathrooms [60], present in water (e.g., fresh, brackish, and ocean) [5], house dust, soil, birds, farm animals and cigarette components (e.g., tobacco, filters, paper) [61]. MAC are thought to be acquired by inhalation or ingestion.

Main disease syndromes produced by MAC in humans are: (1) pulmonary disease, usually in adults whose systemic immunity is intact; (2) disseminated disease, usually in patients with advanced human immunodeficiency virus (HIV) infection; and (3) lymphadenitis, common in children. Additionally, but rarely, MAC can cause disease in other sites, such as cutaneous disease.

Successful treatment of MAC is a challenge. As with therapy of other mycobacterial infections, the use of at least two active drugs is essential to prevent emergence of resistance and to achieve long-term cure [62]. The treatment regimen must be guided by attending to the isolated species, the specific syndromes, clinical experience and individual conditions.

1.1.3.b. *Mycobacterium abscessus*

M. abscessus is a rapidly growing mycobacterium (RGM) in Runyon group IV with *M. chelonae* and *M. immunogenum* [5, 63, 64]. To mention some important clinical situations related with *M. abscessus*:

- *M. abscessus* lung disease: This infection is typically found in cystic fibrosis patients and intensifies destruction of pulmonary architecture. Patients who have *M. abscessus* lung disease are typically older nonsmoking females with no known underlying or predisposing lung disease. This disease clinically and radiographically most closely resembles noncavitary (e.g., nodular bronchiectatic) pulmonary MAI disease. *M. abscessus* and MAI are occasionally isolated concurrently or consecutively in some patients [65].

- Skin and subcutaneous diseases: RGM are probably the most common NTM involved in cases of community-acquired infections of skin and soft tissue, occurring after bacteria that are introduced into the deep subcutaneous tissues by trauma or iatrogenic infections (e.g., intravenous catheter, contaminated wound dressing, prosthetic device such as a heart valve, peritoneal dialysis and bronchoscopy) [6]. Localized traumatic injury, such as puncture wounds from stepping on a nail, insect bite, open lacerations, contamination of a post-leg shaving solution or fractures are the usual scenarios [66]. In ophthalmology, rapid-growing species may cause keratitis and corneal ulceration after surgery, as well as infection after local accidental trauma [9, 50].
- Skeletal disease: RGM have been implicated in chronic granulomatous infections involving tendon sheaths, bursae, bones, and joints after direct inoculation of the pathogen through accidental trauma, surgical incisions, puncture wounds, or injections. Osteomyelitis of the sternum caused by *M. fortuitum* and *M. abscessus* has also been found in clustered outbreaks and sporadic cases after cardiac surgery [63].
- Catheter-related infections: Currently, catheter-related infections, originating from rapid-growing mycobacteria, are the most common nosocomial NTM infections encountered. They are usually seen with long-term central IV catheters, but they may also occur with peritoneal or shunt catheters. These infections may be manifested as fever, local catheter site drainage, bacteremia or occasionally as lung infiltrates or granulomatous hepatitis [67].

1.2. Definition of problems of mycobacterial infections

Despite many remarkable achievements, TB infection remains a major health threat. Namely:

- The TB pandemic has flourished over the past two decades. Epidemiologists once believed the disease would eventually disappear based on some assumptions at the middle of the twentieth century. Although several problems were anticipated, the eradication of tuberculosis was considered feasible [68]. The failure of these predictions became obvious when in 1986 the downward trend of the incidence rate of TB reversed. The reasons are several and complex, including the deterioration of tuberculosis control due to the immigration of people from high-prevalence countries, actions to address direct tuberculosis risk factors (e.g., HIV, undernutrition, diabetes, smoking, drug and alcohol misuse), and underlying social determinants (e.g., poverty, poor living and working conditions) [19, 69].
- The treatment programs of TB failed in some countries. Treatment for TB requires 3–4 drugs given for 6 months or longer. Sometimes, patient's compliance is poor and premature termination of drug therapy. Even worse, new forms of multi drug resistant bacilli are on the rise [70], needing longer treatment with less efficient drugs and more side effects.

- The only vaccine, developed almost a century ago, provides limited protection only during childhood and development of better vaccines has been unsuccessful. Most evidence indicates that BCG vaccination of children results in a 60% to 80% decrease in the incidence of tuberculosis. Although BCG vaccine does not prevent infection, it usually prevents progression to clinical disease, and effectively prevents disseminated disease in young children. The development of a better vaccine for tuberculosis takes a high priority [9]. Additionally, better biomarkers need to be identified that correlate with protective immunity against TB [71].
- In response to the challenge of ominous disease, numerous investigators have been using the best tools of modern science to combat the disease. However, there are still surprising gaps in our knowledge of this infection since appropriate model systems are limited. To battle this bacterial infection effectively, we need to understand its pathophysiology completely [72].
- In addition to TB, NTM infections are increasing nowadays, besides TB. Especially pulmonary NTM is estimated to be at least ten times more common than TB in the U.S with at least 150,000 cases per year. NTM can cause a wide range of infections in humans and animals, and are ubiquitous in the environment [7]. Moreover, differential diagnosis of NTM is problematic.

1.3. Aim of the study

WHO determined that acceleration of the decline towards elimination of this disease will need invigorated actions in four broad areas, which are shown in **Figure 1-3** [69]. Thus, the Treatment Action Group, an activist organization efforts to increase research for deadly infectious diseases, has tracked annual spending on tuberculosis research and development and compared investments in six areas of research (**Figure 1-3**) for the Stop TB Partnership's 2011–2015 Global Plan [73]. From here, basic science forms the foundation on which the development of new diagnostics, drugs, and vaccines should be build. Many kinds of investigations in basic science are orientated on different subjects, for instance *Mycobacterium*, human, models and so on.

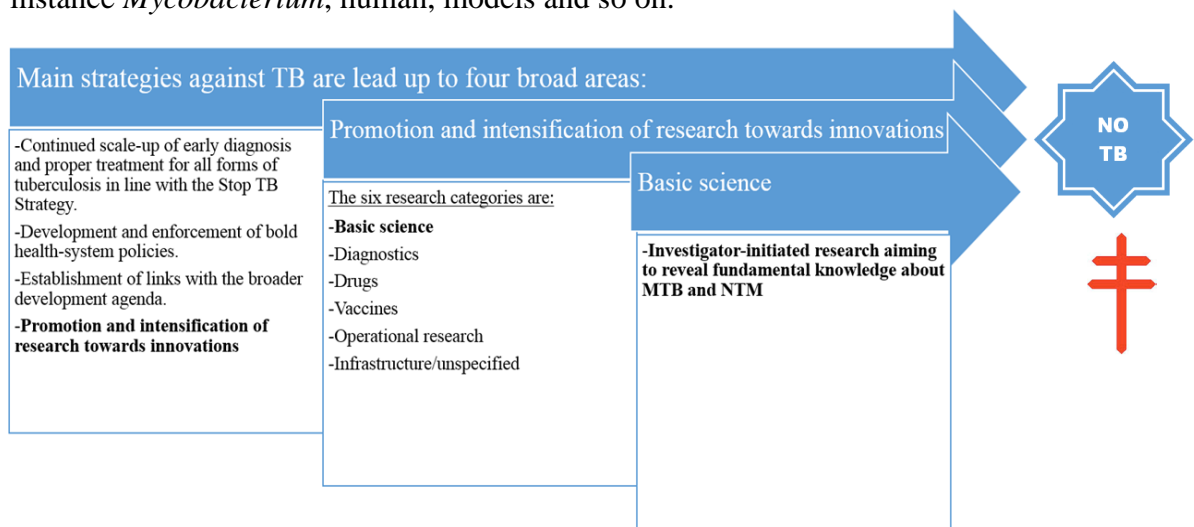


Figure 1-3. Overview of main and sub-strategies against TB.
Postscript*: we try to emphasize our way along to the aim of study in bold print.

Encouraging results have been obtained through animal models, which have provided valuable information about the development of TB, including the pathogenesis, pathology, and immunology [74, 75]. Studies of TB in laboratory animals such as mice [76], rats [77], rabbits [78], monkeys [79] and guinea pigs [80] have been established. Unfortunately, all existing animal models fail to mimic the human disease perfectly. For example, mice are the animals of choice for common scientific studies though, classic TB disease in mice could not be established because of their resistance [81, 82]. Thus to substantially improve the situation, a detailed understanding of the cross-talk between human host and the *Mtb* pathogen is essential.

Regarding *in vitro* models of human cells, the monocytes isolated from peripheral blood are undoubtedly the most important model for primary cell infection [83]. In addition, other human primary phagocyte models, including microglia [84], alveolar macrophages [85] and neutrophils [86] are investigated. Human cell lines have also been used for a long time as infection models, including phagocytic cell lines (THP-1 [87], HL60 [88] and U937 [89]) and non-phagocytic cell lines (like HeLa [90] or A549 [91]). Most of the gathered evidences indicate that it is extremely difficult to induce mycobactericidal activity in purified populations of phagocytes. Probably human phagocytes need the assistance of other cell types or unknown humoral factors to activate properly. Therefore, the development of more complex models may help to elucidate the nature of this infectious diseases in humans. Additionally, mycobacteria can affect any organ, although, the main target is the lung.

On the other hand, TB is the prototype of the life-long, life-threatening, granulomatous disease, followed by formation of granuloma, where persistent T-cell responses to mycobacteria are responsible for chronic aggregates of activated macrophages [9, 92]. Thus, most scientists focus on adaptive immunity. But approximately 50% of individuals exposed to *M. tuberculosis* never become tuberculin skin test positive, which may indicate that the bacterium is removed by the innate immunity [93].

With this attractive hypothesis and based on limitations of human complex models for mycobacterial research, our study intended to establish an *ex vivo* short-term tissue culture model designated as STST (Short-Term Stimulation of Tissue) using human lung tissues. We are convinced that this model allows us to characterize the early steps of mycobacterial infection in humans, as well as, to promote new antimycobacterial mechanisms associated with innate immunity. In science, *ex vivo* refers to experimentation done on tissues in an external environment with the minimum alteration of natural conditions, that would otherwise not be possible or ethical in living subjects [94]. Likewise, the *ex vivo* is a more controlled condition than *in vivo* experiments. Once the vital *ex vivo* STST model contains normal architecture of the lung including all cell types, it would be valuable to establish a more meaningful model for mycobacterial infection, in which cross-talk between human host and infectious agent can be explored, as well as, interaction between different cells, and the initial phase of mycobacterial infection pattern.

In order to combat mycobacterial infections successfully, an improved knowledge of the responses to mycobacterial infection and pathogenic mechanisms are required,

leading to development of future diagnosis, prognosis, and therapy. The use of omics (genomics, transcriptomics, proteomics, metabolomics, plus DNA microarray and bioinformatics) has led to dramatic advances in the understanding of the molecular and genetic bases of disease [95]. Especially transcriptomics provides information about the expression of individual genes at the messenger RNA (mRNA) level and correlates patterns of expression with biological function. A novel fixation technique named HOPE, which preserves nucleic acids well, has been well documented [96-99]. Hence, the combination of short-term cultivation using vital tissues and HOPE-fixation is a useful tool for molecular pathology [100-103]. The focus of this issue, we set out to investigate genes on mRNA level from a genome-wide expression profile upon mycobacterial infection.

2. Materials and Methods

2.1. Collection of samples

Fresh human tissue samples were obtained from patients who underwent thoracic surgery (pneumectomy or lobectomy) at the Lungen Clinic Grosshansdorf due to conspicuous diagnostic findings. Permission of local ethical committee at the University of Lübeck for *ex vivo* cultivation and stimulation of human material, was granted (Approval Nr: 07-157). Totally 65 samples of patients were collected for investigation between march 2012 and february 2013.

2.2. *Ex vivo* STST lung model for mycobacteria

Ex vivo procedures allow experimentation on tissues under more controlled conditions than *in vivo* and ability to perform tests and measurements [94]. That is why we intended to establish an *ex vivo* short-term tissue culture model, designated as STST (Short-Term Stimulation of Tissue) in human lung tissues of mycobacteria, to elucidate some unknown mechanisms during mycobacterial infection.

2.2.a. Preparation of tissues

Applied gross morphologic criteria to choose suitable parts of lung tissues for the study were:

- Without inflammatory consolidation
- Without pleura
- Without anthracosis

Tissues were dissected to obtain pieces of 0.5-1 cm³ size. Specimens were cultured in RPMI Medium 1640 (1x) GlutaMAXtm-I (Invitrogen, Germany) supplemented with 10% FCS (PPA, Austria), 0.02M of HEPES buffer solution (Invitrogen), 0.01mM of Sodium pyruvate (Biochrom, Germany) in Costar 3513 cell culture cluster (12 well, flat bottom with lid) (Lifesciences, USA).

2.2.b. Preparation of suspensions

For every mycobacterial species a type strain and a clinical isolate were used:

- *M. abscessus* 9547/00 (type strain), *M. abscessus* 8562/11 (clinical isolate. Culture origin from Germany in 2011)
- *M. avium* 3725/07 (strain 104), *M. avium* 3439/10 (clinical isolate, Culture origin from Germany in 2010),
- *M. tuberculosis* 9679/00 (type strain), *M. tuberculosis* 1616/12 (clinical isolate, Culture origin from Germany in 2012),

Cultures were grown on Löwenstein–Jensen medium (LJ). For stimulation of human tissues, different concentrations of bacteria were used (10⁴-10⁷ colony forming units

(CFU/ml). Initially a stock suspension was made with 10^8 CFU/ml. For this colony material was taken from the slants by using inoculation loops and dispersed into physiological salt solution using glass sticks. To precipitate clumps of bacteria suspensions were centrifuged at low speed ($100 \times g$) for 5 minutes. The concentration of the supernatant was determined by comparing the solution optically to McFarland 0.5 standard solution. Then final concentrations were prepared by serial 1:10 dilutions into RPMI Medium 1640. BBL™ MGIT™ PANTA™ antibiotic mixture was added to the suspensions to prevent growth of other bacteria. Tissues were infected with 2 ml of the suspensions. To distribute the mycobacteria, medium was resuspended softly several times by pipetting.

2.2.c. Incubation of tissue culture

In general, tissues were incubated at 37°C for different times (~16, 48 and 72 hours) and different concentrations of suspension (10^4 - 10^7 CFU/ml). Two kind of controls were collected, one was directly fixed in HOPE-solution prior to cultivation, another was incubated under same culture conditions without mycobacteria. An overview of the *ex vivo* STST model is illustrated in **Figure 2-1**. The reagents and tools used are listed in **Table 1** in appendix-I.

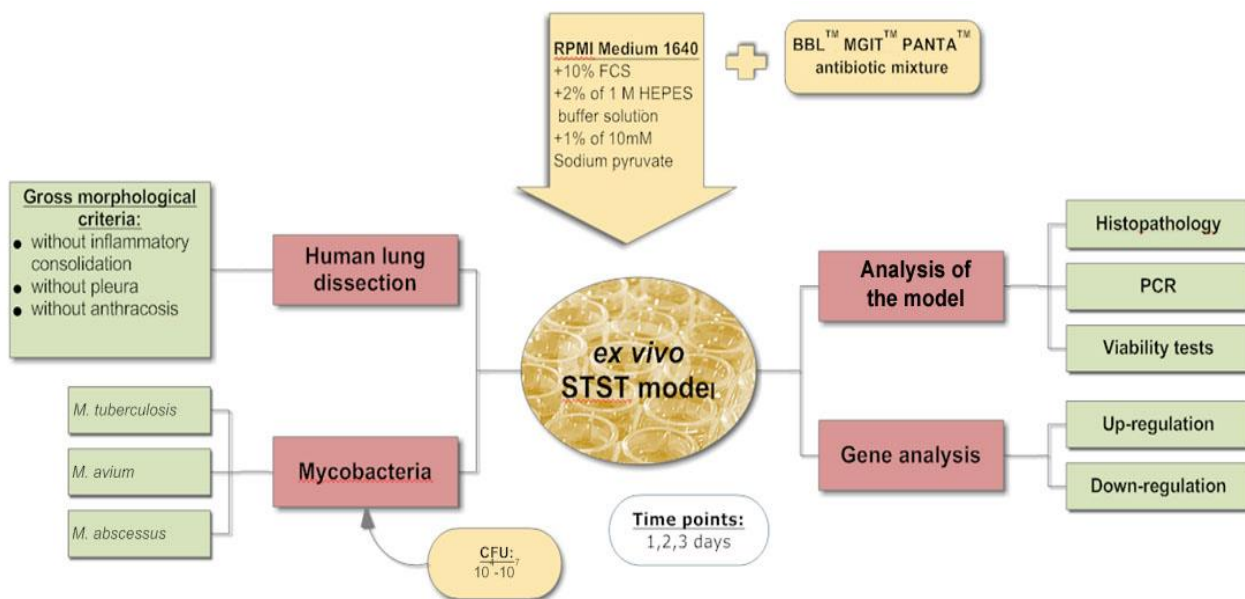


Figure 2-1. General schema of the *ex vivo* STST model and further analysis

2.2.d. CFU control of working suspensions

The concentrations of viable mycobacteria (CFU/ml) in the stock suspensions were determined 3 times during this study. Basically the stock solutions were serially diluted (1:10 each) until 10^0 CFU/ml. From 10^0 - 10^3 CFU/ml 0.3 ml were cultured in petri dishes containing LJ medium. Cultivation time was for *M. abscessus* 1-2 weeks, for *M. avium* and *M. tuberculosis* 4-6 weeks, respectively. Afterwards mycobacterial colonies were counted visually and the CFU/ml were determined.

2.3. Collection of supernatants and tissue processing

At the end of incubation, specimens were transferred into acetone resistant disposable tubes (50 ml) with ice-cold (4°C) HOPE-solution for preservation and incubated at 4°C overnight. After incubation, HOPE-solution was removed, re-filled with 5 ml ice-cold 100% acetone and incubated for 2 hours at 4°C. This step was repeated 4 times with each incubation lasting 2 hours. After 8 hours of dehydration, acetone was discarded and the samples immediately transferred into pre-warmed low-melting paraffin (melting point: 52-54°C) and incubated overnight at 54-55°C in standard cassettes. After infiltration of paraffin, embedding of tissues was carried out in standard cassettes and the specimens kept at 4°C until further use. Supernatants from *ex vivo* stimulation were filtered (pore size of 0.20 µm) to remove bacilli and blood cells and stored at -20°C for further analysis. The reagents and tools used for collection of supernatants and tissue processing steps are listed in **Table 2** in appendix-I.

Above all, 3 randomly selected blocks were completely cut in a series (including *M. abscessus*, *M. avium* and *M. tuberculosis*) in order to enquire how deep infection could infiltrate into tissues. Firstly, the tissues' precise cubic sizes were measured by melting the blocks, then tissue processing was repeated and the block was completely cut with a specimen-thickness of 2 µm. Serial sections were obtained from the samples for ZN staining and IHC (immunohistochemistry).

2.4. Sectioning, deparaffinization and rehydration of HOPE-fixed, paraffin-embedded tissues

Before cutting, the tissue blocks were kept on ice for 30 min and mounted on a microtome as usual. Paraffin-embedded tissues were cut by two types of microtome depending on the purpose. For regular cutting, a manual microtome Leica SM 2000R and for serial cutting an automatic Leica RM 2255 were used. Sections were transferred onto the surface of a water bath first (cold tap water), then transferred on a slide to the heating-plate I (55°C) for a few seconds until the section stretched out completely. Afterwards the sections were placed on a slide rack and drip-dried for a couple of minutes until transfer to heating-plate II (37°C) for overnight incubation. Dried sections were stored at 4°C. For deparaffinization, slides were placed into a first cuvette with 60°C isopropanol for 10 minutes, then transferred to a second cuvette with 60°C isopropanol for washing thoroughly. Rehydrate tissue by incubating it in 70% ice-cold acetone for a minimum of 10 minutes in the fridge for 2 times, afterwards transferred to aqua dest (4°C) for 10 minutes. The reagents and tools used for sectioning, deparaffinization and rehydration of HOPE-fixed, paraffin-embedded tissues are listed in **Table 3** in appendix-I.

2.5. Histochemical stainings

The following stainings were applied:

- Hematoxylin and Eosin (H&E) staining – According to principles of pathological evaluation, initially all samples' general morphological and structural analysis were investigated with H&E staining after *ex vivo* incubation (staining protocol is shown in **Table 4.1** in appendix-I).
- Acid-fast staining– Detection of Mycobacteria (staining protocol is shown in **Table 4.2** in appendix-I). Initially cold Ziehl-Neelsen technique/ Kinyoun staining was used, but HOPE-fixed, paraffin-embedded tissues required some modification of staining. Therefore, we optimized the staining by adding Mayer's hemalum, which is compared in **Figure 2-2 A & B**. The modification of staining allowed us to have good counter staining, even gave a chance to distinguish different infected cells types. In further part of the project, the optimized staining referred just as ZN to make it short once we mentioned here.

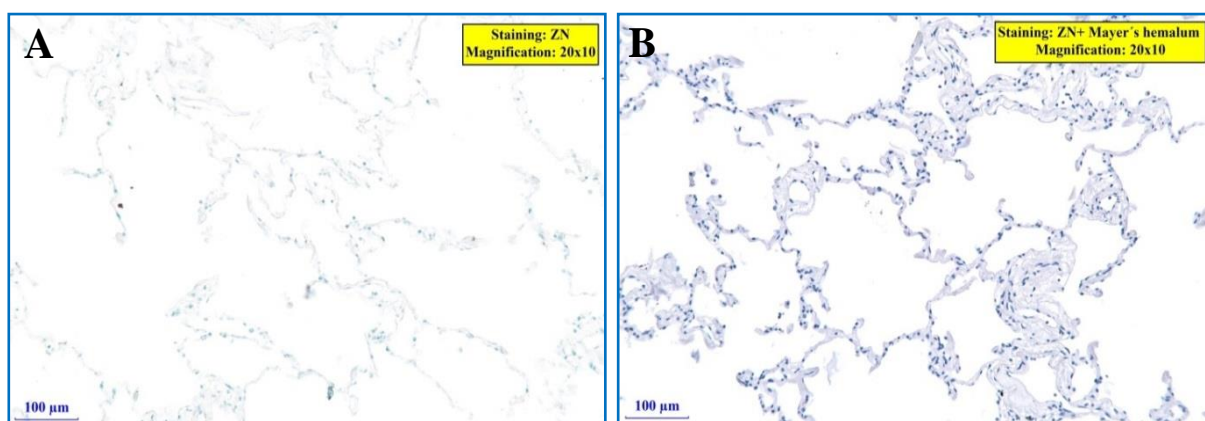


Figure 2-2. Comparison between regular and optimized cold ZN stainings (in HOPE fixed, paraffin-embedded tissues). **A.** A regular cold Ziehl-Neelsen/Kinyoun staining. **B.** A combination of ZN and Mayer's hemalum. The slide thickness (0.5µm) and camera options (exposure time:100, gain: 2, gamma:1) are the same. Images were acquired at ×200 magnification.

- Gram staining – Detection of gram-positive bacterial contamination (staining protocol is shown in **Table 4.3** in appendix-I)
- Immunohistochemical (IHC) staining – Detection and localization of candidate proteins (staining protocol is shown in **Table 4.4** in appendix-I)
- IHC with Auramin-Rhodamin-Fluorescence staining – Double-staining for detection of mycobacteria and target protein (staining protocol is shown in **Table 4.5** in appendix-I)
- Pappenheim staining- The most common stain for blood smears, though it was used for staining of primary alveolar epithelial cells type II (staining protocol is shown in **Table 4.6** in appendix-I)

The reagents and tools used for histochemical stainings are listed in **Table 4** in appendix-I.

2.6. Experiments with nucleic acids

General laboratory practice

Particular care was taken for working with nucleic acids. Generally, working benches were cleaned with 80% ethanol. The microtome was cleaned with chloroform before cutting. Glass and metal ware was baked at 180°C for at least 6 h. Thermostable plastic ware was autoclaved at 121°C for 20 min and sterile gloves were always used during the working-procedures. Chemicals, composition of buffers and reagents as well as instruments used in this study are listed in the Appendix-I.

2.6.1. DNA analysis

A. Purification of DNA from HOPE-fixed, paraffin-embedded tissue blocks

For isolation of DNA from human tissue samples, the QIAamp DNA Mini Kit (Qiagen) was used. This procedure of purification of DNA required no phenol–chloroform extraction and no mechanical homogenization as the tissues are lysed enzymatically via proteinase digestion. The procedure itself was carried out by 2 steps: 1) deparaffinization, 2) DNA isolation. A detailed protocol has been attached in **Table 5** in appendix-I. After deparaffinization proteinase K was used to lyse structural components of tissues and cells. The DNA purification procedure comprises 4 steps, including binding of the DNA, washing with buffer AW1, washing with buffer AW2 and elution. The steps were carried out using QIAamp Mini spin columns, 2 ml collection tubes and standard microcentrifuge tubes. The eluted genomic DNA was collected in standard 1.5 ml microcentrifuge tubes with deionized water and stored at –20°C for further studies.

B. Quantification of nucleic acids

For quantification of DNA a Thermo Scientific NanoDrop™ 2000 Spectrophotometer was used. The modified equation used for nucleic acid calculations is the following:

$$c = (A * \epsilon) / b$$

c = the nucleic acid concentration in ng/microliter

A = the absorbance in AU

ε = the wavelength-dependent extinction coefficient in ng-cm/microliter

b = the pathlength in cm

The extinction coefficients for double-stranded DNA were 50 ng-cm/μL. The ratio of absorbance at 260 and 280 nm is used to assess the purity of nucleic acids. Procedure's protocol and material used are listed in **Table 6** in appendices. Only samples with a ratio > 1.6 were kept at -20°C (DNA), at -80°C (RNA) and used for further analysis.

C. Polymerase chain reaction (PCR)

Purified DNA from *ex vivo* infected tissues was analyzed by PCR for detection of mycobacterial DNA. For means of positive control, mycobacterial DNA was used as template in PCR reactions. Furthermore, negative controls without template and extraction controls were regularly performed. Sequences of used primers are shown in **Table 2-1**.

Description	Site of sequences (5'-3')	Target gene	Specificity	Reference
β-Globin (forward)	GAA GAG CCA AGG ACA GGT AC	β-Globin	Human	[104-106]
β-Globin (reverse)	CAA CTT CAT CCA CGT TCA CC	β-Globin	Human	
B1 (forward)	AGA GTT TGA TCC TGG CTC AG	16S rRNA gene	~all bacteria	[107]
Genus (reverse)	TTT CAC GAA CAA CGC GAC AA	16S rDNAgene	Mycobacteria	[108, 109]
Tub (forward)	CCT GCG AGC GTA GGC GTC GG	IS6110	<i>M. tuberculosis</i>	
Tub (reverse)	CTC GTC CAG CGC CGC TTC GG	IS6110	<i>M. tuberculosis</i>	
Avium (reverse)	ACC AGA AGA CAT GCG TCT TG	16S rDNAgene	<i>M. avium</i>	[105, 109, 110]

PCR master mix was prepared according to **Table 2-2** and the DNA template added. The protocol was designed for a 50 µl reaction volume.

Components	Amount [µl]	Concentration [µM]
Sterile, nuclease free H ₂ O	4.7	-
10x PCR buffer (200 mM Tris-HCL, 500 mM KCL)	5	1
MgCl ₂ (50 mM)	2	2000
dNTPs -10 mM (dATP, dCTP, dGTP and dTTP)	1	200
Forward primer (20 µM)	2	0.8
Reverse primer (20 µM)	2	0.8
<i>Taq</i> DNA polymerase (5 Units /µ 500 U)	0.3	0.03

A thermocycler (UNO, Biometra) was used for the amplification of specific sequences by PCR through multiple cycles of *in vitro* DNA replication. Amplification conditions have been optimized based on the specific characteristics of primers, template and size of the amplicon. Melting temperatures of primers (T_m) were calculated as following: $T_m = 2C(A+T) + 4C(C+G)$ based on length and composition of nucleotides. Programms for the amplification of different targets are shown in **Table 2-3**.

Cycle number: 40 times	Steps Primer combination	B-Globin, Tub (β-Globin forward and reverse, Tub-forward and reverse)	Genus (B1-forward, Genus-reverse)	Avium (B1-forward, avium-reverse)
	Denaturation	94°C (1min)	94°C (1min)	94°C (1min)
Annealing	57°C (1min)	55°C (1min)	55°C (1min)	59°C (1min)
Elongation	72°C (1m 30s)	72°C (1m 30s)	72°C (1m 30s)	72°C (1m 30s)
Final extension	72°C (15 min)	72°C (15 min)	72°C (15 min)	72°C (15 min)
Cooling	4°C (22h)	4°C (22h)	4°C (22h)	4°C (22h)

D. Agarose gel electrophoresis

For separation of PCR products according to their molecular size, 10 µl of amplified PCR products were mixed each with 1.5 µl gel loading buffer. Afterwards PCR products were inserted into holes of 2.4-2.8% agarose gel (Invitrogen) containing 0.001 mg/ml ethidium bromide (Invitrogen). Electrophoresis was conducted in 1xTAE (Tris-Acetate-EDTA) buffer at 80-90 volts (Biometra) for 20-25 min. General protocol for agarose gel electrophoresis is shown in **Table 2-4**. The reagents and tools used for agarose gel electrophoresis are listed in **Table 7** in appendix-I.

Table 2-4. General consideration of agarose gel electrophoresis	
Size of the gel	Minigels (~8 cm long)
Percentage of agarose	2.4-2.8%
Running buffer	1xTAE (50x:2 M Tris; 50 mM EDTA; 1M acetic acid)
Voltage	80-90 V
DNA staining	Ethidium bromide (0.1 mg/ml)
Time	20-25 min
Gel loading buffer	Xylenecyanol (5x TAE buffer 4.6 mM xylenecyanol; 3.3% glycerol) (for β globin, genus); Bromophenol-blue (5x TAE buffer, 5.6% of glycerol, 17.78 mg/ml of bromophenol blue) (for tub, avium, genus)

E. Visualization and analysis of amplified PCR product

Ethidiumbromide as a DNA intercalating dye was used to visualize the separated PCR products. After the electrophoresis, DNA bands were visualized on a UV-transilluminator with digital camera-based gel documentation system (INTAS, Germany). The fragment size was assessed by comparison to a DNA molecular weight marker (pBr322-*Msp*1, New England Biolabs, NJ, USA).

2.6.2. RNA analysis

A. Extraction of total RNA from HOPE-fixed, paraffin-embedded tissue blocks

RNeasy Mini kit (Qiagen, Germany) was used to extract total RNA from HOPE-fixed, paraffin-embedded tissue blocks. Tissues were dewaxed initially according to RNA binding capacity of the RNeasy spin column and the lysing capacity of buffer RLT. After deparaffinization, samples were disrupted and homogenized with an electronic pestle and lysing buffer RLT containing 1% of 14.3M beta-Mercaptoethanol (BME). The total RNA purification procedure comprises several steps. Briefly ethanol was added to the buffer RW1, promoting selective binding of RNA to the RNeasy membrane. Contaminants were washed away by centrifugation with RPE buffer for 3 times. Total RNA was eluted in RNase-free water and stored at -80°C for further studies. A detailed protocol has been attached in **Table 8** in appendix-I.

B. RNA integrity

The Agilent 2100 bioanalyzer (Agilent Technologies, USA) with RNA 6000 Nano kit was used for quality control of extracted total RNA prior to microarray analysis. The detailed protocol has been attached in **Table 9** in appendix-I.

C. Transcriptome analysis

The Agilent Whole Genome 4x44K microarrays with the Low Input Quick Amp Labelling Kit (one-color) (Agilent Technologies) were used for transcriptome analysis. In short, whole RNA was mixed with Spike-In controls and submitted to cDNA synthesis for amplification and reverse transcription. The cDNA was then used for synthesis of complimentary RNA (cRNA) by T7 RNA polymerase, including labelling with Cy3-CTP. This procedure was done by Jasmin Tiebach and Maria Lammers from the department of Clinical and Experimental Pathology at the Research Center Borstel.

2.7. Investigations with primary cells

For *in vitro* infection experiments with mycobacteria, primary alveolar macrophages and alveolar epithelial cells type 2 (AECII) were isolated from human lung tissues. The cells were cultured in modified high glucose DMEM/F12 (Gibco, 21041-025) + 1 % Pen/Strep + 10 % FCS. Cells were generally incubated at 37°C in 5% CO₂ for 24 h and used for further experiments. Isolation of primary cells was done by Bettina Baron-Lühr and Patricia Prilla from the department of Clinical and Experimental Pathology at the Research Center Borstel.

2.7.1. *In vitro* infection of primary cells

Experiments for *in vitro* infection of primary cells with mycobacteria and real time PCR experiments were done by Lisa Niwinski from the Division of Microbial Interface Biology at the Research Center Borstel. Primary alveolar macrophages and type II alveolar epithelial cells were cultured in 500 µl RPMI1640 with 10% FCS and 4 mM L-glutamine in 48-well flat-bottom microtiter plates (Nunc) at 37°C in a humidified atmosphere containing 5% CO₂. Cells were infected with *M. tuberculosis* H37Rv at the indicated MOI. Four hours postinfection, nonphagocytosed bacteria were removed by washing three times with 0.5 ml Hanks' balanced salt solution (HBSS) (Invitrogen, Karlsruhe, Germany) at 37°C. After washing and after 3 days of cultivation, 0.5 ml medium was added to the culture. At day 7, supernatants were completely removed, and macrophage cultures were lysed at 4 hours, 3 and 7 days postinfection by adding 10 microL 10% saponin solution (Sigma, Steinheim, Germany) in HBSS at 37°C for 15 min. Lysates were serially diluted in sterile water containing 0.05% Tween 80 (Merck, Darmstadt, Germany) and plated twice on 7H10 agar containing 0.5% glycerol (Serva) and 10% heat-inactivated bovine calf serum (BioWest, France). After 3 weeks at 37°C, the CFU were counted.

For real time PCR analysis, primary cells were stimulated with *M. tuberculosis* strain H37Rv at an MOI of 10:1. For positive control of immune response LPS was used with 10ng/ml concentration, and for negative control same amount of cells in medium without stimulation were used. In order to investigate reactions of primary cells upon mycobacteria, real time PCR was performed for common cytokines, which are listed in **Table 2-5**.

Table 2-5. The genes list evaluated by real time PCR	
Official abbreviation and full name	Functions related with infections [7]
Wnt3a (wingless-type MMTV integration site family, member 3a)	Multiple functions in cell proliferation and migration as well as tissue organization, regulation of cell fate, secreted signaling protein, regulation of inflammatory processes (anti-inflammatory effects on mycobacteria-infected macrophages)
MCP-1 (monocyte chemoattractant protein-1)	Chemotactic activity (recruits inflammatory cells to the sites of inflammation produced by either tissue injury or infection)
TNF-α (tumor necrosis factor alpha)	Regulate immune cells, potent chemoattractant for neutrophils, stimulate phagocytosis, release upon bacterial products
VEGF-A (Vascular endothelial growth factor A)	It has various effects, including mediating increased vascular permeability, inducing angiogenesis, vasculogenesis and endothelial cell growth, promoting cell migration, and inhibiting apoptosis.
CCL4 (Chemokine (C-C motif))	CCL4, also known as macrophages inflammatory protein-1β (MIP-1β) is a CC

ligand 4)	chemokine with specificity for CCR5 receptors. It is a chemoattractant for natural killer cells, monocytes and a variety of other immune cells
hIL6 (Interleukin 6)	It acts as a pro-inflammatory, to stimulate immune response, during infection and after tissue damage leading to inflammation
CXCL10 (C-X-C motif chemokine 10)	It has pleiotropic effects, including stimulations of immune cells, chemoattraction, angiogenesis.
LNC2/ NGAL (lipocalin-2/neutrophil gelatinase-associated lipocalin)	It is involved in innate immunity by sequestering iron that in turn limits bacterial growth

2.7.2. Vitamin stimulation to induce “self split” cell death

Vitamin C (ascorbic acid) and vitamin K₃ (menadione) were administered to induce oxidative stress leading to a kind of cell death designated “self-split cell death/autoschizis”. 1x10⁵ alveolar macrophages were seeded on 12 mm coverslips in 24-wells in 1 ml medium. Cells were exposed to vitamin combinations (VC:VK₃ ratio of 100:1) at their 90% cytotoxic doses (CD₉₀), which means 8313 μM: 8.313 μM for an hour. DMEM-treated cells served as the negative control. After an hour, the cells washed twice with phosphate-buffered saline (PBS). Cellular morphological changes were analyzed by light microscope after staining by Pappenheim, Mayer’s hemalum and IHC, respectively.

2.8. Viability tests

2.8.1. MTT colorimetric assay (4,5-dimethylthiazol-2-yl)-2,5-diphenyltetrazolium bromide

Cytotoxicity was assessed with a colorimetric assay:

- to investigate viability of tissues after incubation
- to determine 90% cytotoxic doses (CD₉₀) of vitamin combination for inducing “self-split” cell death on alveolar macrophages.

Tetrazolium bromide (Sigma, USA) was dissolved at a concentration of 5 mg/ml in RPMI-1640 without phenol red. The procedure itself was performed in the dark as MTT reagent is sensitive to light. Duration of incubation was 3-4 h for all samples. Fresh lung tissues served as positive controls (alive), tissues treated by 10% Triton X-100 [1 volume of 100% Triton X-100 + 9 volumes of acidified isopropanol (contains 1 μl concentrated hydrochloric acid per 1 ml isopropanol)] for overnight served as negative control. For preparation of negative controls for cells, the duration of 10% Triton X-100 treatment was 1 hour. Absorption was measured in a spectrophotometer plate reader at 550 nm (for cells), and at 570 nm (for tissues) (Nano Quant infinite M 2000, Tecan, Germany). To determine CD₉₀ of vitamin combination (VC:VK₃ ratio of 100:1), a wide range of dosages was explored from 125 μM to 40 mM in 18 different doses.

2.8.2. TUNEL assay (Terminal deoxynucleotidyl transferase dUTP nick end labeling)

For detection of cell death *in situ* evaluating viability of tissues after *ex vivo* short-term stimulation, the TUNEL assay was used, which has the capacity of detection and quantification of apoptosis at single cell level, based on labeling of DNA strand breaks. A

detailed protocol has been attached in **Table 10** in appendix-I. For counter staining and mounting Vectashield mounting medium with 4'-6-diamidino-2-phenylindole (DAPI) was used (Vector Laboratories, Burlingame, USA) and slides were covered with cover slips. The samples were kept at 4°C in dark environment until assessment. Fresh lung tissues served as positive controls (alive), tissues treated by DNase I served as negative control. Examination and capture of images were performed by a fluorescence microscope (Eclipse 80i, Nikon). Numbers of living and dead cells from the samples were analyzed by a cell counting function based on photometric pixel response of “Infinity analyze” software after adjustment of linear contrast.

2.9. Software

Following software was used:

- Thermo Software IQ (version 1.4.2) - NanoDrop 2000 Spectrophotometer
- 2100 Expert Software (version B.02.08.SI648) - Bioanalyzer
- Foto Fix (version 3.20), Image J (version 1.48b), Infinity analyze (version 6.0.02) – micrographs
- Magillen 6 (version 6.2)- MTT assay
- Graph Pad > Quick Calcs > Molarity Calculator [111]
- IBM SPSS (version 20.0.0) and Graph Pad Prism 6 (version 6.04) - Statistical analysis
- Creative Research Systems - Sample size calculator [112]
- INTAS GDS (version 3.29 18.12.2009)- Gel documentation system

2.10. Statistics

Totally 65 patients' samples were collected for our study. According to principles of statistics, firstly the sample size was determined, in which the goal is to choose the number of observations with sufficient statistical power. “Sample Size Calculator” from Creative Research Systems survey software was used for computation of sample size.

According to real terms, in our case sample size can be minimum number of 26, using for any empirical study. But we preferred a sample size of 30, which is even and would be easy to calculate for any statistical analysis. The following statistical tests were performed:

Descriptive statistics and test assumptions associated with data sets: Regarding to principles of statistics, data characteristic and test assumptions were determined prior to choice of inferential statistical tests. Herein:

- Tests for distribution:
 - Normality tests: Shapiro-Wilk's test: Kolmogorov–Smirnov's test and D'Agostino's K^2 test.

- Skewness and kurtosis: Z-value of skewness and kurtosis, which are determined by calculating the measures divided by their standard errors.
- Visual inspection of histograms, normal Q-Q plots, and outliers.
- Independence and measurement of scales: depending on data
- Homogeneity of variances: depending on distribution of variables parametric and non-parametric Levene's test for homogeneity of variances were used.
- Homoscedasticity: Scatter plots associated with linear regression of standardized variables, and outliers.

Inferential statistics associated with data sets: Usage of inferential statistics depended on the purpose of analysis and satisfaction of assumptions. As listed:

- Group comparison test:
 - Analysis of variance/ one way ANOVA
 - Nonparametric Mann–Whitney *U* test
 - Nonparametric Kruskal-Wallis test
 - Median test
 - Independent-samples T test
 - Factorial ANOVA
- Multiple comparison test/ Post Hoc test:
 - Tukey's HSD test
 - Nonparametric multiple comparison test
- Correlation and association:
 - Streamlined Pearson correlation matrix
 - Spearman's rank correlation
 - Chi square test
 - Cramér's V and Phi coefficient
- Regression
 - Linear regression
 - Nonlinear regression
- Multivariable analysis:
 - Correspondence analysis (Dr. Kurt Fellenberg; Division of Bioinformatics at the Research Center Borstel)
 - GeneSpring (Dr. Sebastian Marwitz; Division of Experimental and Clinical Pathology at the Research Center Borstel)

3. Results

The different mycobacterial species and their respective strains were abbreviated in the following manuscript as indicated here:

- *M. abscessus* 9547/00 (type strain) AB1
- *M. abscessus* 8562/11 (clinical isolate) AB2
- *M. avium* 3439/10 (clinical isolate) AV1
- *M. avium* 3725/07 (strain 104) AV2
- *M. tuberculosis* 1616/12 (clinical isolate) TB1
- *M. tuberculosis* 9679/00 (type strain) TB2

3.1. Establishment of the STST *ex vivo* model for mycobacteria

In order to establish the conditions for *ex vivo* mycobacterial infection in human lung tissues, the STST model was assessed by 2 main criteria: 1) viability of tissues, 2) infection of tissues. Each category comprises of 2-3 methods, which are illustrated in **Figure 3-1**.

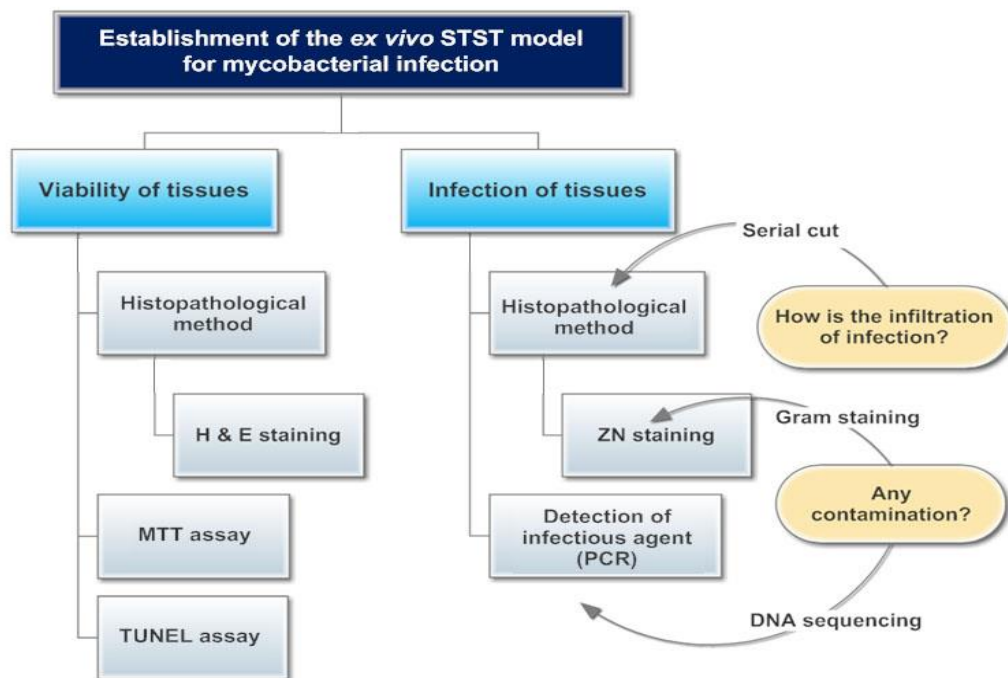


Figure 3-1. The overview of the establishment of the *ex vivo* STST model.

3.1.1. Viability of tissues

3.1.1.a. Histopathological overview

Throughout histopathological examination the morphology of mycobacteria-stimulated and unstimulated tissues were explored and compared to fresh lung tissues, without incubation. As a result, regarding microscopic anatomy of the lung, specimens had not noticeable differences among samples from all collected donors' material, except some

mechanical injuries of tissues caused by cutting process. A representative sample section from the *ex vivo* STST model is shown in **Figure 3-2**, in which terminal components of the lung containing intact interalveolar septum, clean lumen and visible nuclei of cells, indicating acceptable background structure after overnight incubation. Likewise, neither destructive changes (such as atelectasis, emphysema) nor inflammatory consolidation have been observed, indicating the applied gross morphologic criteria had satisfied.

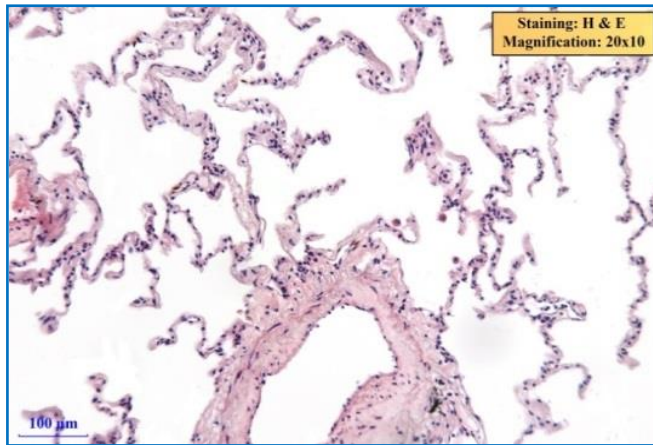
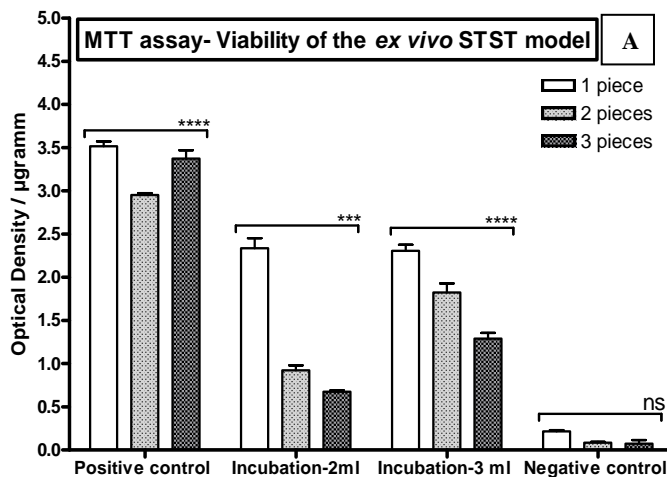


Figure 3-2. A representative mycobacteria-stimulated sample's image. Stain: H&E, Magnification: 200 fold

3.1.1.b. MTT colorimetric assay

In order to determine the viability of tissues after incubation, as well as the suitable amount of tissues and volume of culture medium, MTT assays were performed. Theoretically, NAD(P)H-dependent oxidoreductase from alive cells convert tetrazolium dye MTT to insoluble purple formazan reflecting the amount of viable cells present, and the formazan is quantified by measuring at optical density of 570 nm wavelength. Two kinds of culture volumes were used for the assay: 1) 2 ml medium per well, 2) 3 ml medium per well for overnight incubation without mycobacteria. The samples were compared with positive (preparations from fresh lung) and negative (tissues treated by Triton X-100) controls. Additionally, in each volume, either 1, 2, or 3 pieces of lung specimens were incubated in the wells and the results are depicted in **Figure 3-3**.



B		Descriptive Statistics of MTT assay		
		Absorbance of formazan		Average of weight (by piece)
		Mean	Std. Deviation	
1 piece	positive control	0.0963	±0.0011	27.4 milligram
	incubation-2ml	0.0640	±0.0032	
	incubation-3ml	0.0632	±0.0019	
	negative control	0.0059	±0.0004	
2 pieces	positive control	0.1983	±0.0011	67.2 milligram
	incubation-2ml	0.0620	±0.0039	
	incubation-3ml	0.1226	±0.0071	
	negative control	0.0058	±0.0006	
3 pieces	positive control	0.3540	±0.0071	104.9 milligram
	incubation-2ml	0.0708	±0.0016	
	incubation-3ml	0.1354	±0.0068	
	negative control	0.0078	±0.0043	

Figure 3-3. Influence of culture conditions on tissue viability. In the graph (A), the ratios of measurements of optical density (formazan quantified by measuring at 570 nm wavelength) and tissue weights (μ gramm) are on Y axis. The 4 groups, having 1 (white bar), 2 (light grey bar with pattern) or 3 (dark grey bar with strong pattern) pieces of tissue dissections in each group are located on X axis. Table (B) shows absorbances of formazans in each group with average weights of pieces (N=15 in each group). The statistics of group comparison (one-way ANOVA analysis), within each condition related to the different numbers of tissues in the wells have been applied on the graph. ***= $p \leq 0.001$, **** $p \leq 0.0001$, ns= not significant.

The graph (**Figure 3-3.A**) summarizes that viabilities of all incubated samples intervened between positive and negative controls, and tissue viabilities decreased with increased numbers of lung pieces per well. As particularly, in positive controls the ratio of optical density and weights were 3.52 ± 0.06 (1 piece), 2.95 ± 0.02 (2 pieces), 3.37 ± 0.1 (3 pieces), while the ratios were in negative controls 0.22 ± 0.01 (1 piece), 0.09 ± 0.01 (2 pieces), 0.07 ± 0.04 (3 pieces). The estimations of observed tissues' viability with regards to amount of tissue-input and incubation was between positive and negative controls' values. In particular, the samples incubated in 2 ml containing 1 piece ranged between 2.34 ± 0.12 , the range of variables of 2 pieces was ranged between 0.92 ± 0.06 , variables of 3 pieces were between 0.67 ± 0.02 . For samples incubated in 3 ml medium, the ratios were 2.31 ± 0.07 (1 piece), 1.82 ± 0.11 (2 pieces), 1.29 ± 0.06 (3 pieces), indicating overnight incubation was matchable for tissue viability.

Although, as compared together decreases of tissue viabilities to positive control after incubation, the decreases of viability using 1 piece per well did not differ in 2 or 3 ml medium and were 33.52 % and 34.38%, respectively, of the positive control. By contrast, using 2 or even 3 pieces of lung specimens per well, the viability was further decreased dependent on the volume per well. Estimated reductions of viability for 2 pieces of lung were 68.81% (in 2ml) and 38.31% (in 3ml). For 3 pieces per well, reductions of viability were 80.12% (in 2 ml) and 61.72% (in 3ml) of the positive control, respectively, in the respective medium conditions. Therefore, 1 piece tissues (~30 milligram) were optimal for *ex vivo* STST model either in 2 ml or 3 ml.

Inferential statistics associated with MTT assay

Summary of test assumptions and data characteristic:

[all detailed performances have attached in appendix II (3.1.1.b. Results of MTT assay)]

- **Distribution:** *In terms of Shapiro-Wilk ($p > 0.05$) and Kolmogorov-Smirnov test ($p > 0.05$), regarding skewness and kurtosis (skew $< |2|$, kurtosis $< |9|$, Z values were between ± 1.96 in all variables), we can assume that all variables in data set of MTT assay for tissue viability are approximately normally distributed.*
- **Equality of variance:** *all variables of Levene's F tests were in the positive control $F(2,15)=1.775$, $p=0.211$, in the negative control $F(2,15)=5.240$, $p=0.073$, for samples incubated in 2ml $F(2,15)=0.431$, $p=0.660$, for samples incubated in 3 ml $F(2,15)=1.573$, $p=0.247$, which indicates that the data set has equal variances.*

1. To test the hypothesis whether there are any statistical significant differences within every group associated with numbers of pieces, a group comparison test was performed (**Table 3-1**).

Table 3-1. One way ANOVA associated MTT assay for tissue viability

		ANOVA				
		Sum of Squares	df	Mean Square	F	Sig.
positive control	Between Groups	.168	2	.084	4826.654	.000
	Within Groups	.000	12	.000		
	Total	.169	14			
negative control	Between Groups	.000	2	.000	.980	.403
	Within Groups	.000	12	.000		
	Total	.000	14			
incubation-2ml	Between Groups	.000	2	.000	11.122	.002
	Within Groups	.000	12	.000		
	Total	.000	14			
incubation-3ml	Between Groups	.015	2	.007	221.960	.000
	Within Groups	.000	12	.000		
	Total	.015	14			

Analysis of variance showed that:

- There is a significant difference between 3 groups of the positive control depending on numbers of pieces, $F(2,12)=4826.654$, $p<0.0001$,
- There is no significant difference dependent on the numbers of pieces in the negative control, $F(2,12)=0.980$, $p=0.403$, showing quality of negative control was good due to effect of Triton X-100.
- There is a significant difference between 3 groups of samples dependent on the numbers of tissues when incubated in 2 ml medium per well, $F(2,12)=11.112$, $p=0.002$,
- There is a significant difference between 3 groups of samples incubated in 3 ml depending on number of piece, $F(2,12)=221.9604$, $p<0.0001$.

2. Once, significant differences of viability depending on numbers of pieces, in order to evaluate the strength of correlations, a streamlined correlation matrix was calculated (Table 3-2):

Table 3-2. Streamline correlation matrix associated MTT assay for tissue viability

		Correlations			
		positive control	negative control	incubation-2ml	incubation-3ml
pieces	Pearson Correlation	.992**	.313	.594*	.925**
	Sig. (2-tailed)	.000	.256	.020	.000
	N	15	15	15	15

** . Correlation is significant at the 0.01 level (2-tailed).

* . Correlation is significant at the 0.05 level (2-tailed).

- The variables in the positive control were strongly correlated, $r(15)=0.992$, $p<0.0001$,
- The variables of the negative control were not correlated, $r(15)=0.313$, $p=0.256$,
- The variables of samples incubated in 2 ml were moderately correlated, $r(15)=0.594$, $p=0.02$,

- The variables of samples incubated in 3 ml were strongly correlated, $r(15)=0.925$, $p<0.0001$.

3. In addition, to test the hypothesis whether there are any statistical significant differences between groups associated with number of piece, Tukey HSD's multiple comparison test was performed. There were no significant differences only between 1 piece samples in 2ml and 3ml, $p=0.917$. All other groups' comparisons showed significant differences, thus it can be concluded that positive and negative control's qualities were reliable, and that the tissue viability for 2 and 3 pieces was highly dependent on the amount of used medium per well.

3.1.1.c. TUNEL assay

Besides metabolic activity, the viability of tissues after incubation was furthermore assessed by detection of DNA double-strand breaks via TUNEL assay. In **Figure 3-4** fluorescence images of a representative *ex vivo* stimulated tissue sample has been depicted comparing with positive (untreated lung specimen) and negative controls (DNase I treated lung specimen).

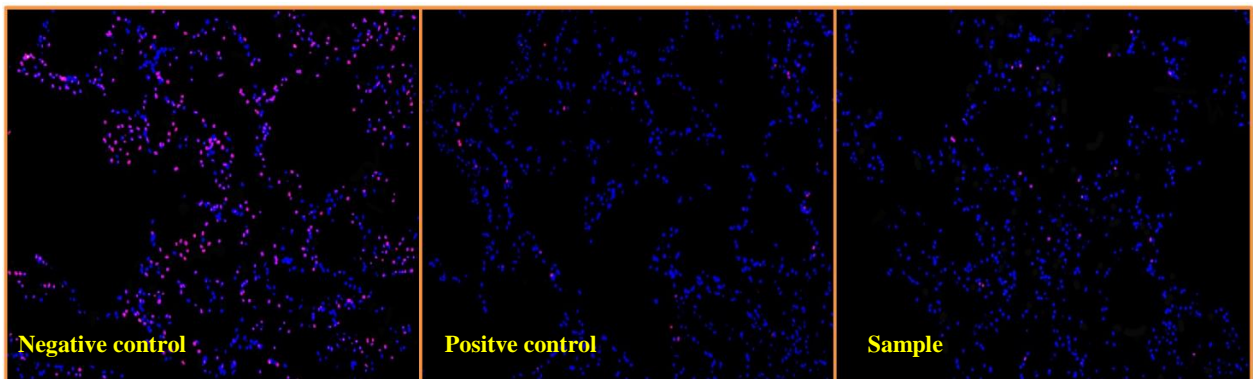


Figure 3-4. No increase of DNA-double strand breaks upon tissue culture. Fluorescence photographs of TUNEL assay of lung tissues, including positive control (preparation of fresh lung), negative control (treated by DNase I) and sample (a representative sample of the *ex vivo* STST model, which was incubated overnight with and without mycobacteria). Living cells are indicated by DAPI-staining in blue, while cells with DNA double-strand breaks were positive for TRITC (red). Images were acquired at $\times 100$ magnification (N=79).

According to structural features of the lung, in a single microscopic field of view at $\times 100$ magnification, the numbers of all cells' nuclei ranged from 155 to 730 (404.62 ± 140.15) and the areas of all cells' nuclei ranged from 13.47 to 14.97 mm^2 (58.95 ± 32.65) as ascribed all groups.

In the positive controls, numbers of living cells' nuclei ranged between 169-552, having an area of 17.64-12.04 mm^2 , whereas the number of observed dead cells' nuclei ranged between 2-39 in an area of 0.07-4.16 mm^2 . In contrast, the negative controls displayed a range of living cells between 280-552 in an area of 37.75-105.6 mm^2 , and a range of observed dead cell between 111-311 in 9.68-28.69 mm^2 of area. The investigated

samples displayed a range of 166-678 living cells in 13.28-131.5 mm² of area with dead 1-111 cells in 0.04-8.95 mm² area. Comparisons of counting analysis of TUNEL assay in these 3 groups were depicted in **Figure 3-5** with the way of measurements.

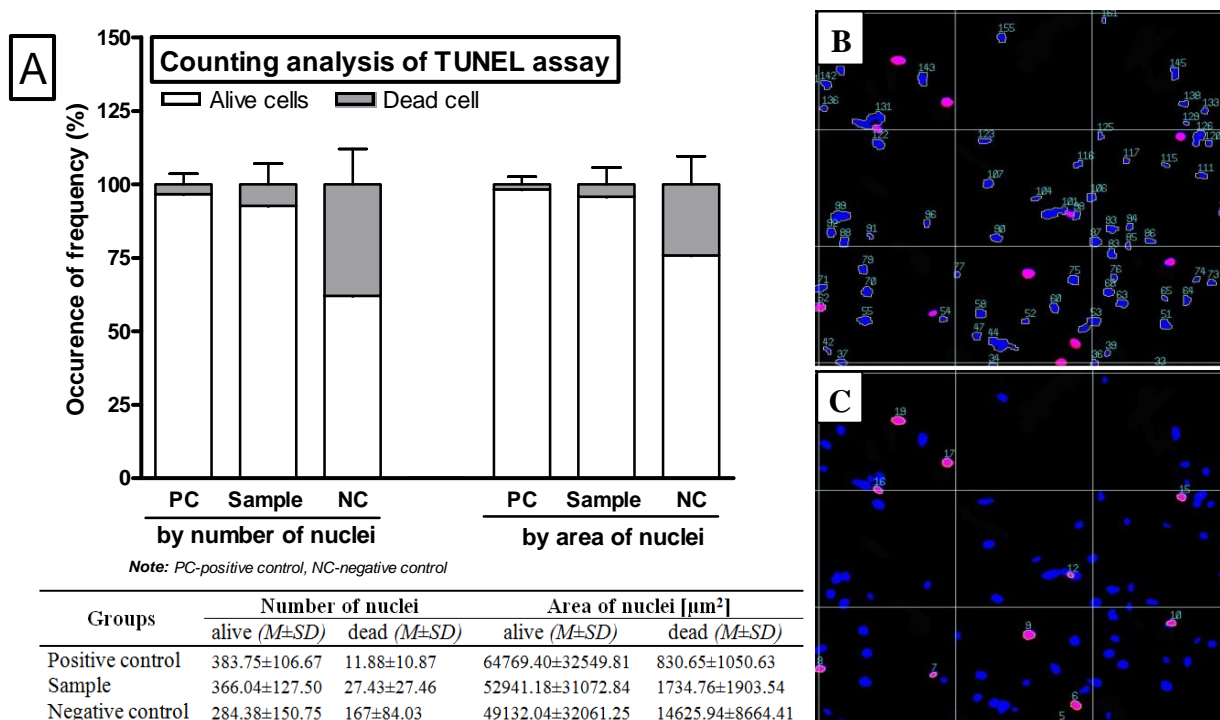


Figure 3-5. Influence of the *ex vivo* culture on tissue viability. **A.** Graph and table of counting analysis of TUNEL assay. The graph is created by percentage of alive and dead cells' nuclei in each group for areas and numbers. The table contains the variables of number and area of alive and dead cells' nuclei, respectively. Note: PC-positive control, NC-negative control. **B and C.** The samples were analyzed by cell counting function based on photometric pixel response of "Infinity analyze" software after adjustment of linear contrast. Then numbers and areas of alive and dead cells' nuclei were obtained, respectively. B. Alive cells' nuclei, C. Dead cells' nuclei.

As recount from the figure (**Figure 3-5**), 96.64 \pm 3.65% of cells in the positive controls were alive compared to 62.09 \pm 11.95% in negative control. The *ex vivo* STST samples had 92.85 \pm 6.99% of alive cells in total cells, while 7.15% were apoptotic as demonstrated by positive staining for TRITC and hence, presumably dead.

Furthermore, the area per nucleus of living cells was 162.06 unit, compared to 73.41 unit in dead cells, indicating nuclear shrinkage, which was calculated by mean nuclei numbers and mean nuclei areas.

3.1.2. Infection of tissues

3.1.2.a. CFU determination of suspensions

In order to determine suitable concentrations of viable mycobacteria for *ex vivo* infection model, in a first approach, some tissues were incubated with different concentrations of mycobacterial suspensions (10^4 - 10^7 CFU/ml). As a result, the concentration of 10^7 CFU/ml induced highest number of infected cells, therefore this dose was used for all further experiments.

3.1.2.b. Histopathological overview

In order to detect mycobacterial infection and other bacterial contaminations, all infected samples were stained with ZN and gram stainings in parallel. As a consequence, all cases of ZN staining were positive and all gram-stainings were negative. Photomicrographs of representative lung specimens are depicted in **Figure 3-6**.

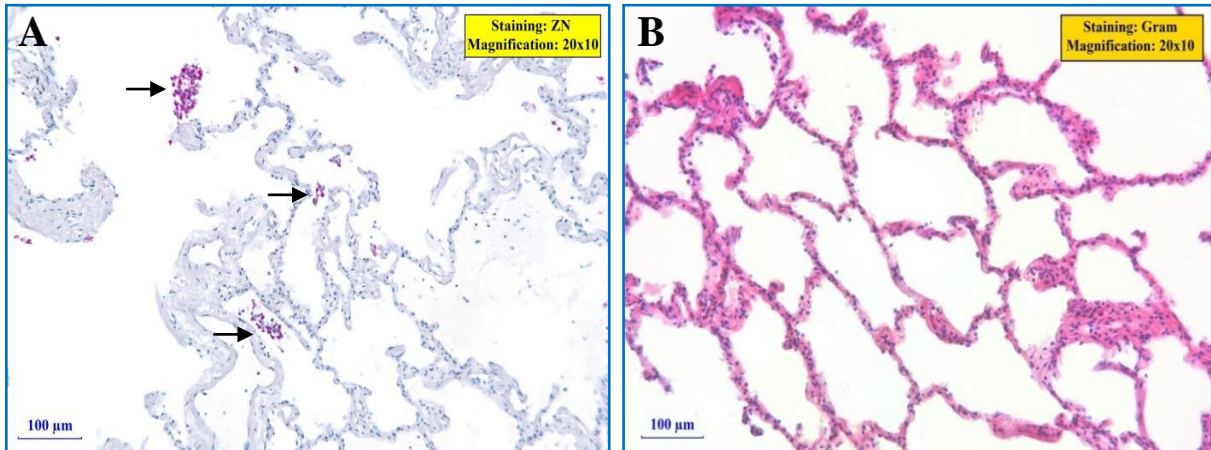


Figure 3-6. Successful mycobacterial infection using the *ex vivo* STST model. **A.** Photomicrograph of lung tissue from *ex vivo* STST model. The image shows the presence of numerous acid-fast bacilli (arrows) visualized by Ziehl-Neelsen staining in pink color **B.** Gram staining of *ex vivo* lung tissue, no gram positive microorganism could be detected. Images were acquired at $\times 200$ magnification, bar = $100\mu\text{m}$.

Once the *ex vivo* model of mycobacterial infection was established successfully, we encountered an interesting question: Since the mycobacteria are non-motile, how deep could the infection infiltrate into the tissues? To address this question, serial sections from one whole paraffin block were done with a thickness of $2\ \mu\text{m}$. In **Figure 3-7.A**, the block infected by *M. tuberculosis* is exemplified.

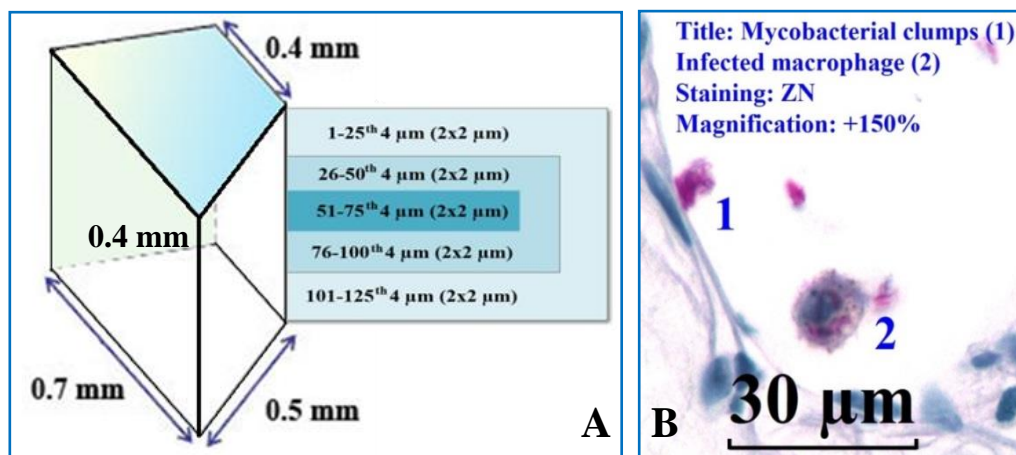


Figure 3-7.A. Observation of serial sections of the whole block. Its 3D trapezoid size was approximately $0.7 \times 0.5 \times 0.4 \times 0.4$ mm, the serial cuts of the whole block produced around 125 pieces of $4\ \mu\text{m}$ sized-pairs; Note that, because of technical handling few cuttings have been lost. **B.** Photomicrograph of intra- and extra-cellular mycobacteria, mycobacterial clumps (1), infected macrophage (2), the images was acquired at $\times 400$ magnification, zoomed in 150%, bar = $30\mu\text{m}$.

As illustrated **Figure 3-7.A**, the 1-25th and 101-125th sections were considered to be identical (same peripheral condition) as well as the 26-50th and 76-100th sections (same

para-peripheral condition). Thus, all infected cells on 1-25th (peripheral 25 slides) and 51-75th (central 25 slides) slides were counted. The 1-25th slides were associated with a number of infected cells 47.87 ± 38.9 . On the contrary, 51-75th slides were associated numerically more numbers of infected cells 126.92 ± 59.47 . A visual comparison of the result with statistics can be seen in **Figure 3-8** and more detailed statistical analysis has been attached in appendix-II. 3.1.2. b. Histopathological overview.

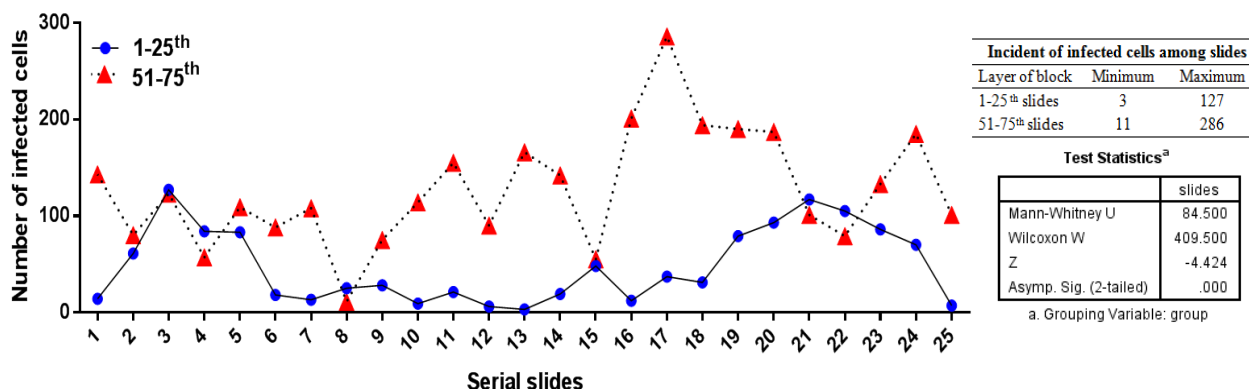


Figure 3-8. Distribution of infected cells according to depth of tissue with associated statistics. The numbers of infected cells in peripheral (N=25) and central (N=25) serial sections of a single paraffin block integrated in the graph and the 2 groups are indicated by the blue and red symbol. On the right side, (upper table) the ranges of infected cells are given. Statistical results of nonparametric tests are summarized in the table below.

Inferential statistics associated with histopathology

Summary of test assumptions and data characteristic:

[More detailed performances have attached in appendix II (3.1.2.b. Histopathological overview)]

- **Distribution:** Variables' distribution of central slides were sufficiently normal for the purpose of conducting a mean comparison test, in terms of Shapiro-Wilk ($p=0.011$) and Kolmogorov-Smirnov test ($p=0.024$), also regarding skewness and kurtosis ($skew < |2|$, $kurtosis < |9|$, Z values were between ± 1.96). Whereas distribution of peripheral slides 'variables were not normally distributed, in terms of Shapiro-Wilk ($p=0.2$) and Kolmogorov-Smirnov test ($p=0.57$), and were also negative kurtotic.
- **Equality of variance:** An assumption of homogeneity of variances was verified via nonparametric Levene's test, $F(1.48)=0.044$, $p=0.835$.

To test the hypothesis that the peripheral and central slides in block were associated with statistically significantly different mean numbers of infected cells, a Mann-Whitney test was performed. The nonparametric test indicated that the mean rank of infected cells on the peripheral ($Mrank=16.38$) is significantly lower than the rank mean of infected cells on the central slides ($Mrank=34.62$), $U=84.5$, Z value= -4.424 , $p<0.0001$ (**Figure 3-8**).

While detecting mycobacteria in all cases, some micro clumps have been found (**Figure 3-7.B**) though, which did not interrupt successful infection of the *ex vivo* STST model systematically.

3.1.2.c. Detection of mycobacterial DNA in the *ex vivo* infected tissues

To further verify the successful infection of human tissues by mycobacteria, DNA of 26 randomly chosen patients' material has been used for the detection of mycobacterial

DNA by PCR. **Figure 3-9** shows exemplary results of PCR. No mycobacterial DNA could be detected in the medium control. Amplification of DNA-sequences from mycobacterial species, including clinical isolates and type strains of each *M. abscessus*, *M. avium* and *M. tuberculosis* are shown in bands 2-7 as indicated. From every strains, specific sequences were detectable in the *ex vivo* infected patient tissues and their fragments of mycobacterial species had presence of bands can be seen in Figure 3-9. Purity and specificity of PCR reactions were assessed by extraction control in lane 8, negative control in lane 9 and a positive control in lane 10.

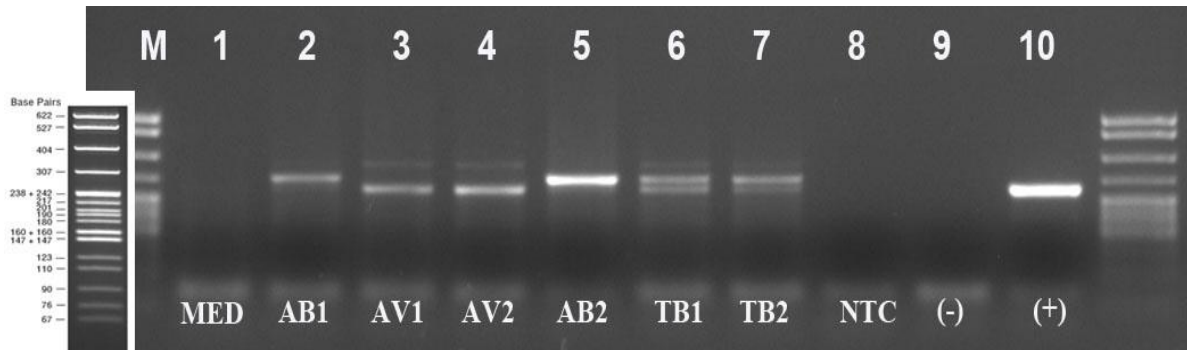


Figure 3-9. Mycobacterial DNA can be detected in infected *ex vivo* human tissue samples. Image of EtBr-stained agarose gel from electrophoretic separation of PCR products. Amplification of mycobacterial sequences from DNA of human tissues was done with genus primer. Med= medium control tissue, AB1= *M. abscessus* (type strain), AV1= *M. avium* (clinical isolate), AV2= *M. avium* (strain 104), AB2= *M. abscessus* (clinical isolate), TB1= *M. tuberculosis* (clinical isolate), TB2= *M. tuberculosis* (type strain), NTC= no-template control, (-)= negative control, (+)= positive control (*M. szulgai*), M= Molecular weight marker (*pBR322 DNA-MspI*).

In order to detect the amount of mycobacterial DNAs and specificities, total DNAs were purified from randomly chosen *ex vivo* STST samples, then both real time PCR and sequencing were performed. The results can be seen in **Figure 3-10. A and B.**

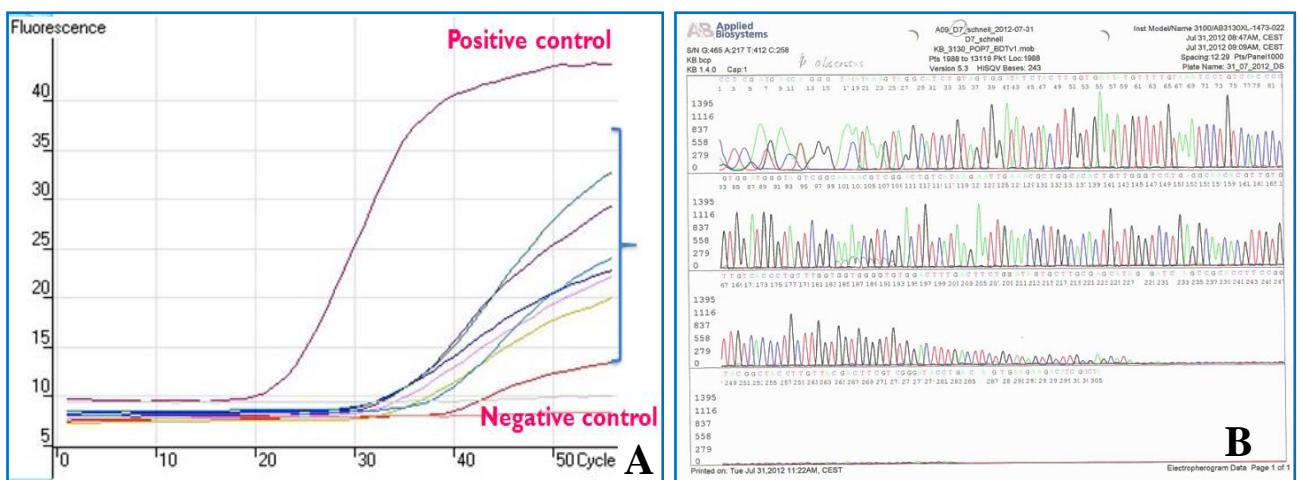


Figure 3-10. A. A plot of RT-PCR reaction of mycobacterial DNA isolated from *ex vivo* infected lung tissues. X-axis: cycle number, y-axis: amount of DNA measured by fluorescence. The PCR-curves for the negative and positive controls are indicated. **B.** A chromatograph of DNA sequencing of *M. abscessus*, isolated from a single *ex vivo* infected lung specimen. The peaks had been color-coded to correspond to each base pair-A (green), C (blue), G (black) and T (red). The nucleotide positions in the sequence are indicated above the corresponding peaks.

Figure 3-10.A shows that all 7 samples of *ex vivo* infected lung tissues exhibit a variable amount of specific mycobacterial DNA that is considerably lower than in the positive control (the highest amplitude) but certainly higher than in the negative control (lowest amplitude). **Figure 3-10.B** demonstrates the specificity of the DNA for *M. abscessus* that has been isolated from a single infected lung tissue sample, according to internal transcribed spacer (ITS) in the genetic material of *M. abscessus*. Furthermore, one can see the good quality of chromatogram's features, including distinguishable peaks with even spacing, consistent shoulder width, low background signal underneath the peak, and relatively even signal intensity throughout the run.

3.2. Findings using the *ex vivo* STST model

The results of the *ex vivo* lung tissue model of mycobacterial infection can be divided into 3 main aspects 1) different infected cell types 2) change of cellular morphology 3) gene analysis, which are illustrated in **Figure 3-11** with their relationships.

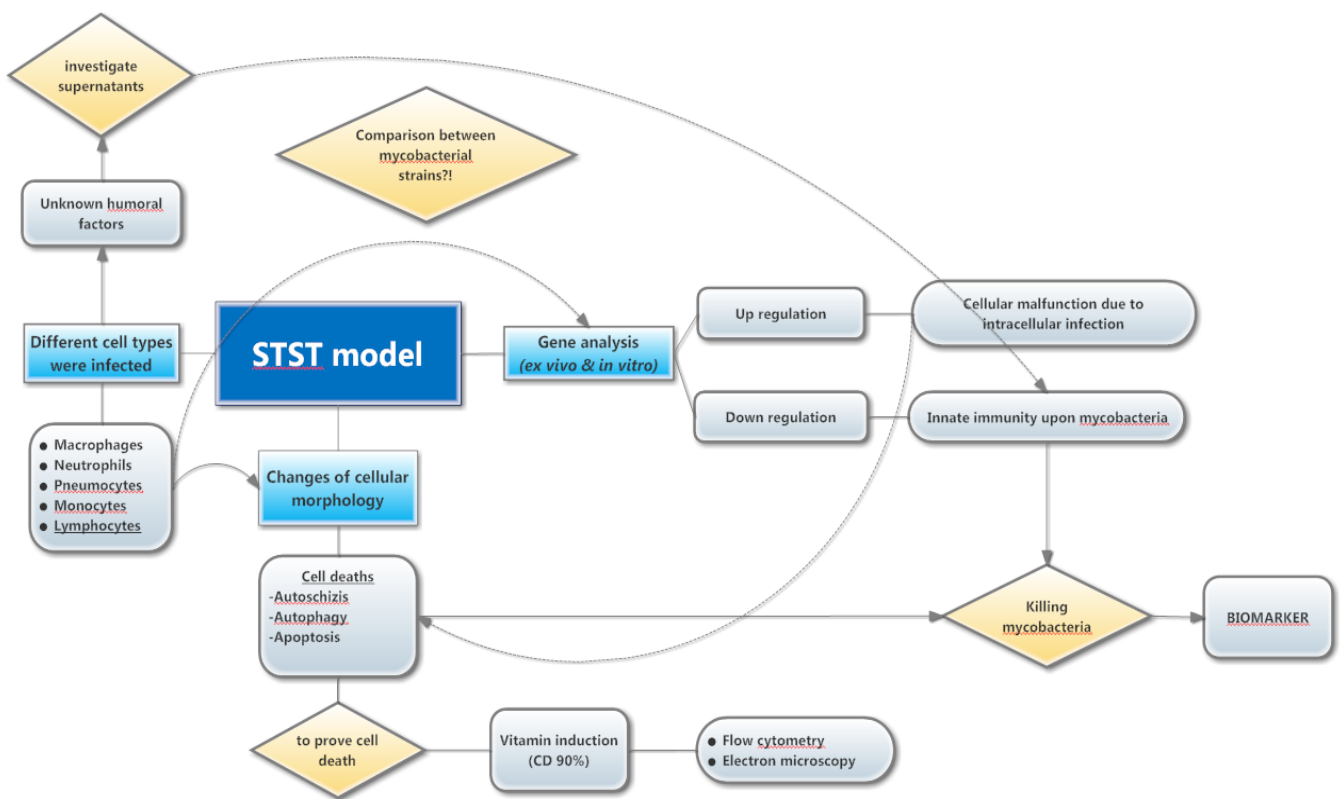


Figure 3-11. Overview of findings from *ex vivo* STST model and their relationship.

3.2.1. Infected cell types

During observations of slides with high magnification (400 fold), different infected cell types were detected (**Figure 3-12. A, B**), including macrophages, neutrophils, monocytes, lymphocytes and pneumocytes-II/alveolar type II cells.

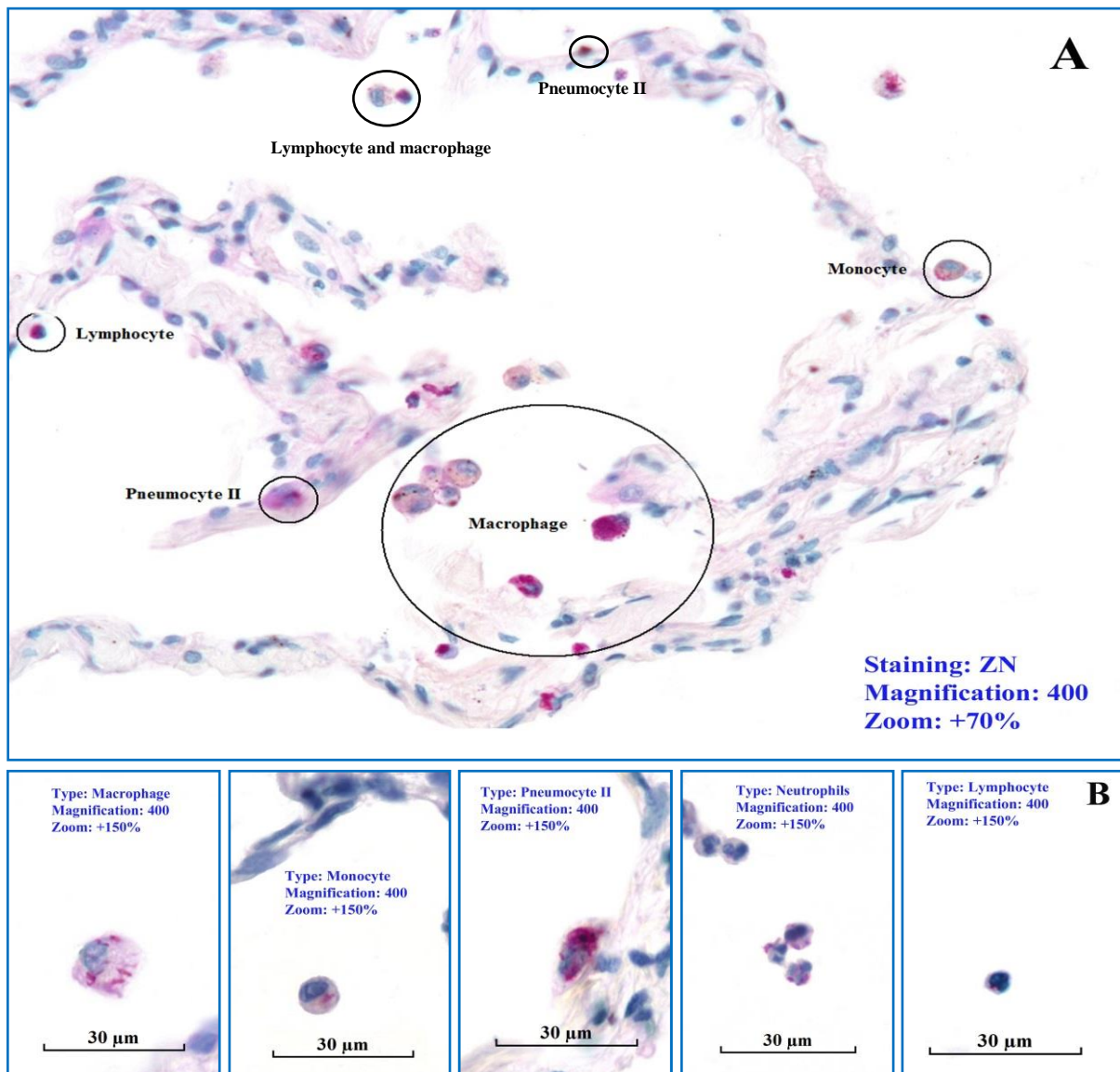


Figure 3-12. Mycobacteria invaded different cell types in the *ex vivo* human lung tissues **A**. Infected cell with labels, at $\times 400$ magnifications, zoomed in 70%; intracellular bacilli were visualized by Ziehl-Neelsen stain in pink color. **B**. Infected cell types were shown separately with labels, the images were acquired at $\times 400$ magnification, zoomed in 150%, bar =30 μ m.

In order to characterize the infected cell types, 30 infected cells were counted from each slide among 2 diagonal lines due to include the whole tissue equivalently (**Figure 3-13.B**). On the following graph, the frequency of occurrence of infected cell types in each strain is shown (**Figure 3-13.A**) and from this graph has yielded following results. Among 6 mycobacterial strains, overall incidences of infected neutrophils ranged from 24 to 55 (4.69%) in 900 cells. Infected pneumocytes-II exhibited a range of infection between 14-59 (3.54%), whereas lymphocytes ranged between 83-119 (11.07%). Monocytes were rarely infected [with a range of 49-75 (6.44%)], while macrophages were the most frequently infected cells with 645-709 (74.26%) in a total of 900 cells. This observation prompted us to do more specific statistical tests to determine each type of infected cell, which was associated with statistically significant difference among mycobacterial strains.

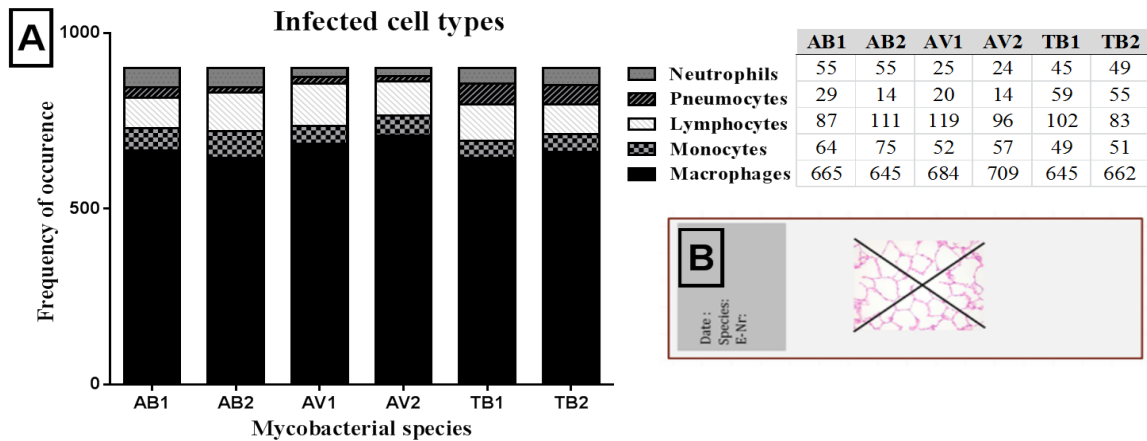


Figure 3-13. Cellular populations infected by 6 mycobacterial strains. **A.** Graph and table of occurrence of infected cell types induced by 6 different strains of mycobacteria for 30 randomly chosen human lung tissues. **B.** 30 infected cells were counted among 2 diagonal lines in each slide, in order to involve whole tissue equivalently (including central and peripheral parts of the slides) as illustrated. Sometimes 4 sectors or additional slides were needed to check, when there were not enough infected cells.

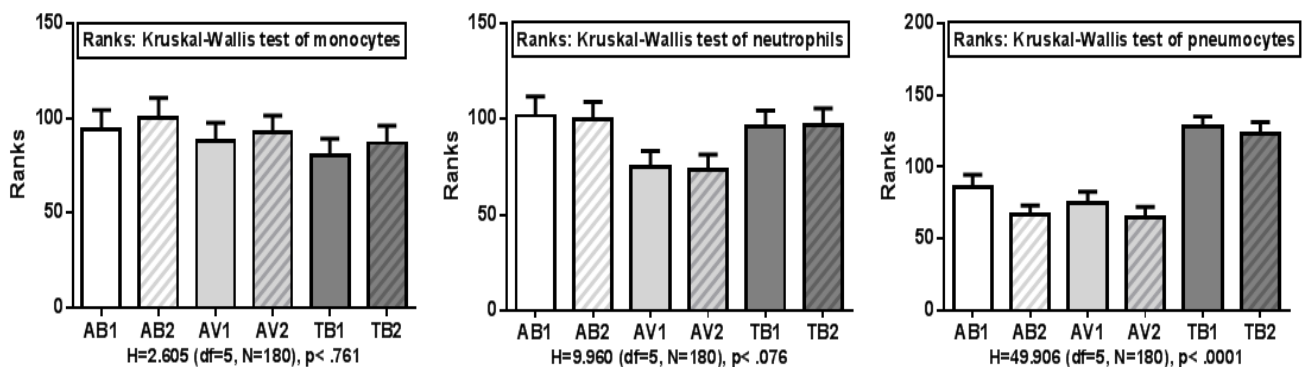
Inferential statistics associated with infected cell types

Summary of test assumption and data characteristic:

[More detailed performances have been attached in appendix II (3.2.1. Infected cell types)]

- **Distribution:** In terms of Shapiro-Wilk and Kolmogorov-Smirnov test, skewness and kurtosis, visual inspections of the histograms showed that all data sets were far from being normally distributed, having some outliers, and some variables' distribution were skewed and kurtotic.
- **Equality of variance:** nonparametric Levene's F tests, were in monocytes $F(5,180)=1.108$, $p=0.358$, in macrophages $F(5,180)=1.177$, $p=0.322$, in pneumocytes $F(5,180)=1.397$, $p=0.228$, in neutrophils $F(5,180)=1.380$, $p=0.234$, in lymphocytes $F(5,180)=0.763$, $p=0.577$, which indicated that all variables have equal variances. Therefore, for group comparison, a nonparametric Kruskal-Wallis test was selected based on assumptions' satisfaction and group numbers.

1) In order to test the hypothesis that each type of infected cell was associated with statistically significant differences among mycobacterial strains, the Kruskal-Wallis tests have been performed via 2 alternatives: 1) comparisons in 6 locations [each strain, including AB1, AB2, AV1, AV2, TB1, TB2, form a single group], 2) comparisons in 3 locations [the 2 strains of same strains form 1 group AB1+AB2, AV1+AV2, TB1+TB2]. The only results of 6 locations were illustrated in **Figure 3-14** with statistical reports which is more detailed than 3 locations. Likewise, almost all tests of 3 and 6 locations showed the same outcome, except for neutrophils. Therefore, 3 location-test of neutrophils was included in **Figure 3-14** (lower panel, most right graph).



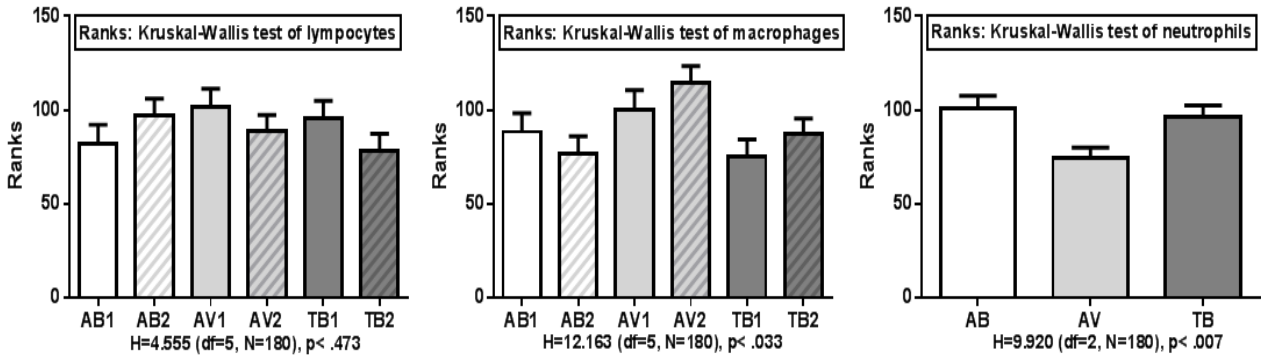
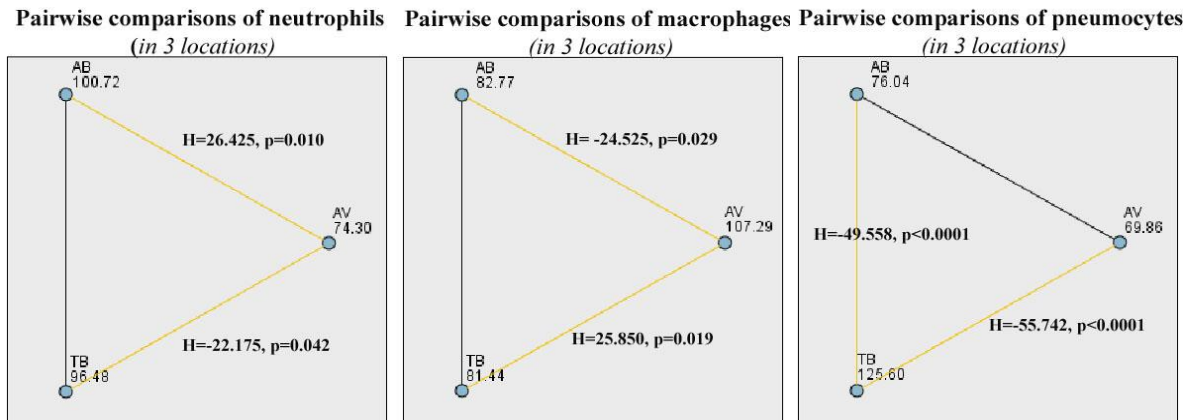


Figure 3-14. Comparisons of each cell type separately among mycobacterial strains

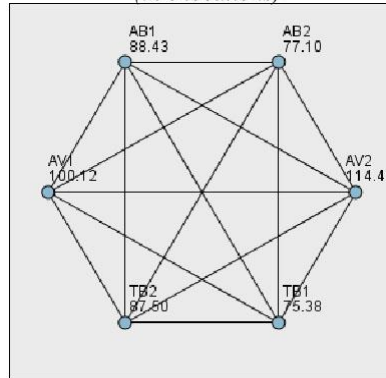
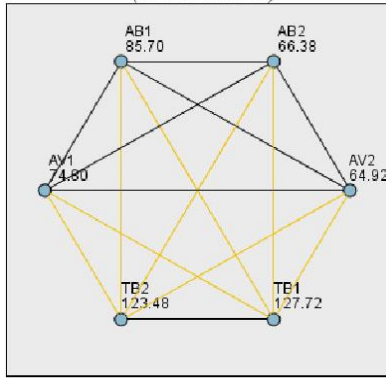
As can be seen in **Figure 3-14**, the Kruskal-Wallis tests showed that:

- Groups having a significant difference in mean rank:
 - Pneumocytes, either in 6 or 3 location tests, H=49.906 (df=5, N=180), p<0.0001 and H=46.847 (df=2, N=180), p<0.0001,
 - Macrophages, either in 6 or 3 location tests, H=12.163 (df=5, N=180), p=0.033 and H=9.474 (df=2, N=180), p=0.009,
 - Neutrophils, in 3 locations, H=9.920 (df=2, N=180), p=0.007.
- All other cell types did not reveal any significant differences between the rank means. Herein:
 - Lymphocytes, either in 6 or 3 location tests, H=4.555 (df=5, N=180), p=0.473 and, H=0.764 (df=2, N=180), p=0.683,
 - Monocytes, either in 6 or 3 location tests, H=2.605 (df=5, N=180), p=0.761 and, H=2.085 (df=2, N=180), p=0.353,
 - Neutrophils in 6 locations, H=9.960 (df=5, N=180), p=0.076.

2) A specific comparing test (post hoc) was proceeded to explore exactly which groups are different. The comparisons are summarized in **Figure 3-15** via yellow and black lines with statistical reports. Briefly, a pairwise comparison revealed significant differences of infection events in neutrophils between AV and AB (p=0.01), as well as between AV and TB (p=0.042). In cases of macrophages, the significant differences existed in between AV and AB (p=0.029), in between AV and TB (p=0.019). A pairwise comparisons of mean ranks of pneumocytes-II showed that there was a significant difference between TB and AB (p<0.0001), and a significant difference between TB and AV (p<0.0001).



Pairwise comparisons of pneumocytes (in 6 locations) **Pairwise comparisons of macrophages** (in 6 locations)



Pairwise comparisons of pneumocytes	
Species	Test statistics & significance
AB2-TB1	H= -61.333, p<0.0001
AB2-TB2	H= -57.100, p<0.0001
AV1-TB1	H= -52.917, p<0.0001
AV2-TB1	H= -62.800, p<0.0001
AV1-TB2	H= -48.683, p=0.002
AV2-TB2	H= -58.567, p<0.0001
AB1-TB1	H= -42.017, p=0.013
AB1-TB2	H= -42.017, p=0.042

Pairwise comparisons of macrophages	
Species	Test statistics & significance
AV2-TB1	H=39.083, p=0.003
AB2-AV2	H= -37.367, p=0.005
TB2-AV2	H=26.967, p=0.044
AB1-AV2	H= -26.033, p=0.052

Figure 3-15. *Ex vivo* infected human lung tissues reveal significant differences of infected cell types regards to mycobacterial strains. Nonparametric specific comparing tests (post hoc) for neutrophils, macrophages and pneumocytes among mycobacterial strains in 3 and 6 locations. On the graphs each blue node shows the mean ranks of variables with name of strains. Black line indicates no significant difference and yellow line indicates significant difference between variables. In 3 location tests, the test statistics reported beside of the yellow lines, while test statistic of 6 location tests reported in the table separately.

3) Since the tissue samples originated from different donors with different genetical and pathological backgrounds, the possible influence on the infection events was assessed by Kruskal-Wallis test (**Table 3-3**) with the hypothesis that there are no significant difference between 30 patients in each mycobacterial strains.

Table 3-3. Kruskal-Wallis Test for patient’s comparisons among all mycobacterial strains

Test Statistics ^{a,b}						
	AB1	AB2	AV1	AV2	TB1	TB2
Chi-Square	5.816	4.371	6.256	4.716	3.439	2.243
df	29	29	29	29	29	29
Asymp. Sig.	1.000	1.000	1.000	1.000	1.000	1.000

a. Kruskal Wallis Test

b. Grouping Variable: Patient ID

The tests showed that, mean rank of AB1 ranged from 99.63 to 140.31, test statistics was H=5.816 (df=29, N=240), p=1, mean rank of AB2 ranged between 107.06-143.38, the test statistics was H=4.371 (df=29, N=240), p=1, for AV1 range was 91.75-135.44, H=6.256 (df=29, N=240), p=1, for TB1 range was 101.88-134.44, H=3.439 (df=29, N=240), p=1, the mean rank of TB2 ranged from 101 to 130.94, the test statistics was H=2.243 (df=29, N=240), p=1.

Conclusion: There were no statistically significant differences among the infected cell types in all 30 patients analyzed, regardless of which mycobacterial strains was applied.

Since there were some significant differences regarding the types of cells infected by the different mycobacterial strains, it was worthwhile to identify which cell type might be more susceptible to a particular mycobacterial strain. Thus, a simple correspondence analysis, which is a statistical visualization method for picturing the associations between cell types versus mycobacterial strains (a two-way contingency table), was performed with

Dr. Kurt Fellenberg (Division of Bioinformatics at the Research Center Borstel) and the results of the analysis are summarized in **Figure 3-16**.

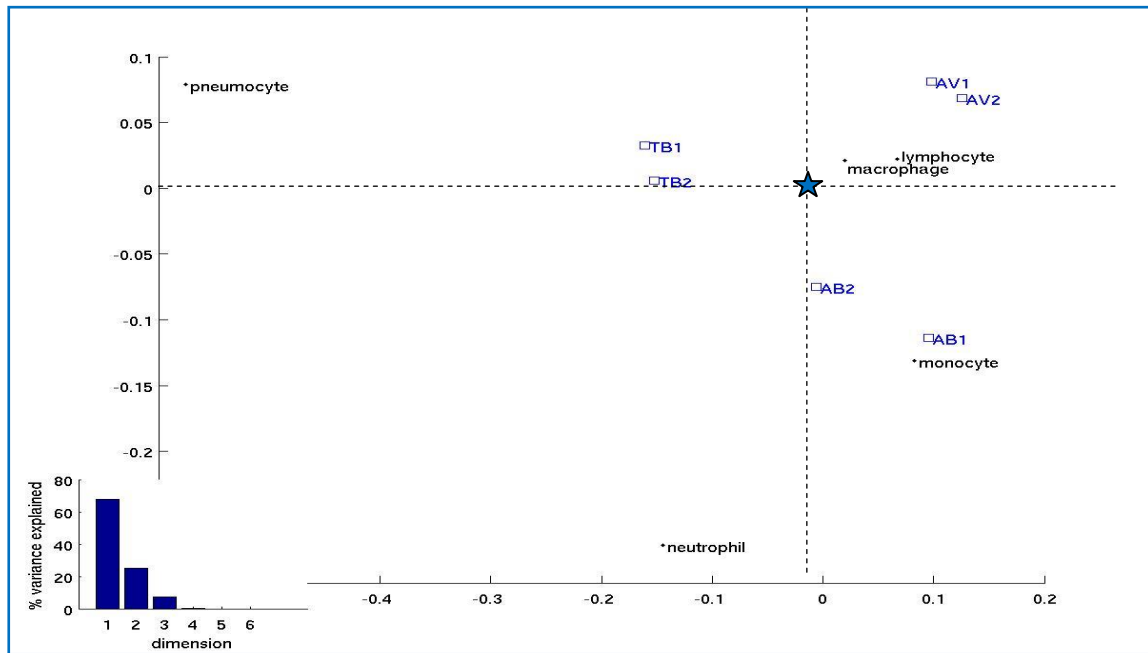


Figure 3-16. Correspondence analysis map for mycobacterial strains and cell types. Dispersions of all profile points (sets of relative frequencies) produced an asymmetric map. The centroid was labeled by a star, which is the point of no correlation. Around the centroid, the profile points of the various mycobacterial species (blue square) and of the different cell types (black dot) were plotted. A barplot of variances is shown at the left bottom part of the map. The Y and X axis are showing values of corresponding correlation coefficients.

The map of profile points was derived from two-crosstabulation: 1) cell types, which consists of 5 elements, including neutrophils, monocytes, macrophages, lymphocytes, pneumocytes-II and 2) mycobacterial strains, which has 6 elements, including AB1, AB2, AV1, AV2, TB1, TB2. Dispersions of all profile points produced an asymmetric map, since their weighted average (centroid) is not in the center of all unit points.

The profile points of all mycobacterial strains lie around the centroid-indicating no correlation. Likewise, the strains are plotted near to each other and indicate commonalities of the strains. Regarding positions of profile points associated with infected cell types: the points of macrophages and lymphocytes were clustered near to the centroid within the region of all strains, showing no special association with any strains. Thus, infection of these two cell types by 3 strains of mycobacteria was the same. By contrast, the point unit of the pneumocytes coordinated located far from centroid in the quadrant of TB1, TB2, indicating that the infection of this cell type was closely associated with these strains. In addition, the point units of neutrophils and monocytes plotted in the quadrant of AB1, AB2 strains, demonstrating a close relation between these cell types with these two strains.

In order to prove the identity of infected cell types via advanced molecular pathological methods, parallel stains of IHC and ZN from serial sections, as well as double-stainings of immunofluorescence and immunohistochemistry were carried out

(**Figure 3-17**). In consequence, double-stains allowed molecular identification of infected cell types, including neutrophils (NE-elastase), macrophages (CD68) and pneumocytes type II (SPC). In case of monocyte, there was no antibody available, which can distinguish macrophages from monocytes. According to lymphocytes, we could not prove via double staining, concluding they were most likely progressive cellular shrinkage of phagocytes. Therefore, Kruskal-Wallis tests were re-performed after integrating data of macrophages and lymphocytes in 2 locations. The test showed that there were no significant differences, neither in 6 nor 3 location tests, $H=4.072$ ($df=5$, $N=180$), $p=0.539$ and $H=2$ ($df=2$, $N=180$), $p=0.368$.

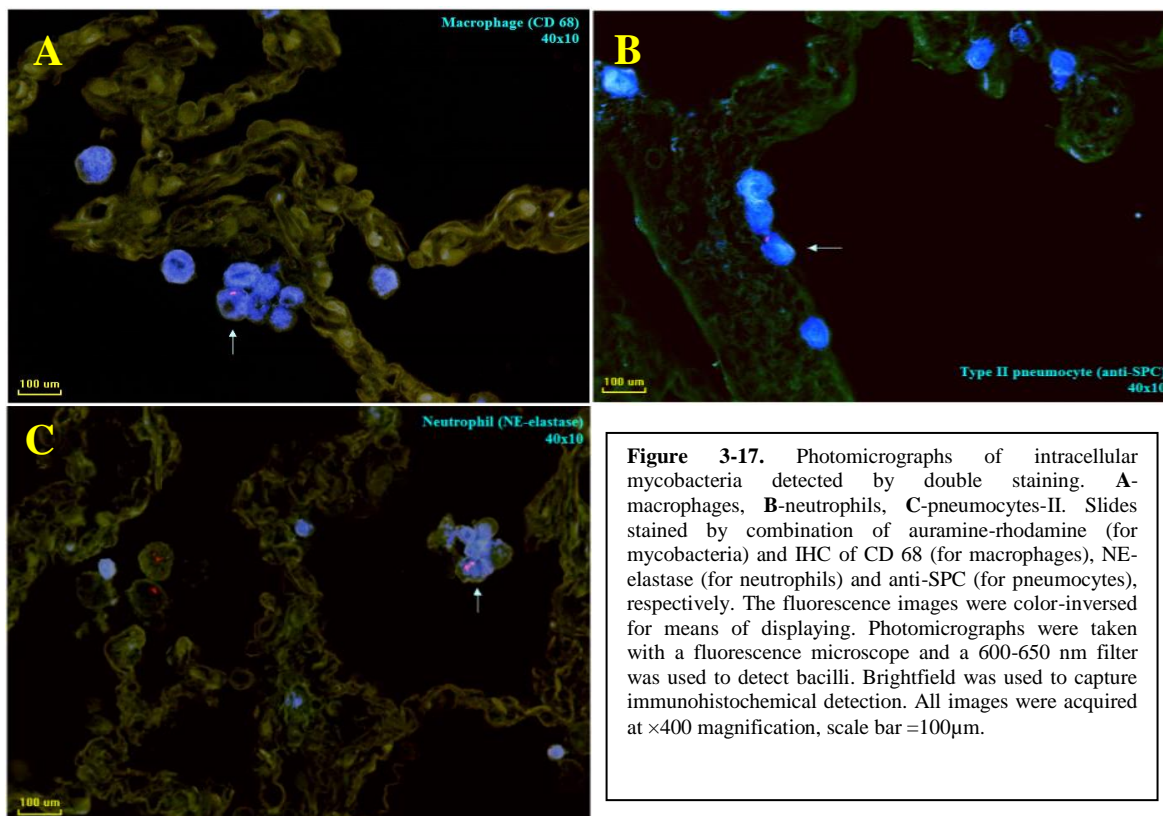


Figure 3-17. Photomicrographs of intracellular mycobacteria detected by double staining. **A**-macrophages, **B**-neutrophils, **C**-pneumocytes-II. Slides stained by combination of auramine-rhodamine (for mycobacteria) and IHC of CD 68 (for macrophages), NE-elastase (for neutrophils) and anti-SPC (for pneumocytes), respectively. The fluorescence images were color-inversed for means of displaying. Photomicrographs were taken with a fluorescence microscope and a 600-650 nm filter was used to detect bacilli. Brightfield was used to capture immunohistochemical detection. All images were acquired at $\times 400$ magnification, scale bar = $100\mu\text{m}$.

3.2.2. *In vitro* infection of primary cells

Ex vivo infections of lung tissues with mycobacteria led to issues which suggested *in vitro* infection of primary alveolar macrophages and type II epithelial cells (pneumocytes-II):

- A wide range of phagocytosis capacity was observed in macrophages (**Figure 3-18.A**).
- In addition, there were formations of vacuoles in infected macrophages. It might seem that high invasion of mycobacteria resulted in intracellular starvation followed by macroautophagy (**Figure 3-18.B**).
- The findings of infected pneumocytes-II in *ex vivo* infection with mycobacteria were interesting. Furthermore, it was remarkable that the ability of phagocytosis of

this non-professional phagocytes was comparable to that seen by the professional phagocytes (**Figure 3-18.C&D**).

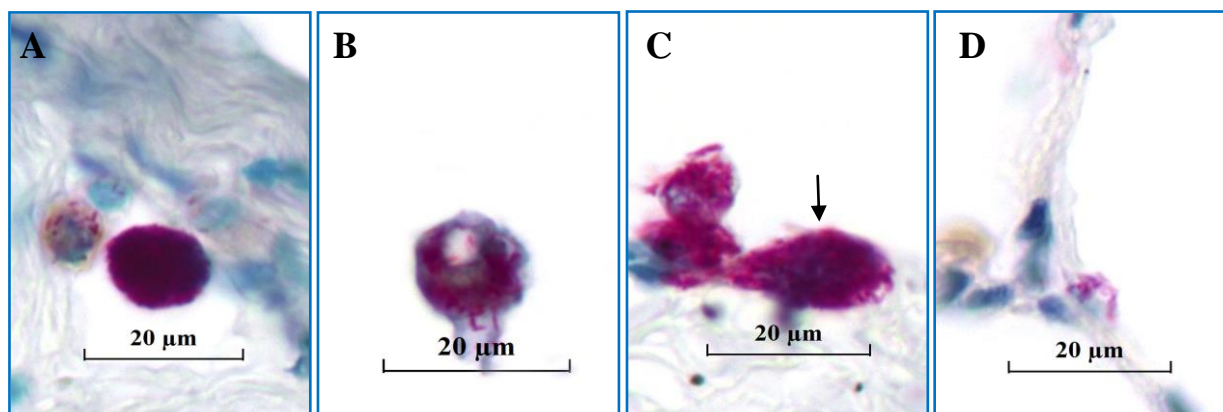


Figure 3-18. Observations of the *ex vivo* infected macrophages and pneumocytes-II by mycobacteria. Intracellular bacilli were visualized by Ziehl-Neelsen staining (pink color). The images were acquired at $\times 400$ magnification, zoomed in 200%. Scale bar =20 μ m. **A.** High and low internalization of mycobacteria in macrophages **B.** A vacuole in an infected macrophage by mycobacteria. **C.** High internalization of mycobacteria in pneumocyte (arrow) **D.** A pneumocyte-II phagocytosed few mycobacteria.

One should note that all *in vitro* experimental results were obtained through 2 independent experiments, which were repeated 2 times technically. The inoculum of bacilli and amount of cells used for the study were presented in **Table 3-4**.

Table 3-4. The amount of cells and bacilli used for the study				
Cell types	Number of cells	Inoculum of <i>M. tuberculosis</i> strain H37Rv (mean\pmSD) $\times 10^5$		
		MOI of 1:1	MOI of 3:1	MOI of 10:1
Pneumocytes-II	4×10^5	2.5 ± 0.57	7.5 ± 2.1	25 ± 7
Macrophages	2.5×10^5	1.6 ± 0.37	4.7 ± 1.35	26.5 ± 6.5

To begin with, the actual inoculum was estimated from number of cells and inoculum as percentage and resulted in an MOI of $62.5 \pm 14.28\%$ for pneumocytes-II and $62 \pm 14.69\%$ for macrophages. In **Table 3-5**, all experimental results from *in vitro* infections of primary cells using *M. tuberculosis* H37Rv with an MOI of 1:1, 3:1 and 10:1 are summarized. The replication of the intracellular mycobacteria was determined after 3 and 7 days, respectively.

Table 3-5. The amounts of intracellular mycobacteria				
Time Points	Cell type	Bacterial number (mean\pmSD) $\times 10^3$		
		MOI of 1:1	MOI of 3:1	MOI of 10:1
4 hours	Pneumocytes-II	5.10 ± 0.08	28.25 ± 4.25	65.0 ± 20.0
	Macrophages	18.25 ± 1.02	95.0 ± 25.0	70.0 ± 10.0
3 days	Pneumocytes-II	3.50 ± 0.41	11.25 ± 0.75	37.50 ± 1.0
	Macrophages	9.25 ± 0.20	67.50 ± 7.50	150.0 ± 30.0
7 days	Pneumocytes-II	0.93 ± 0.43	8.75 ± 2.75	11.25 ± 0.75
	Macrophages	10.50 ± 1.63	105.0 ± 20.0	157.350 ± 22.5

The results of *in vitro* infection of primary cells can be divided into 2 aspects: a) invasion into primary cells, b) replication within primary cells.

3.2.2. a. Cellular uptake of primary cells by *M. tuberculosis* strain H37Rv

In order to estimate the degree of interaction (binding and uptake) of mycobacteria into primary cells, the latter were incubated with strain H37Rv for 4 hours followed by washing off extracellular bacilli. Afterwards, the bacilli interacting with the cells were counted and the results are depicted in **Table 3-5** and comparisons between the different MOIs after 4 hour incubation are illustrated in **Figure 3-19**.

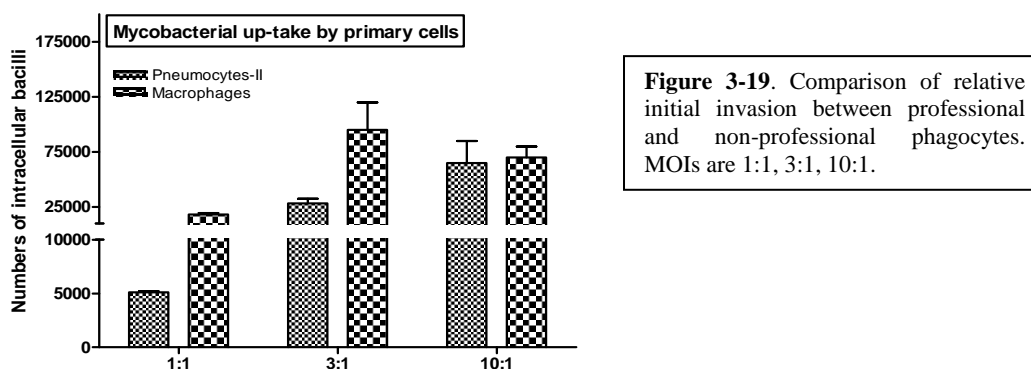


Figure 3-19. Comparison of relative initial invasion between professional and non-professional phagocytes. MOIs are 1:1, 3:1, 10:1.

Regarding the different amounts of inoculum, macrophages phagocytosed *M. tuberculosis* H37Rv with an efficiency of $12.67 \pm 4.68\%$ at a MOI of 1:1. At MOIs of 3:1 and 10:1, the relative efficiencies $22.82 \pm 12.52\%$ and $2.82 \pm 1.1\%$, respectively. In comparison, strain H37Rv invaded into pneumocytes-II with much less efficiency of $2.16 \pm 0.67\%$ at MOI of 1:1 and of $4.1 \pm 1.78\%$ at MOI of 3:1, respectively and almost to the same low degree of $2.6 \pm 0.08\%$ at MOI of 10:1.

Although it could not be distinguished whether each cell engulfed a single pathogen or several bacilli, approximately 1.3% of all seeded pneumocytes-II were infected at MOI of 1:1. At MOIs of 3:1 and 10:1, the percentages of infected cells increased to 7.1% and 16.25%, respectively. By contrast, in macrophages, 7.3% and 28% of all seeded cells were infected at MOI of 1:1 and of MOI 10:1, respectively. Interestingly, at MOI of 3:1, the percentage of infected cells was even 38%, showing most efficient infection than in all other cases. At MOI of 10:1, professional and non-professional phagocytes engulfed almost the same amount of bacilli, thus, a concentration of MOI 10:1 was chosen for a direct comparison of infection rates of mycobacteria in these two cell types.

3.2.2. b. Replication of *M. tuberculosis* strain H37Rv within primary cells

In order to examine the ability of *M. tuberculosis* H37Rv to replicate within primary cells, incubation of these cells proceeded for 3 and 7 days after initial invasion and intracellular bacilli numbers were assessed at the indicated time points.

According to **Table 3-5**, it can be hypothesized that there may be differences of engulfed bacilli numbers associated with MOIs and cell types, and bacterial growth depending on cell types. **Figure 3-20** summarizes the mycobacterial replication rates

within primary macrophages (left bars) and primary pneumocytes-II (right bars) at MOI of 10:1 for indicated 3 different incubation times.

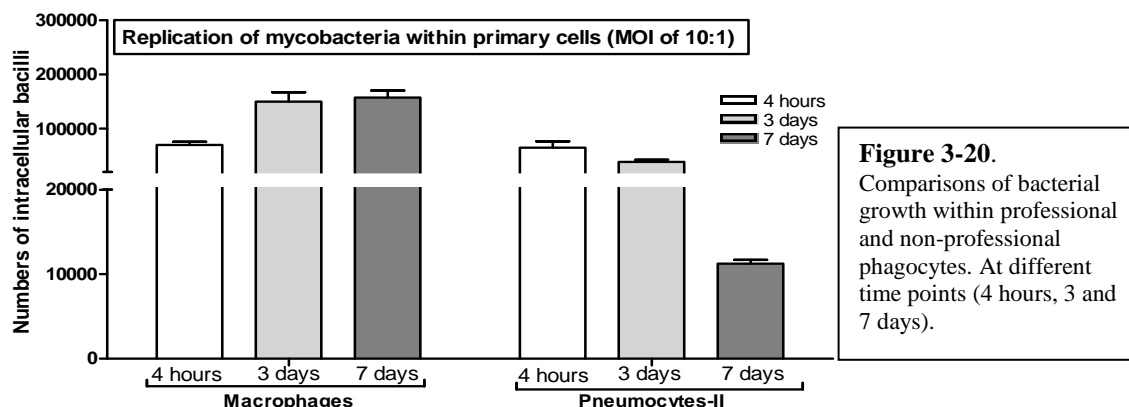


Figure 3-20. Comparisons of bacterial growth within professional and non-professional phagocytes. At different time points (4 hours, 3 and 7 days).

The intracellular mycobacterial numbers showed different tendencies within each primary cell following different *in vitro* incubation times (Table 3-5). As particularly, within the macrophages, the initial amount of internalized bacilli was $70 \pm 10.0 \times 10^3$ that increased to $150.0 \pm 30.0 \times 10^3$ bacilli by 3 days and to $157.35 \pm 22.5 \times 10^3$ bacilli on 7 days. In contrast to the macrophages, the number of mycobacteria within pneumocytes-II decreased with increasing incubation time. While $65.0 \pm 20.0 \times 10^3$ bacilli were counted after first inoculum, then numbers of bacteria decreased to $37.50 \pm 1.0 \times 10^3$ and to $11.25 \pm 0.75 \times 10^3$ on 3 and 7 days, respectively.

Since there were differences of the internalized numbers of bacteria by the different types of primary cells at all time points, the association between cell type and bacterial growth was determined. For this purpose, the changes of bacilli number by calculating ratios between posterior and anterior bacilli numbers were determined, particularly, between initial uptake and 3th day, as well as between 3 and 7 days. Afterwards, in order to convert numerical data to categorical ones for analysis by Chi square test, the ratios were given a label as “down” for a decrease, and “up” for an increase.

The assumptions of Chi square test were satisfied, such as a minimum expectation of 5 occurrences in each category and values for the variables are mutually exclusive. A total of 36 values were sampled that were related to changes of bacterial growth in both pneumocytes-II and macrophages. The frequencies of both actual observed values and expected values are shown in following Table 3-6.

Table 3-6. Contingency table for Chi square (A), and association (B) tests

bacterial growth * cell type Crosstabulation					
A			cell type		Total
			Pneumocytes-II	Macrophages	
bacterial growth	down	Count	17	6	23
		Expected Count	11.5	11.5	23.0
	up	Count	1	12	13
		Expected Count	6.5	6.5	13.0
Total	Count	18	18	36	
	Expected Count	18.0	18.0	36.0	

B Chi-Square Tests			
	Value	df	Sig. (2-sided)
Chi-Square test	14.569 ^a	1	0.000
Nominal by Nominal			
Phi	0.636		0.000
Cramer's V	0.636		0.000

a. 0 cells (0.0%) have expected count less than 5. The minimum expected count is 6.50.

As summarized in **Table 3-6 A and B**, the actual frequency of bacterial increase in macrophages was 12, while in pneumocytes-II was 1. On the other hand, the actual frequency of bacterial decrease in macrophages was 6 and in pneumocytes-II was 17. Regarding Chi square test, there is a significant association between cell types and intracellular bacterial growth rates, because the observed frequencies differ significantly from the expected frequencies in each category, the $\chi^2 (1) = 14.569$, $p < 0.0001$. Likewise, Cramér's V, a measure of association two nominal variables, and Phi coefficient, a measure of the degree of association between two binary variables, were calculated, which indicated positive strong association between bacterial growth and cell types, both ϕ_c and $r_\phi = 0.636$, $p < 0.0001$.

Based on this high association between bacterial growth and cell type, changes of intracellular bacilli numbers over the time was examined. Results are depicted in the next **Figure 3-21**.

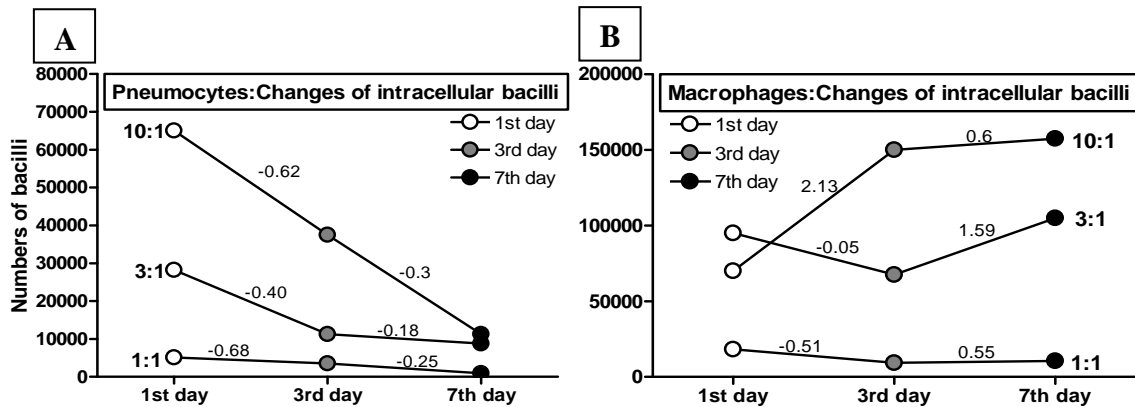


Figure 3-21. Intracellular changes within primary cells. **A.** Pneumocytes-II, **B.** Macrophages. The coefficient of changes was calculated from anterior and posterior numbers. Note: the decrease of coefficient was labeled by negative numbers, the increases were indicated by positive numbers.

In all cases of within pneumocytes-II, intracellular bacilli decreased. In particularly, the sums of coefficients of changes in pneumocytes-II among incubations were -0.93 (MOI of 1:1), -0.58 (MOI of 3:1), and -0.92 (MOI of 10:1). By contrast in macrophages, the sum of the coefficients from counted bacilli of related days showed that infection increases. Namely, at MOI of 1:1 the sum was 0.04, while at MOIs of 3:1 and 10:1 the coefficients showed more increase, 1.54 and 2.73 respectively. Interestingly, at MOI of 1:1 was being shown the highest decrease of mycobacteria in pneumocytes-II and only decreases of mycobacteria in macrophages.

3.2.2. c. Results of real-time PCR of antimycobacterial activity

In order to investigate reactions of primary cells upon mycobacteria, RT-PCR was performed for common cytokines, which are listed in **Table 2-5** (material and methods part). In **Figure 3-22**, the overview of real time PCR can be seen comparing the different responses of primary macrophages and pneumocytes-II. The data shown are preliminary data. The data show high variances and missing values. Thus, more experiments should be

performed. In this presented result, the productions of macrophages, including MCP-1, TNF- α , CCL4, hIL6, and CXCL10, were higher than in pneumocytes-II's response. While, VEGFA, and LNC2 from stimulated pneumocytes-II were higher than macrophages' production.

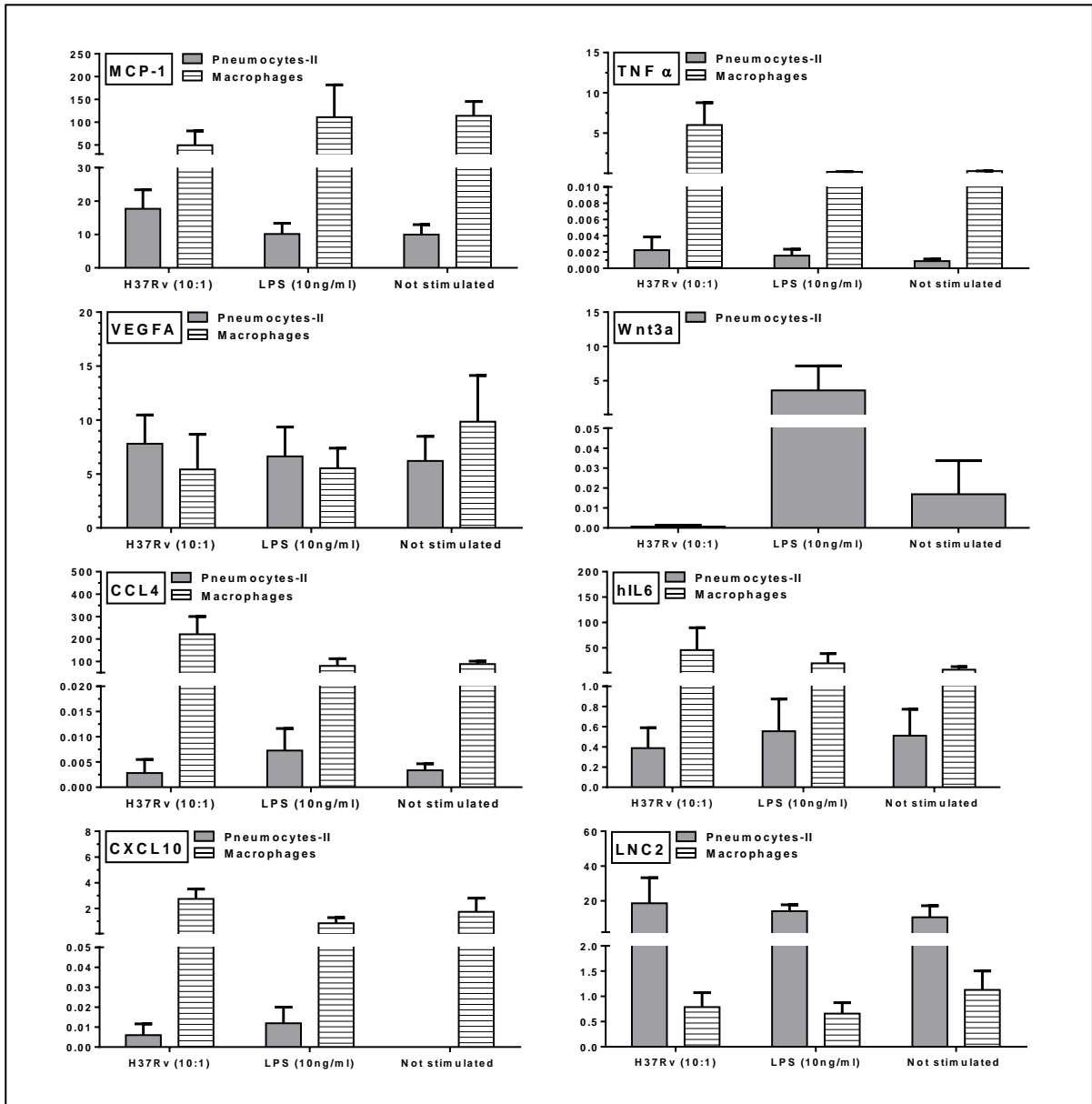


Figure 3-22. Detection and comparisons of cytokines released in the culture supernatant of human primary cells. The comparisons included three groups: 1) primary cells stimulated by H37Rv at MOI of 10:1, 2) primary cells presence in the LPS [10ng/ml], 3) non-stimulated primary cells. RT-PCR of 8 primers, including MCP-1, TNF-alpha, VEGFA, Wnt3a, CCL4, hIL6, CXCL10, and LNC2.

3.2.3. Changes of cellular morphology

3.2.3.a. Types of cellular changes

While counting cell types with high magnification (400fold), some types of morphological changes of infected macrophages have been found (**Figure 3-23**), including

cellular shrinkage, and some nuclear alterations, including karyopyknosis, karyolysis and karyorrhexis of infected macrophages.

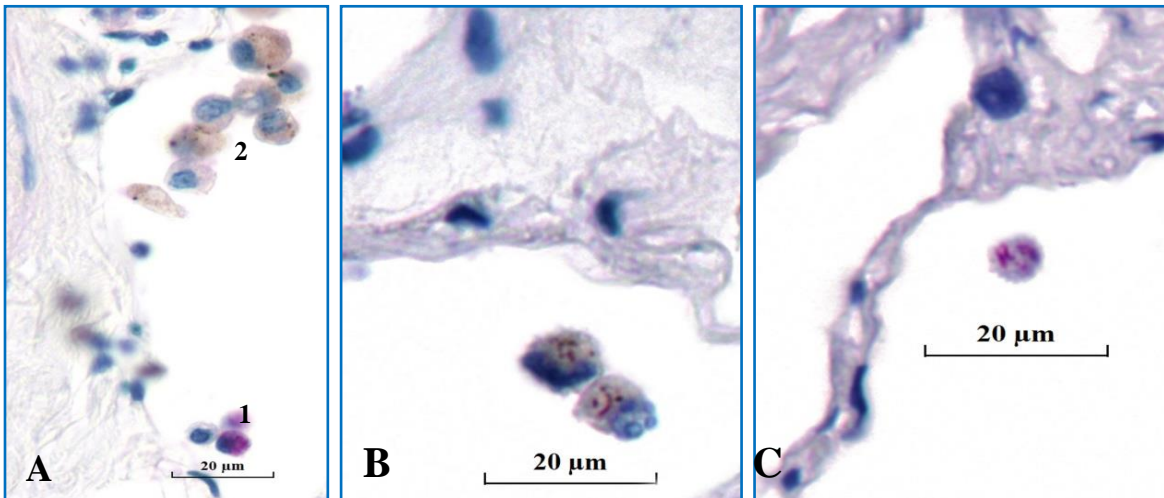


Figure 3-23. Cellular changes in infected cells. Intracellular bacilli were visualized by Ziehl-Neelsen stain in pink color, the images were acquired at $\times 400$ magnification, bar =20µm. **A.** Cellular shrinkage of infected macrophages (1) and normal macrophages (2), zoomed in 70% **B.** Karyorrhexis of infected macrophages, zoomed in 150% **C.** Karyolysis of a single infected macrophage, zoomed in 150%.

In order to illustrate how many proportions of all macrophages changed due to mycobacterial infection, **Figure 3-24** was created with numbers of incidences. From this graph has yielded following results: The total incidences of infected macrophages in AB1, AB2, AV1, AV2, TB1, and TB2 strains were 816, 731, 855, 862, 796 and 796, respectively. Overall, in all 6 different mycobacterial strains, the infected macrophages exhibited karyolysis ranging from 0 to 41 ($1.58 \pm 2.18\%$) with high variance, karyorrhexis also varying between 1-48 (2.18 ± 2.52), while karyopyknosis was observed in 192-295 ($32.77 \pm 4.04\%$) macrophages. In the cases of intact infected cells, the number of macrophages ranged between 436-492 ($56.25 \pm 4.49\%$), and the range of monocytes was between 49-75 ($7.23 \pm 1.62\%$). In the AB1 strain, 31.86% of the 816 macrophages had cellular morphological changes, in the AB2 strain, 27.77% of 731 identified macrophages, which had been infected, showed morphological alterations. In the TB1 and TB2 strains, morphological lesions in all infected macrophages were evident in 37.44% and in 37.19%, respectively. Whereas, the percentages of morphological alterations caused by AV1 and AV2 strains were 42.11% and 42.81%, respectively. These effects were comparably higher than seen in the former 4 strains of mycobacteria, prompting precise statistical tests to verify which kind of cellular lesions were associated dependent on the types of mycobacterial strains.

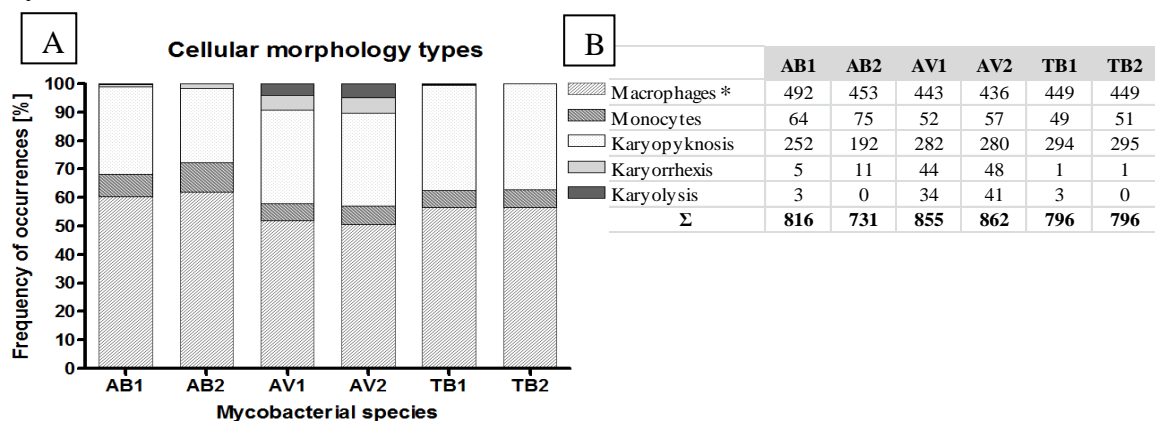


Figure 3-24. Frequency of indicated morphological changes in the infected macrophages (induced in the different 6 strains of mycobacteria). The Graph (A) reflects the frequency of occurrences of cellular morphology types within whole infected macrophages among 6 mycobacterial strains. The table (B) reports number of incidences and sum of morphological types. *: normally shaped macrophages

Summary of test assumption and data characteristic:

[More detailed performance has attached in appendix II. 3.2.3.a. Types of cellular changes]

- **Distribution:** In terms of Shapiro-Wilk and Kolmogorov-Smirnov tests showed that all distributions in data set were not normal. In visual inspections of the histograms, the bell-shaped normal curve appeared to not be fitted to all variables, having some outliers. Furthermore, in terms of skewness and kurtosis, some variables have skewed and kurtotic distributions.
- **Equality of variance:** all variables of Levene’s F tests were in monocytes $F(5,180)=1.108, p=0.358$, in intact macrophages $F(5,180)=0.827, p=0.532$, in karyolysis of infected macrophages $F(5,180)=58.049, p<0.0001$, in karyopyknosis $F(5,180)=0.465, p=0.802$, in karyorrhexis $F(5,180)=48.857, p<0.0001$, which indicated that we can keep the null hypothesis for macrophages, monocytes and karyopyknosis. Thus, for group comparison of these variables, a nonparametric Kruskal-Wallis test was selected based on assumptions’ satisfaction and group number (more than 2 groups) (Figure 3-22). On the contrary, in the cases of karyolysis and karyorrhexis, the null hypothesis is rejected ($P<0.0001$) indicating these variables have heterogeneous variances. Therefore a median test (Figure 3-23) for group comparison was performed for these 2 variables, which does not assume equality of variances.

Table 3-7. Kruskal-Wallis tests for changes of cellular morphology. Monocytes, intact and karyopyknotic macrophages among mycobacterial strains. The tests have been performed in 2 alternatives, one was for comparing 6 locations (A) (6 strains separately, AB1, AB2, TB1, TB2, AV1, AV2) and another is for comparing 3 locations (B) (same strains are integrated, AB1+AB2, AV1+AV2, TB1+TB2).

A				B			
Test Statistics ^{a,b}				Test Statistics ^{a,b}			
	macrophage	monocyte	karyopyknosis		macrophage	monocyte	karyopyknosis
Chi-Square	5.482	2.605	7.324	Chi-Square	4.146	2.085	3.996
df	5	5	5	df	2	2	2
Asymp. Sig.	.360	.761	.198	Asymp. Sig.	.126	.353	.136

a. Kruskal Wallis Test
b. Grouping Variable: species

a. Kruskal Wallis Test
b. Grouping Variable: species2

As can be seen in **Table 3-7**, Kruskal-Wallis test’s evaluations either in 3 (the 2 strains of same species form 1 group) (A) or in 6 locations (each strain; AB1, AB2, AV1, AV2, TB1, TB2 form a single group) (B) all p values of group comparison were greater than critical value ($p>0.05$), verifying no significant differences mean ranks of all mycobacterial groups associated with macrophages, monocytes and karyopyknosis. To mention in detail, statistical tests for macrophages were $H(5,180)=5.482, p=0.360$ and, $H(2,80)=4.146, p=0.126$ for 3 or 6 locations, respectively. In case of monocytes, analysis of mean rank were $H(5,180)=2.605, p=0.761$ and $H(2,80)=2.085, p=0.353$ for 3 or 6 locations, respectively. Likewise, the respective statistics of karyopyknosis were $H(5,180)=7.324, p=0.198$ and $H(2,80)=3.996, p=0.136$, respectively. **Figure 3-25** depicts Kruskal-Wallis test’s results for infected macrophages, monocytes and karyopyknosis for all 6 locations separately.

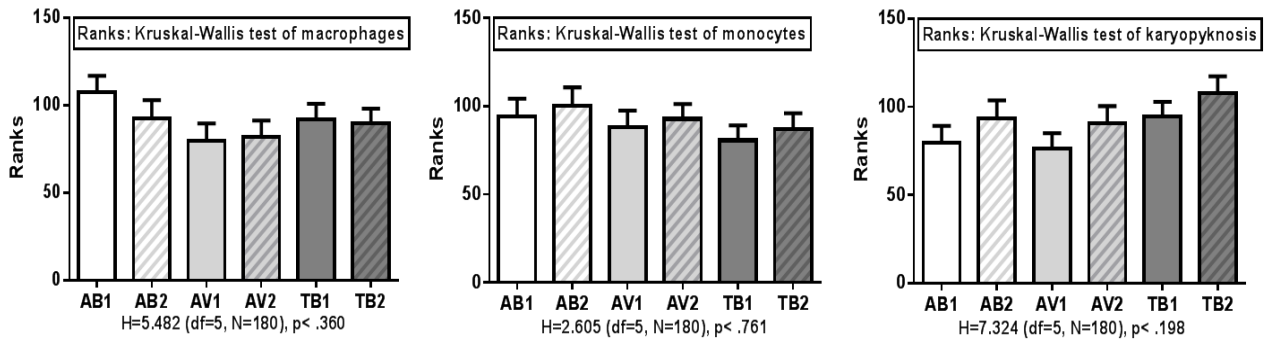


Figure 3-25. The nonparametric Kruskal-Wallis tests for cellular changes in infected cells. Herein, monocytes, intact and karyopyknotic macrophages among all mycobacterial strains (6 locations).

In section **3.2.1. Infected cell types**, some infected cells had been classified initially as lymphocytes due to their morphological similarities, but this was subsequently corrected and instead was associated with progressive pyknosis of infected macrophages. Therefore, in this paragraph, the data of lymphocytes were integrated into the results for karyopyknotic cells. These combined data's assumptions of distribution and homogeneity of variances were tested and satisfied, leading to one-way ANOVA test for group comparisons. The analysis of variance showed that there is no significant difference in variables of all karyopyknotic cells in 6 locations too, $F(5,179)=0.982$, $p=0.43$.

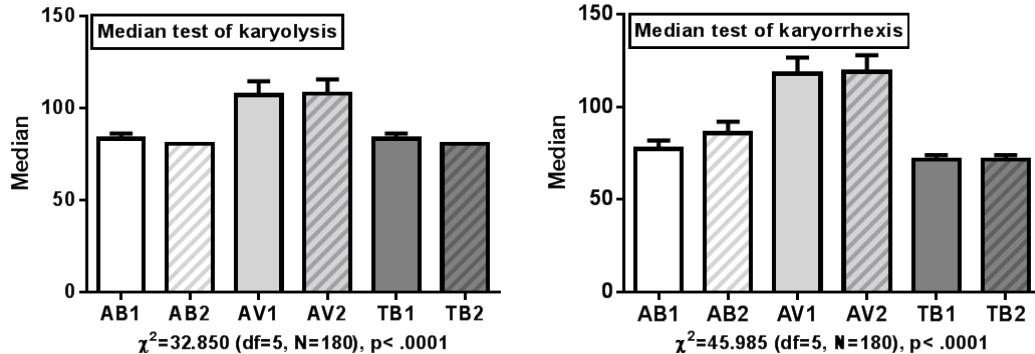


Figure 3-26. The median tests for cellular changes, including karyolysis and karyorrhesis of infected cells among all mycobacterial strains

The nonparametric median tests in both 3 and 6 locations of karyolysis and karyorrhesis indicated that there were significant differences between the median of these 2 variables. In detail, the median test of karyolysis were in 6 locations $\chi^2=32.850$ (df=5, N=180), $p < 0.0001$ and in 3 locations $\chi^2=32.513$ (df=2, N=180), $p < 0.0001$, the median test of karyorrhesis were in 6 locations $\chi^2=45.985$ (df=5, N=180), $p < 0.0001$ and in 3 locations $\chi^2=45.160$ (df=2, N=180), $p < 0.0001$, which is presented in **Figure 3-26**. In order to explore location and number of the difference among groups, a multiple comparison test with transformed data was performed (Parametric Post Hoc). Since there is not median multiple comparison test, data were transformed via logarithm. In **Table 3-8** Tukey's HSD tests for both karyolysis and karyorrhesis in 3 locations showed that both TB and AB species

significantly differ from AV species, however, they did not differ significantly from each other. Tukey’s HSD tests for karyolysis and karyorrhesis in 6 locations have been attached in Appendix-II.

Table 3-8. Tukey’s HSD tests for log transformed data of karyolysis (A) and karyorrhesis (B) in 3 locations.

Multiple Comparisons: Post Hoc test							Multiple Comparisons: Post Hoc test						
Dependent Variable: Log(karyolysis)							Dependent Variable: Log(karyorrhesis)						
Tukey HSD							Tukey HSD						
(I) species2	(J) species2	Mean Difference (I-J)	Std. Error	Sig.	95% Confidence Interval		(I) species2	(J) species2	Mean Difference (I-J)	Std. Error	Sig.	95% Confidence Interval	
					Lower Bound	Upper Bound						Lower Bound	Upper Bound
AB	AV	-.18982*	.03651	.000	-.2761	-.1035	AB	AV	-.23271*	.03691	.000	-.3199	-.1455
	TB	.00000	.03651	1.000	-.0863	.0863		TB	.05481	.03691	.301	-.0324	.1420
AV	AB	.18982*	.03651	.000	.1035	.2761	AV	AB	.23271*	.03691	.000	.1455	.3199
	TB	.18982*	.03651	.000	.1035	.2761		TB	.28752*	.03691	.000	.2003	.3748
TB	AB	.00000	.03651	1.000	-.0863	.0863	TB	AB	-.05481	.03691	.301	-.1420	.0324
	AV	-.18982*	.03651	.000	-.2761	-.1035		AV	-.28752*	.03691	.000	-.3748	-.2003

*. The mean difference is significant at the 0.05 level.

*. The mean difference is significant at the 0.05 level.

Since there were some significant differences regarding effects on cellular morphology after infection with the indicated mycobacterial species, it was worthwhile to inspect which cellular changes were induced more frequently depending on a particular mycobacterial strain. Thus, a simple correspondence analysis, a statistical visualization method for picturing the associations between the levels of a two-way contingency table (cellular changes x mycobacterial strains), was performed and the performance of analysis is summarized in **Figure 3-27**.

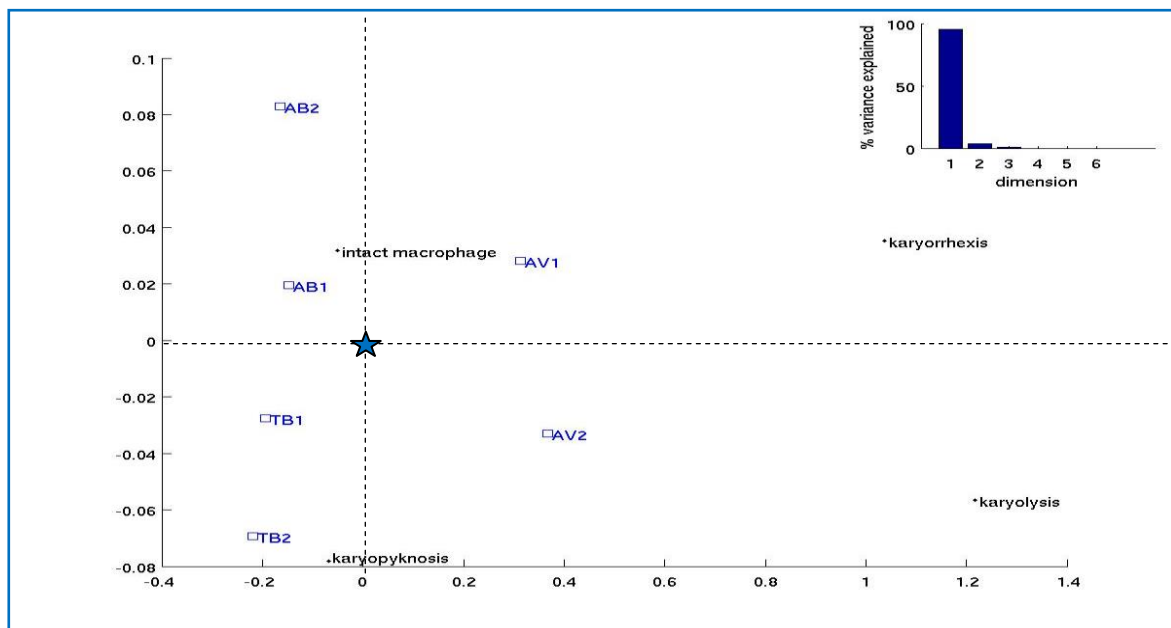


Figure 3-27. Correspondence analysis map for mycobacterial strains and cellular changes. Dispersions of variables produced an asymmetric map, its centroid (point of no correlation) was labeled by a star. All profile points were plotted around this weighted average. A barplot of variances is shown at the right top part of the map. The map of profile points was derived from a two-cross tabulation: 1) cellular morphology types, which consisted of 4 elements, such as macrophages, karyorrhesis, karyopyknosis, karyolysis, and 2) mycobacterial strains, which consisted of 6 elements, including AB1, AB2, AV1, AV2, TB1, TB2.

The plot of all profile points summarizes the relationship between mycobacterial strains and cellular morphology changes. All profile points lie around the centroid-indicating no correlation. It can be easily seen in **Figure 3-27**, there are high association between karyopyknosis and TB1, TB2, AV2 strains. Because the position of pneumocytes’

unit coordinated away from the centroid in the side of above three species. Intact structures of macrophages occurred after infection of AB1 and AB2. While the sets of relative frequencies of karyolysis and karyorrehxis coordinated far from the centroid in the side of AVs, demonstrating close relationships between these cellular changes with these two strains.

Furthermore, viability of tissues after incubation was determined by TUNEL assay, which is special for a kind of cell death referred to as apoptosis. The samples were comprised of non-infected (medium control) and infected samples, including infected by *M.tuberculosis*, *M.avium* and *M.abscessus*, respectively. A direct comparison of all groups can be seen in **Figure 3-28.A**.

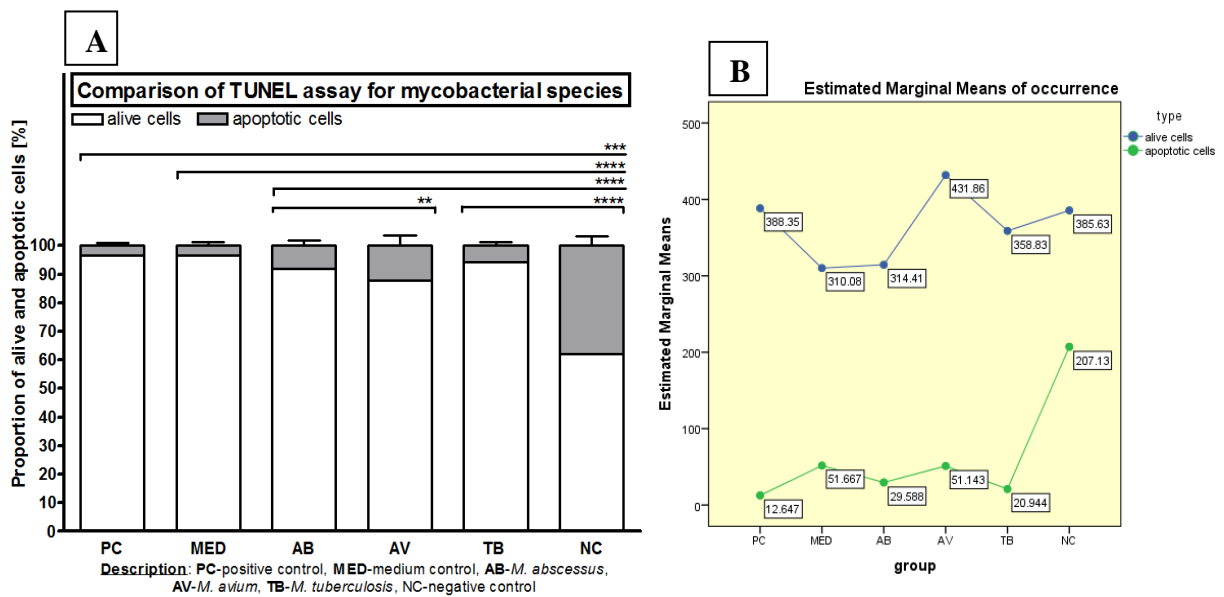


Figure 3-28. The counting analysis of TUNEL assay. **A.**The percentages of alive and dead cells' nuclei in each group with their SD are shown. Positive control (preparation of fresh lung), negative control (treated by DNase I) and *ex vivo* STST samples, including medium control (non-infected tissue), infected tissues by three mycobacterial species. Apoptotic cells are indicated as dead cells. Mean difference is significant at the $\alpha=0.05$. **B.** Profile plot of 2x6 designed factorial ANOVA for TUNEL assay. On the graph each node labeled with mean of variables. The magnitudes of means are different among each group category, likewise, the distance between magnitudes of alive and apoptotic cell groups is high.

As recount from the figure, in the positive controls represented by fresh lung tissue without incubation time, $3.36 \pm 3.65\%$ ($N=17$) of all estimated cells were apoptotic, whereas $37.91 \pm 11.95\%$ ($N=8$) of all estimated cells were apoptotic in negative controls. The percentages of apoptotic cells in MED, AB, and TB species were $3.36 \pm 3.34\%$ ($N=12$), $8.49 \pm 7.64\%$ ($N=17$), and $6.15 \pm 5.45\%$ ($N=18$), respectively. In contrast, AV strains induced higher apoptosis of $12.24 \pm 9.7\%$ ($N=7$), indicating that strain of AV cause more cell deaths than the other 2 mycobacterial species.

In order to determine whether there are any significant differences in results' of TUNEL assay related with effects of multiple factors, a factorial ANOVA test was performed by 2x6 factorial design. The between subject factors were cell type (1-alive and 2-apoptotic cells) and groups (1-PC, 2-MED, 3-AB, 4-AV, 5-TB, 6-NC, the labels' description can be seen in legend of **Figure 3-28.A**). After testing the test assumptions,

the adjustment conformed into Model type III, because of unequal sample sizes and heterogenous variances. 76.1% of the variability in all occurrences main accounted for this model design.

The hypothesis related the main effect of cell types (alive and apoptotic cells), there is a significant difference in all occurrence, $F(1,158)=351.854$, $p<0.0001$, $\eta=0.707$; and a main effect of groups showed significant difference between groups $F(5,158)=3.395$, $p=0.001$, $\eta=0.139$. About the interaction of main effects showed that dependent variables differ significantly from each other $F(6,158)=3.395$, $p=0.006$, $\eta=0.104$, and the magnitudes of mean difference were depicted in **Figure 3-28.B** by split plot between subject factors. The different groups were determined via pairwise comparisons which is applied in **Figure 3-28.A** with symbols of significant values. Namely, the mean of negative control differs from mean of PC ($p=0.001$), MC ($p<0.0001$), AB ($p<0.0001$) and TB ($p<0.0001$), likewise mean of AB differs significantly from mean of AV ($p<0.022$). But there was no difference between AV and NC ($p=0.115$).

3.2.3.b. Cellular measurements

While calculating numbers of types of cellular changes, it became obvious that some infected cells underwent measurable shrinkage, which was characterized by allround shape without blebbing and nuclear fragmentation (unlikely apoptosis), high condensation of cytoplasm and nucleus together. In order to study the characteristics of this atypical pyknotic changes in more detail, 100 normal and 100 infected pyknotic macrophages were randomly sampled from all cases and strains, then following parameters were measured and compared:

- Cytoplasmic diameter & nuclear diameter (**Figure 3-29.A**)
- N/C ratio (It is a ratio of the nuclear size to the cytoplasmic size)
- Light density (LD) of cytoplasm & light density of nucleus (**Figure 3-29.B**)

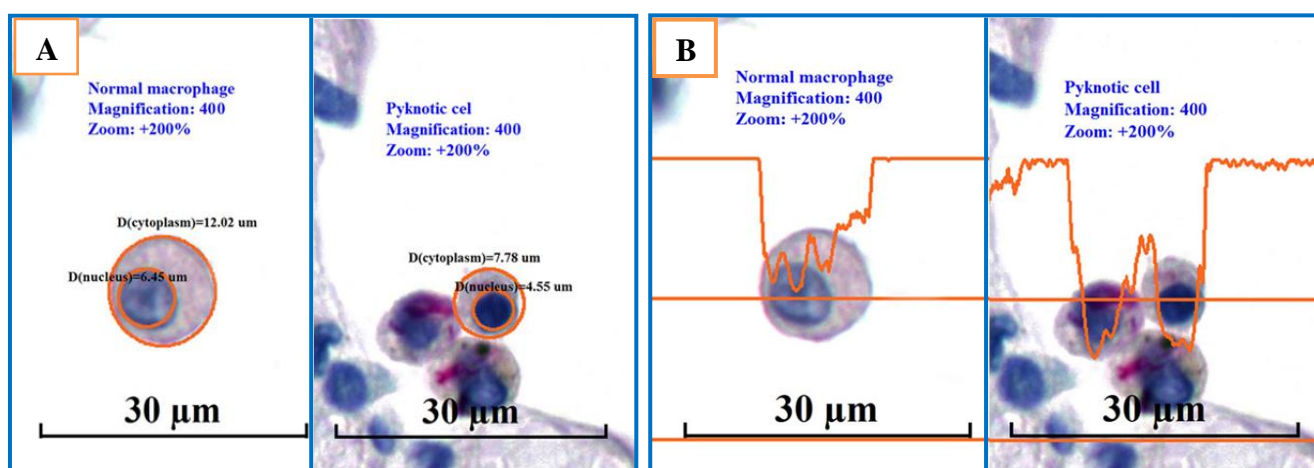


Figure 3-29. Measuring of cellular diameters and light densities **A.** General ways to measure above scales by using Infinity analysis software. Cell size (nuclear and cytoplasmic diameter, respectively), **B.** Light density (nuclear and cytoplasmic light density, respectively). To keep measuring light density of cells equivalently, certain camera control options were used (magnification: 400, exposure: 200, gain: 2, gamma: 1), light source at daylight, camera control extended with default before measuring, then used white balance and area white balance.

All results of measurements are combined in **Table 3-9**, the following contexts cellular sizes and light densities of 2 groups, and association of them are analyzed separately.

Table 3-9
Cellular measurements of infected and non-infected cells (Mean±SD)

Parameters of measurements	Infected cell		Non-infected cell	
	Nucleus	Cytoplasm	Nucleus	Cytoplasm
Light density	-22.83±22.53	43.21±22.59	23.84±17.23	60.71±21.40
Diameter (µm)	4.30±0.77	8.40±1.80	7.53±1.48	14.26±2.31
AM of LD	10.19±18.89		42.28±16.62	
N/C ratio	0.52±0.08		0.53±0.09	

Abbreviation: AM of LD- Arithmetic mean of nuclear and cytoplasmic LD

A. Measurements of cytoplasmic and nuclear sizes

As detailing the data of cellular sizes in **Table 3-9**, the diameter of cytoplasmic size in non-infected cells (N=100) ranged from 10.87 to 25.29 µm (14.25±2.30), while the diameter of cytoplasmic size in infected cells (N=100) was associated with a numerically smaller size of 5.1-14.75 µm (8.39±1.79). The diameter of nuclear size in non-infected cell ranged from 5.11-11.91 µm (7.53±1.48), while the diameter of nuclear size in infected cell was associated with a numerically smaller size of 2.54 to 6.42 µm (4.29±0.76). The N/C ratio in non-infected cells ranged from 0.33 to 0.88 (0.53±0.09), while the N/C ratio in infected cells was associated with a numerically smaller size of 0.35-0.73 (0.52±0.079), prompting precise statistical tests to verify these differences are significant.

Inferential statistics associated with cell sizes

Summary of test assumption and data characteristic:

[More detailed performance is attached in appendix II (3.2.3.b. Cellular measurements-1)]

- **Distribution:** In terms of Shapiro-Wilk and Kolmogorov-Smirnov tests and visual inspection of histograms showed that 4 data in data set were not normally distributed, having residuals. Skewness and kurtosis Z values for every independent value were estimated, which indicated our data were skewed and kurtotic, they differ significantly from normality. Only the Z value of nuclear size (infected cells) and N/C (infected cells) were approximately normally distributed, in terms of skewness and kurtosis.
- **Equality of variance:** Cytoplasmic and nuclear size of nonparametric Levene's F test, $F(1) < 0.0001$, $p=1.0$, N/C of Levene's F test, $F(1)=0.0001$, $p=0.981$, which indicate that we can keep the null hypothesis. Hence for group comparison, Mann-Whitney U test (**Figure 3-30**) was selected based on assumptions' satisfactions.

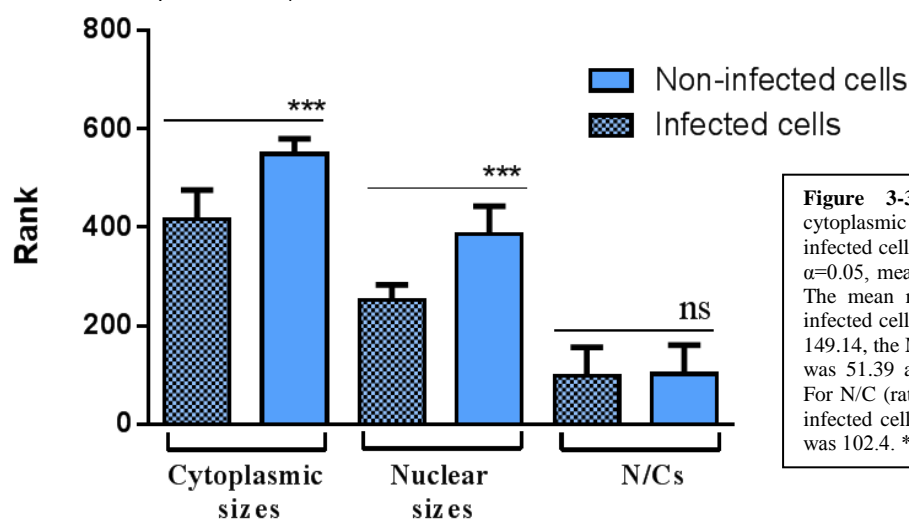


Figure 3-30. Comparisons of nuclear and cytoplasmic sizes between infected and non-infected cells. Mean difference is significant at the $\alpha=0.05$, meanings of p values labeled as asterisks. The mean rank (Mrank) of cytoplasmic size of infected cells was 51.86, in non-infected cells was 149.14, the Mranks of nuclear sizes in infected cell was 51.39 and in non-infected cells was 149.61. For N/C (ratio of nuclear and cytoplasmic size) in infected cells was 98.60 and in non-infected cells was 102.4. ***= $p \leq 0.001$, ns=not significant

size in non-infected cells, $U=136$, Z value= -11.885 , $p<0.001$. The Mann–Whitney U test for nuclear size of mean rank in both groups showed that there is a significant difference, $U= 89$, Z value= -12 , $p<0.001$. Nevertheless, the mean rank of N/C in infected cells does not differ from the rank mean of N/C in non-infected cells, $U=4810$, Z value= -0.465 , $p= 0.642$.

B. Measurements of cytoplasmic and nuclear light density (LD) of the atypical pyknotic cells

As detailing the data of LDs in **Table 3-9**, the rank of cytoplasmic LD in non-infected cells ($N=100$) ranged from 24 to 105 (60.7 ± 2.14), while the cytoplasmic LD in infected cells ($N=100$) was associated with a numerically darker LD of $-23.5-79.5$ (43.2 ± 2.25). The nuclear LD in non-infected cells ranged from -9.01 to 64.51 (23.84 ± 1.72), while nuclear LD in infected cells was associated with a numerically darker LD of $-70.01-44.50$ (-22.82 ± 2.25). Overall, the average LD of cytoplasmic and nuclear in non-infected cells ranged from 7.50 to 84.51 (42.27 ± 16.61), while the average LD of cytoplasmic and nuclear in infected cells was associated with a numerically darker LD of $-45.05-54.33$ (10.18 ± 18.89).

Inferential statistics associated with light density

Summary of test assumption and data characteristic:

[More detailed performance is attached in appendix II (3.2.3.b. Cellular measurements-2)]

- **Distribution:** A visual inspection of the histograms showed that there is not enough evidence to assume all sampled population is normally distributed due to outliers. Skewness and kurtosis Z value were estimated, regarding them: our data were a little bit skewed and kurtotic, they don't differ significantly from normality, except kurtosis Z value of cytoplasmic LD in infected and non-infected cells were beyond in the span of $|1.96|$. The results of normality tests show that all data are not normally distributed.
- **Equality of variance:** Cytoplasmic LD of Levene's F test, $F(199) < 0.0001$, $p=.996$, nuclear LD of Levene's F test, $F(199) < 0.0001$, $p=1$, which indicate that we can keep the null hypothesis. Conclusion: for group comparison, nonparametric Mann-Whitney U test (**Figure 3-31**) was selected based on assumptions' satisfaction.

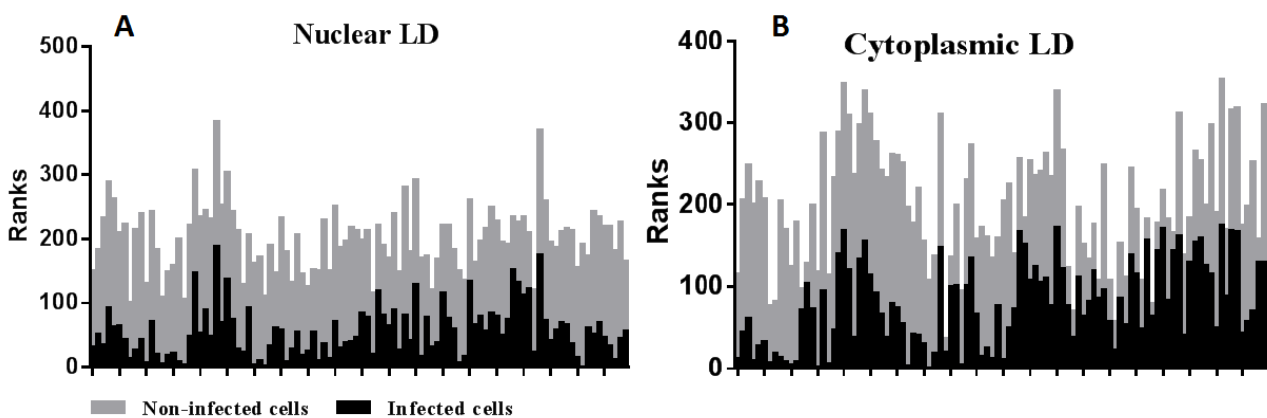


Figure 3-31. Comparisons of nuclear (A) and cytoplasmic (B) LDs between infected and non-infected cells. The graph was created by transformed data of LDs comparing with infected and non-infected cells of nuclear ($N=100$) and cytoplasmic ($N=100$) LDs, respectively, for Mann-Whitney U tests. The mean rank (Mrank) of cytoplasmic LDs in infected cells was 80.58 , in non-infected cells was 120.43 , Mrank of nuclear LD in infected cells was 56.02 and in non-infected cells was 144.98 .

The representation of graph and table in **Figure 3-31** demonstrates that the Mann–Whitney U test indicated that the mean rank of cytoplasmic LD in infected cells is significantly darker than mean rank of cytoplasmic LD in non-infected cells, $U=3007.5$, Z value= -4.869 , $p<0.001$. The Mann–Whitney U test for nuclear size of mean rank in both groups was associated with a statistically significant difference, $U= 552$, Z value= -10.86 , $p<0.001$.

C. Relationship between cell sizes and light density of the atypical pyknotic cells

In order to disclose whether there is a statistical significant relationship between changes of cell sizes and light densities, two-way scatter plots were performed initially, which are illustrated in **Figure 3-32 (A&B)**, likewise cytoplasmic and nuclear sizes were plotted due to inspect of their association.

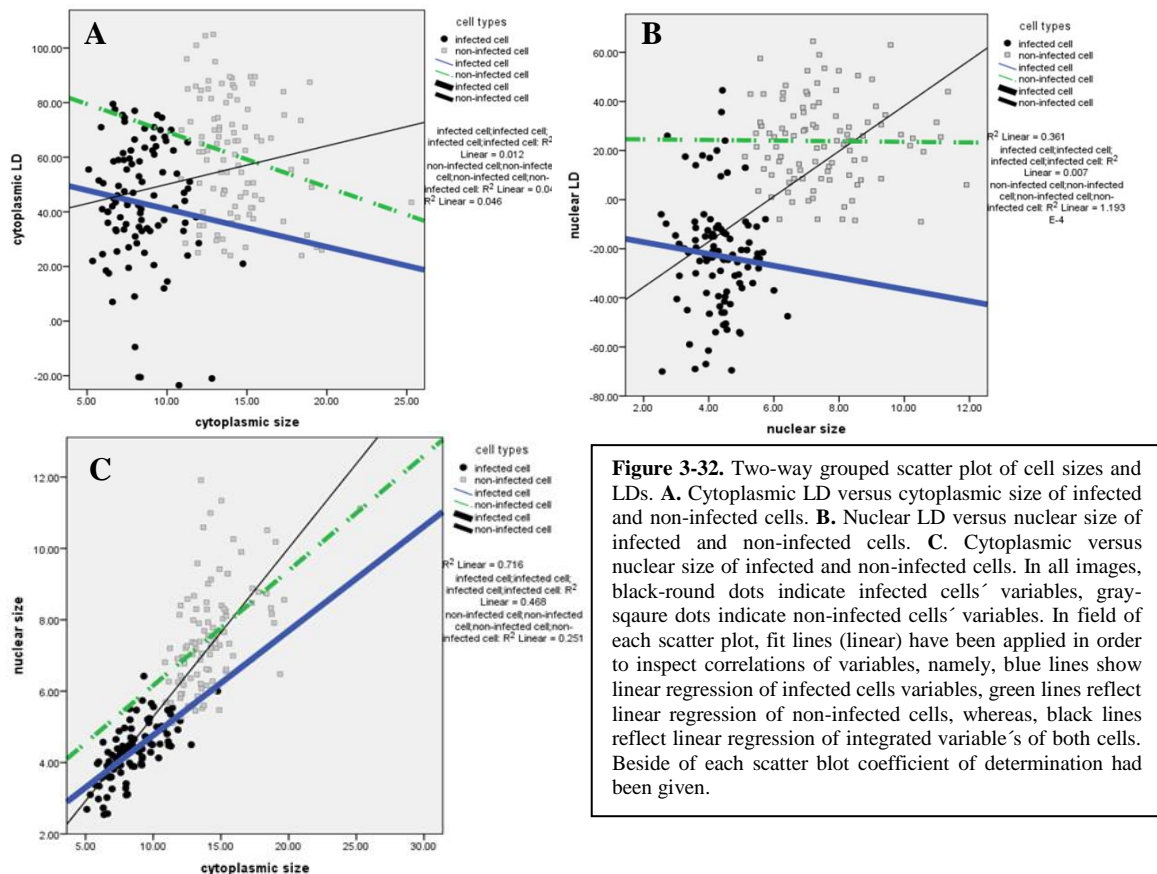


Figure 3-32. Two-way grouped scatter plot of cell sizes and LDs. **A.** Cytoplasmic LD versus cytoplasmic size of infected and non-infected cells. **B.** Nuclear LD versus nuclear size of infected and non-infected cells. **C.** Cytoplasmic versus nuclear size of infected and non-infected cells. In all images, black-round dots indicate infected cells' variables, gray-square dots indicate non-infected cells' variables. In field of each scatter plot, fit lines (linear) have been applied in order to inspect correlations of variables, namely, blue lines show linear regression of infected cells variables, green lines reflect linear regression of non-infected cells, whereas, black lines reflect linear regression of integrated variables of both cells. Beside of each scatter blot coefficient of determination had been given.

In **Figure 3-32** demonstrates in visual inspection of two-way scatter plots show, there are kinds of relationships and co-movement, which prompted more specific statistical tests to verify their relationships.

Summary of test assumption and data characteristic:

[More detailed performance is attached in appendix II (3.2.3.b. Cellular measurements-3)]

- *Standardized residual on the standardized predicted values in infected cells' variables indicate typical conventional manifestation of heteroscedasticity, while in non-infected cells' indicates approximately homoscedasticity.*
- *Distribution was mentioned above separately.*

- In scatter plot, variables' patterns fitted to linear form.

Measurement of scales and randomization were satisfied. Therefore, a Spearman's rank correlation matrix was performed to detect any existing relationships in all variables (Table 3-10).

Table 3-10. Spearman's rank correlation matrix for cellular sizes and LDs in infected and non-infected cells

			Correlations					
			cytoplasmic size	nuclear size	N/C	cytoplasmic LD	nuclear LD	arithmetic mean of LD
Spearman's rho	cytoplasmic size	Correlation Coefficient	1.000	.894**	-.182	.234**	.606**	.538**
		Sig. (2-tailed)	.	.000	.010	.001	.000	.000
		N	200	200	200	200	200	200
	nuclear size	Correlation Coefficient	.894**	1.000	.237**	.290**	.628**	.582**
		Sig. (2-tailed)	.000	.	.001	.000	.000	.000
		N	200	200	200	200	200	200
	N/C	Correlation Coefficient	-.182	.237**	1.000	.106	.061	.100
		Sig. (2-tailed)	.010	.001	.	.134	.389	.157
		N	200	200	200	200	200	200
	cytoplasmic LD	Correlation Coefficient	.234**	.290**	.106	1.000	.515**	.801**
		Sig. (2-tailed)	.001	.000	.134	.	.000	.000
		N	200	200	200	200	200	200
	nuclear LD	Correlation Coefficient	.606**	.628**	.061	.515**	1.000	.917**
		Sig. (2-tailed)	.000	.000	.389	.000	.	.000
		N	200	200	200	200	200	200
	arithmetic mean of LD	Correlation Coefficient	.538**	.582**	.100	.801**	.917**	1.000
		Sig. (2-tailed)	.000	.000	.157	.000	.000	.
		N	200	200	200	200	200	200

** . Correlation is significant at the 0.01 level (2-tailed).

* . Correlation is significant at the 0.05 level (2-tailed).

As recount from the table, the cytoplasmic LD and the cytoplasmic size were correlated weakly and significantly, Spearman's ρ (198)= 0.234, $p=0.001$ with positive covariance. The nuclear LD and the nuclear size were correlated strongly and significantly, Spearman's ρ (198) =0.628, $p<0.0001$ with positive covariance. Likewise, the nuclear size and the cytoplasmic size were correlated strongly and significantly, Spearman's ρ (198)= 0.894, $p<0.0001$ with positive covariance. While N/C has correlated both of them weakly and significantly, Spearman's ρ (198)=0.237 and -0.182, $p<0.0001$ and $p<0.01$ with positive covariance to nuclear size, but negative covariance to cytoplasmic size. For the 100 infected and 100 non-infected cells, the cytoplasmic LD and the nuclear LD were correlated strongly and significantly, Spearman's ρ (198)= 0.515, $p<0.0001$ with positive covariance. Arithmetic mean of LD has strong and significant relationship with all variable with positive covariance, except N/C, it indicates significant relationship of cell sizes and LDs.

In order to determine how these correlations vary together, linear regression analysis (Figure 3-33) was performed. For this reason, it was necessary that the variables have been transformed, as a consequence, the data set was standardized by creating Z score due to be on the same scales.

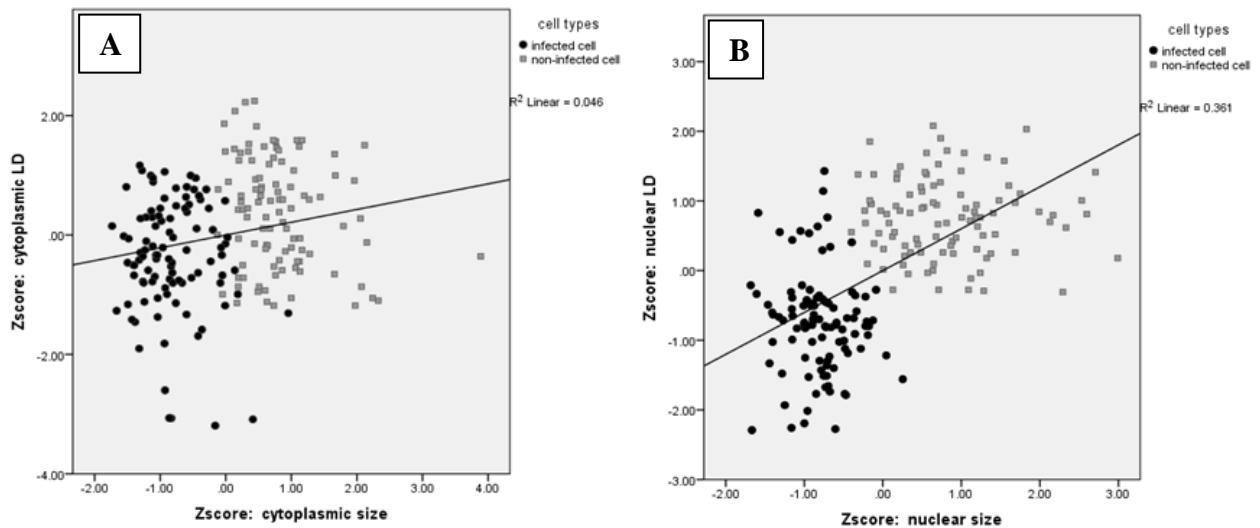


Figure 3-33. Scatter plots associated with linear regression of standardized variables. **A.** Cytoplasmic measurements, **B.** Nuclear measurements. The coefficient of determination (R^2) is 0.046 in cytoplasmic size and LD, 4.6% of the variability in cytoplasmic LD can be explained by this linear relationship with cytoplasmic size, the other 95.4% is random variation that is unexplained by this linear relationship; while nuclear size and LD the R^2 is 0.361, verifying 36.1% of the variability in nuclear LD can be explained by the linear relationship with nuclear size, the other 63.9% is random variation that is unexplained by this linear relationship.

Coefficients^a

Model		Unstandardized Coefficients		Standardized Coefficients	t	Sig.	95.0% Confidence Interval for B	
		B	Std. Error	Beta			Lower Bound	Upper Bound
1	(Constant)	-1.581E-016	.069		.000	1.000	-.137	.137
	Zscore: cytoplasmic size	.214	.069	.214	3.086	.002	.077	.351

a. Dependent Variable: Zscore: cytoplasmic LD

Z scored value of cytoplasmic size significantly predicted standardized cytoplasmic LD, $\beta=0.214$, $t(198)=3.086$, $p<0.002$. It supported also a significant proportion of variance in cytoplasmic LD, $F(1,198)=9.524$, $p=0.002$. So, linear regression line would be $\hat{Y} = -1.581E-016 + 0.214 * X + 0.069$. So we can predict that each Z scored value of cytoplasmic size can change the cytoplasmic LD by a Z score of 0.214.

Coefficients^a

Model		Unstandardized Coefficients		Standardized Coefficients	t	Sig.	95.0% Confidence Interval for B	
		B	Std. Error	Beta			Lower Bound	Upper Bound
1	(Constant)	1.045E-015	.057		.000	1.000	-.112	.112
	Zscore: nuclear size	.601	.057	.601	10.584	.000	.489	.713

a. Dependent Variable: Zscore: nuclear LD

Z scored value of nuclear size significantly predicted standardized nuclear LD, $\beta=0.601$, $t(198)=10.584$, $p<0.0001$. It also explained a significant proportion of variance in nuclear LD, $F(1,198)=112.028$, $p<0.0001$. So, linear regression line would be $\hat{Y} = 1.045E-015 + 0.601 * X + 0.057$. Thus, there is enough evidence to say that each unit of nuclear size change can influence 0.601 amount of nuclear LD.

Coefficients^a

Model		Unstandardized Coefficients		Standardized Coefficients	t	Sig.	95.0% Confidence Interval for B	
		B	Std. Error	Beta			Lower Bound	Upper Bound
1	(Constant)	1.247E-015	.038		.000	1.000	-.075	.075
	Zscore: nuclear size	.846	.038	.846	22.328	.000	.771	.921

a. Dependent Variable: Zscore: cytoplasmic size

Z scored value of nuclear size significantly predicted standardized cytoplasmic size, $\beta=0.846$, $t(198)=22.328$, $P<0.0001$. It supported also a significant proportion of variance in cytoplasmic size, $F(1,198)=498.542$, $p<0.0001$. So, linear regression line would be $\hat{Y}=1.247E-015+0.846*X+0.53$. Thus, there is enough evidence to say that each unit of nuclear size change can influence 0.846 amount of cytoplasmic standardized size. R square of 0.716 values indicates, that 71.6% of variables can be explained by this model.

Since arithmetic mean of LD has strong correlation with nuclear and cytoplasmic size both leading multi-regression. R^2 is 0.557, so we can conclude that our two predictor variables can explain 55.7% of the arithmetic mean of LD by model. The remainder is error or explained by other effects. Regarding to collinearity statistics, tolerance=0.284, variance inflation factor (VIF) =3.518 provide that these variables are not multi-collinearity, thus an important assumption of multi-linear regression has satisfied. Z scored value of cytoplasmic and nuclear size significantly predicted standardized the arithmetic mean of LD, $F=38.302$, $p<0.0001$. Multi-linear regression's equation would be $\hat{Y}=1.072E-015+0.129*X_1+0.416*X_2+0.85$. So it can be predicted that each Z scored value of cytoplasmic and nuclear diameter can affect cytoplasmic LD by standardized score of 0.545. According to standardized coefficient beta, in our model nuclear size ($\beta=0.416$, $t=3.66$, $p<0.0001$) can make strong contribution to prediction of outcome comparing cytoplasmic size.

Coefficients^a

Model		Unstandardized Coefficients		Standardized Coefficients	t	Sig.	95.0% Confidence Interval for B		Correlations			Collinearity Statistics	
		B	Std. Error	Beta			Lower Bound	Upper Bound	Zero-order	Partial	Part	Tolerance	VIF
1	(Constant)	1.072E-015	.060		.000	1.000	-.119	.119					
	Zscore: cytoplasmic size	.129	.113	.129	1.133	.258	-.095	.352	.480	.080	.069	.284	3.518
	Zscore: nuclear size	.416	.113	.416	3.668	.000	.192	.640	.525	.253	.222	.284	3.518

a. Dependent Variable: Zscore: arithmetic mean of LD

3.2.4. Vitamin stimulation of “self-split” cell death

Theoretically, the progressive overall cellular changes are representing a kind of cell death, named “self split” cell death/autoschizis, among nearly 15 different types of cell deaths. Thus, in order to verify that it can occur in macrophages upon intracellular infection, *in vitro* primary alveolar macrophages were induced by combination of Vitamin C (ascorbic acid) and K_3 (menadione).

Initially, the 90% level of cytotoxic dose (CD_{90}) of vitamins treatment was determined by using a colorimetric assay within a wide range of dosages (from 125 μ M to 40 mM in 18 different doses). Experiments were repeated 3 times and each experiment involved $N_1=324$, $N_2=204$, $N_3=216$ measurements, respectively. To determine CD_{90} , the

concentration at which the serving fraction is 90%, the non-linear regression model with sigmoidal curve for best-fit values (dose-response curve) was created, which can be seen in **Figure 3-34**.

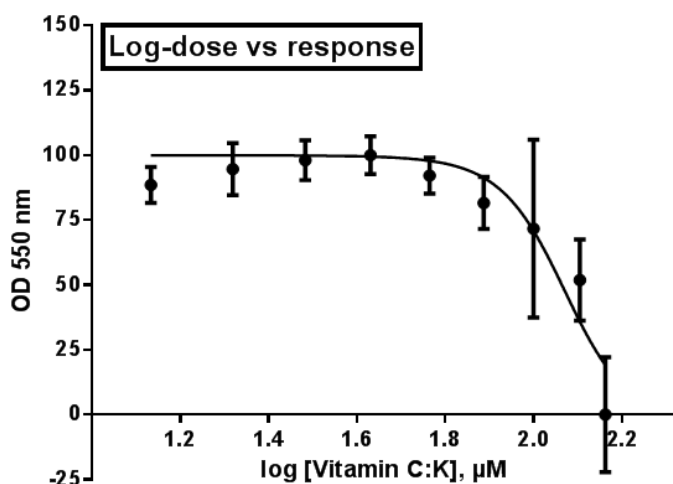


Figure 3-34. Dose-response curve of vitamin combination-treated alveolar macrophages. The Y axis plots response, which is measurements of optical density (formazan quantified by measuring at 550 nm wavelength). The X axis plots concentrations (125 μM to 40 mM in 18 different doses), which are logarithmic transformed for non-linear regression. Statistical analysis was performed at 95% of confidence intervals. N=744 representing the summary of all measurements.

In a first approach, the dose-response curve created in 2 alternatives: 1) different curve for each data set 2) one curve for all data set. But, the coefficient of determinations were $R^2_1=0.5223$, $R^2_2=0.1852$, $R^2_3=0.2462$ in integrated data set, respectively, indicating 52.23%, 18.52% and 24.62% of the variability can be explained by the non-linear relationship of dose-exposure, which is enough evidence to use one curve for 3 data sets. And the rest of percentages are random variation that were unexplained by this model. The non-linear regression model with sigmoidal curve showed that, HillSlope ranged between 6364(bottom)-10859(top), $CD_{90}= 8313\mu\text{M}$: 83.13 μM (VC:VK₃ ratio of 100:1).

Additionally, in order to inspect the structural changes, the vitamin treated-primary cells stained immunohistochemically and histochemically, respectively, and compared with untreated primary cells (**Figure 3-35**). As a result, vitamin stimulated cells were noticeable smaller with pyknotic nuclei than non-stimulated cells resembling lymphocytes, and mixed with few lysed cells (**Figure 3-35.A&B**). In order to distinguish between pyknotic macrophages and lymphocytes, immunohistochemical stainings with an antibody against CD 68 were performed, in which all pyknotic cells were positive (**Figure 3-35.C**). Likewise, to distinguish between programmed and accidental cell deaths, immunohistochemical stainings with a specific antibody directed at Caspase-3 were performed, and the majority of the macrophages remained negative (**Figure 3-35.D**), demonstrating that vitamins did not induce apoptosis in primary alveolar macrophages.

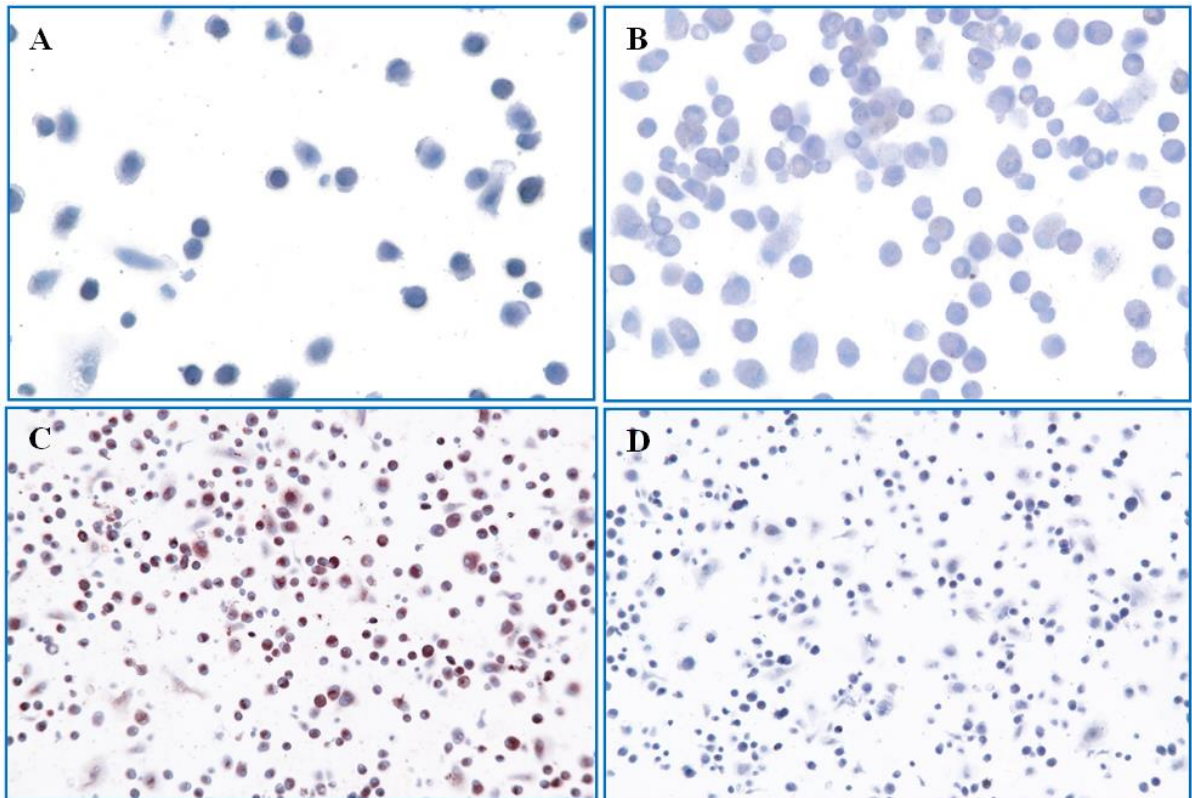


Figure 3-35. “Self-split” cell death of primary alveolar macrophages. All images were acquired at $\times 200$ magnification. **A** (stimulated) and **B** (non-stimulated) Comparison of vitamin stimulated and non-stimulated primary cells, zoomed in +200%. At same camera control options were used (exposure: 100, gain: 2, gamma: 1), light source at daylight, camera control extended with default before measuring, then used white balance and area white balance. Counter staining of Mayer’s hemalum. **C.** Immunohistochemical detection of CD68, which is positive for all cells. **D.** Immunohistochemical detection of Caspase-3, which was almost negative for all cells (only 1-3 cells were positive on a single field).

3.2.5. Transcriptome analysis of mycobacterial infection

In order to analyze the expression of individual genes on mRNA level from a genome-wide expression profile upon mycobacterial infection, including *M. tuberculosis*, *M. avium* and *M. abscessus*, a transcriptome analysis was performed from HOPE-fixed paraffin embedded tissues of *ex vivo* STS model.

3.2.5.a. Transcription profiling

Initially, to inspect gene expressions patterns of tissue responses due to different strains, a hierarchical clustering from all the samples (N=3 for each species or condition) was computed from the genes that exhibited a fold change >2 against the medium control (**Figure 3-36**).

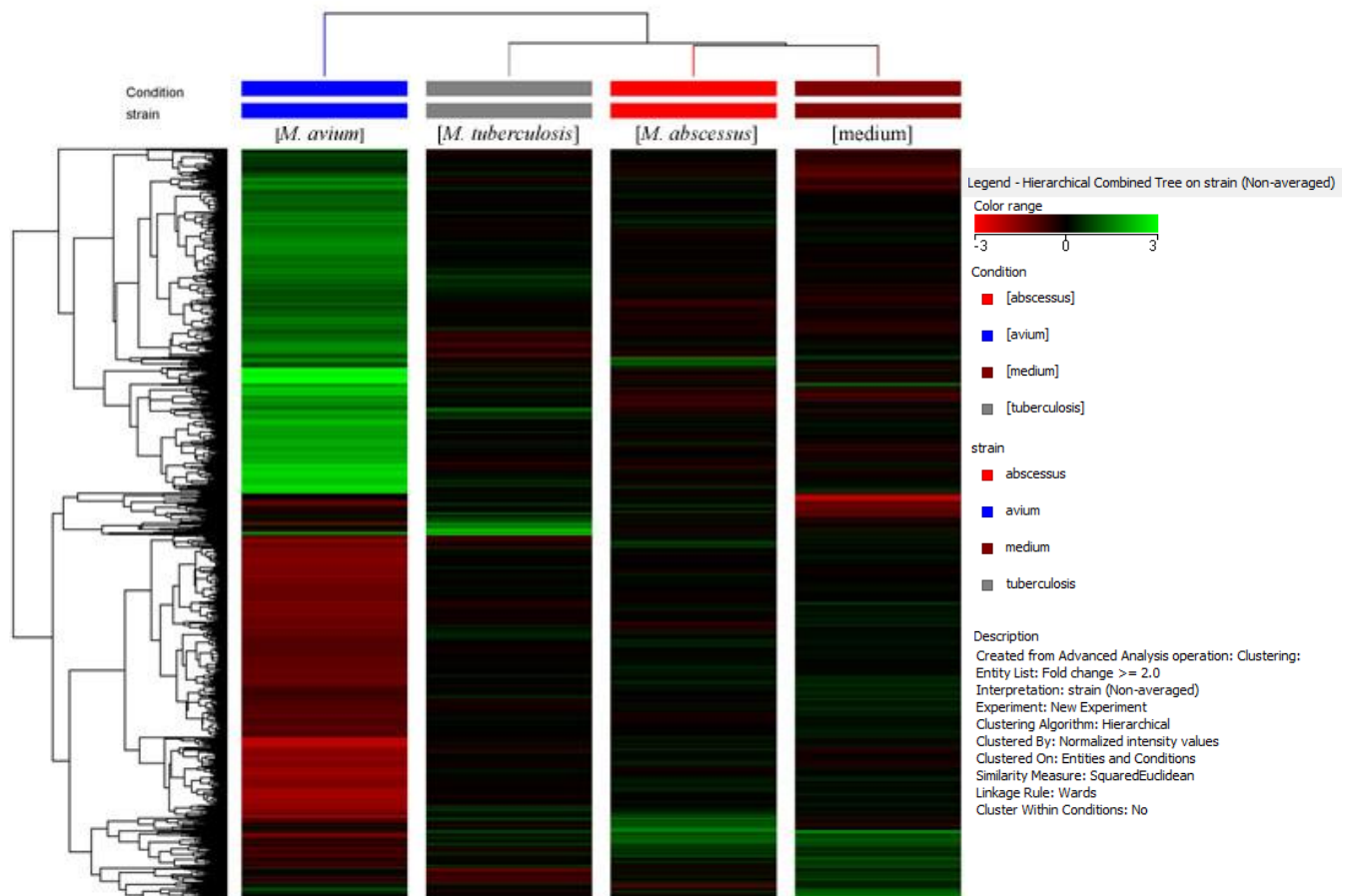


Figure 3-36. Hierarchical clustering of the transcriptomes from *ex vivo* infected human tissues with mycobacteria. Mean values of 3 independent experiments are displayed for each column which represents the different species of mycobacteria (*M. tuberculosis*, *M. avium* and *M. abscessus*) or non-infected tissue samples.

According to hierarchical clustering (**Figure 3-36**), one can see that the expression patterns of non-infected samples and infected samples with *M. tuberculosis* and *M. abscessus* transcriptomes cluster together, indicating they are more similar in their gene expression pattern with each other compared to *M. avium*. Within this cluster, the expressed genes from medium controls and *M. abscessus* show a higher similarity than to *M. tuberculosis*. *M. avium* infected tissues displayed the strongest differences in gene expression compared to all other samples.

3.2.5.b. Transcriptome analysis

In order to determine the individual response to each strain of mycobacteria, a venn diagram from up-regulated genes in 3 species of mycobacteria was created against non-infected control sample's transcriptome (**Figure 3-37**). This diagram displays the amount of genes which are only induced by each mycobacterial species (i.e 840 genes only by *M.*

abscessus) and in the overlapping parts, those genes which are induced by more than one individual species.

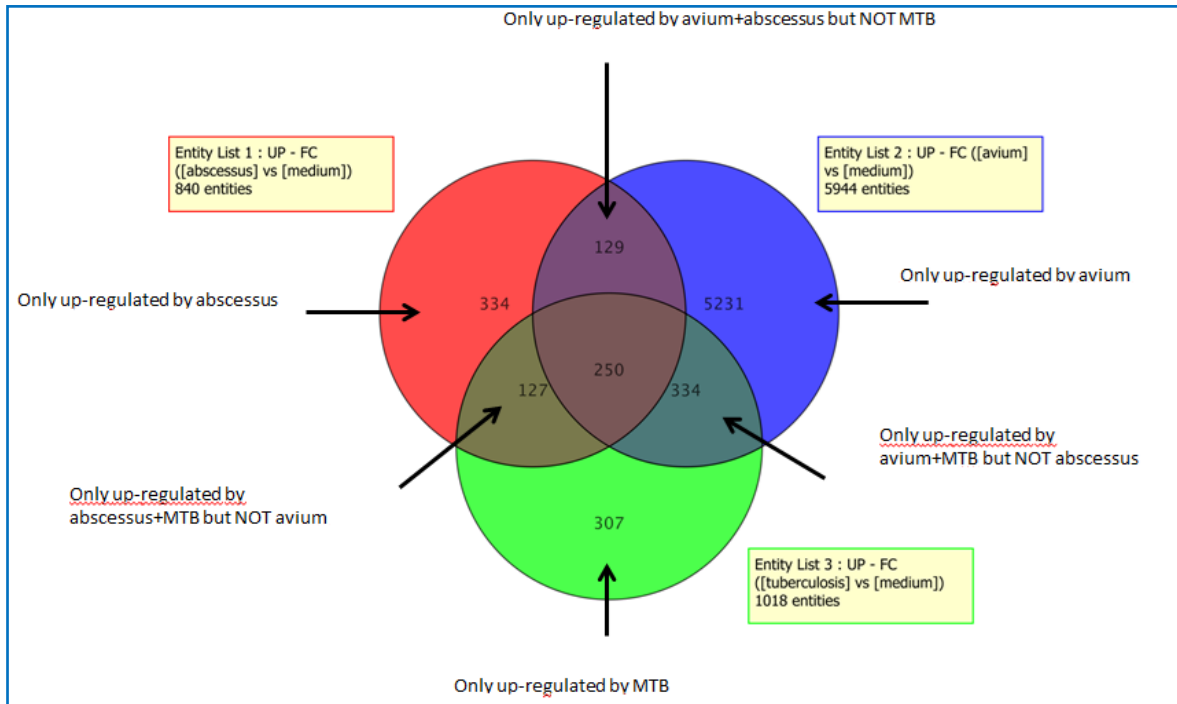


Figure 3-37. Venn diagram from up-regulated genes upon 3 mycobacterial strains (all against medium control).

In sets of *M. abscessus* (red) and *M. tuberculosis* (green) 840 and 1018 genes were found to be up-regulated due to intracellular infection and at their intersection 127 same genes had been shared. In case of *M. avium* (blue) 5944 genes were up-regulated upon stimulation compared to medium control. 5231 of these were regarded as induced exclusively by *M. avium*. Intersections between *M. abscessus* and *M. avium* showed 129 genes induced by both species, whereas between *M. tuberculosis* and *M. avium* 334 genes displayed co-expression. Finally 250 up-regulated genes were found to be induced by all mycobacteria and thus, comprise the core response to these bacteria. Additionally, 334 (*M. abscessus*), 5231 (*M. avium*) and 307 (*M. tuberculosis*) up-regulated genes seemed to be exclusively up-regulated by each strain.

3.2.6. Validation of genes

Among all up-regulated genes upon mycobacterial infection that have been identified by GeneSpring analysis, some candidate genes were validated using immunohistochemical staining of the respective proteins. The chosen genes are *SELE* (E-selectin, also known as CD62E) and *PCDHB16* (Protocadherin β -16), and the representative results are shown in **Figure 3-38**. Both PCDHB16 and anti-human CD62E antibodies appeared to show positive signals in all specimens concerning IHC with membranous pattern in macrophages, pneumocytes-II and bronchial epithelium (**Figure 3-38. A and B**) or in macrophages and endothelium, respectively (**Figure 3-38. C**).

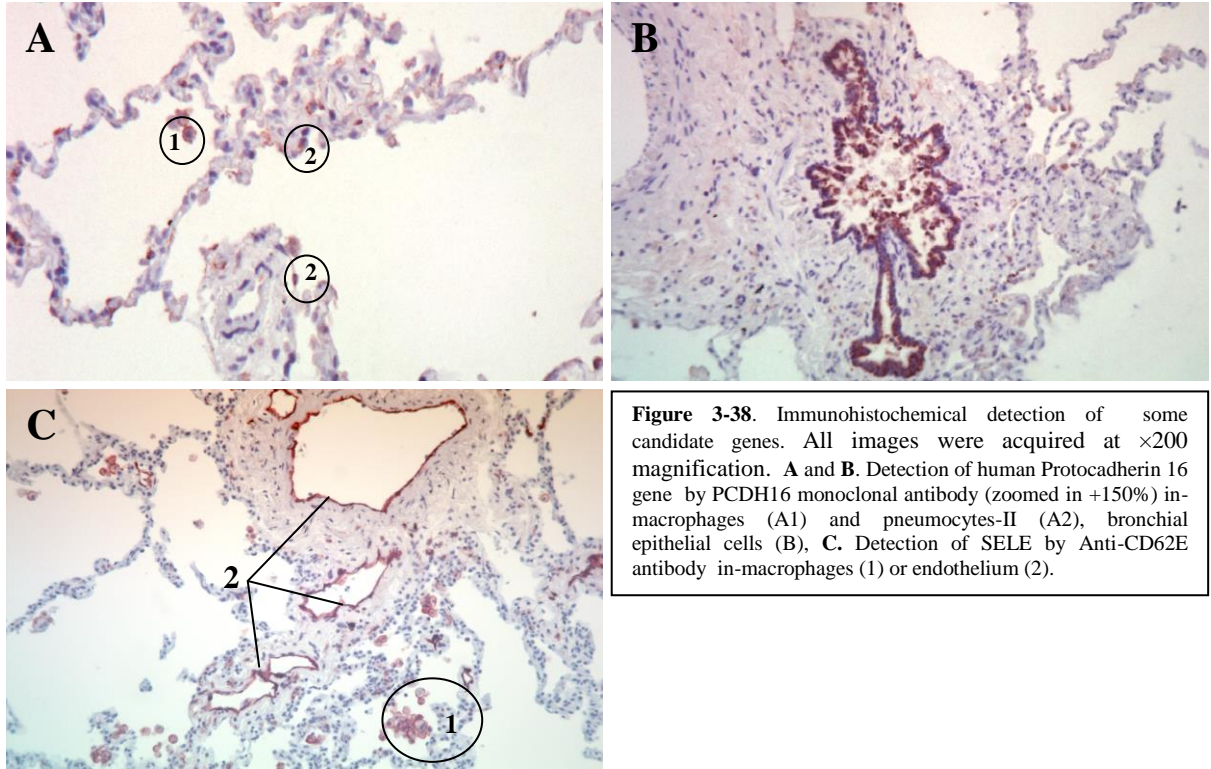


Figure 3-38. Immunohistochemical detection of some candidate genes. All images were acquired at $\times 200$ magnification. **A** and **B.** Detection of human Protocadherin 16 gene by PCDH16 monoclonal antibody (zoomed in +150%) in-macrophages (A1) and pneumocytes-II (A2), bronchial epithelial cells (B). **C.** Detection of SELE by Anti-CD62E antibody in-macrophages (1) or endothelium (2).

4. Discussion

4.1. Establishment of the *ex vivo* STST model for mycobacteria

Mycobacterial infections, particularly tuberculosis, remain a major health threat. At the middle of the twentieth century the total eradication of tuberculosis was considered feasible. In 1986 the downward trend of the incidence rate of tuberculosis reversed, besides nontuberculous mycobacterial (i.e., *M. avium*, *M. abscessus*, *M. chelonae*) diseases increased. The reasons are rather complex, including spread of HIV infection [113], the immigration of people from high-prevalence countries and the deterioration of tuberculosis control [68], the lack of an effective vaccine [114], emergence of drug-resistant forms, lack of sensitive and rapid diagnostics [115], lack of reliable biomarkers, and surprising gaps in our knowledge of these diseases [8]. Nowadays, the long-term goal to eliminate tuberculosis has been set for 2050 [116]. Thus, numerous investigators are using the best tools of modern science to combat mycobacterial infections in many fields.

Interestingly, research on tuberculosis is limited by suitable models. Indeed, many of the mechanisms leading our understanding of the immunopathology of mycobacterial infections have been obtained through animal models, which have provided valuable information about the development of TB. Many different species of animals had been involved in the research of mycobacteria since Robert Koch's period. However, all existing animal models so far fail to mimic the human disease perfectly, since they exhibit some disadvantages including variable patterns of pathological reactions, relative resistances (mice and rats), high costs (non-human primates), or less immunological reagents than humans (guinea pigs and rabbits) [117-121]. For this reason various *in vitro* infection models using human cells have been established [28]. Besides of biosafety concerns, the manipulation of mycobacteria is, however, technically very demanding and the optimization of *in vitro* infection protocols has been difficult. As a result, there are large numbers of variations in the methodology that make it hard to compare and conclude the results of the different research groups [28]. There are various factors that influence to a wide variability in the results obtained from different *in vitro* models, including cell types (monocytes, macrophages, neutrophils, and microglia [84-86, 122]), cell lines (macrophage-like cells and non-phagocytic cell lines [87, 88, 90, 91, 123]), source of donor (human, healthy or patients, and animals [83, 124, 125]), incubation media (containing supplements or not [126, 127]), amount of inoculum [128, 129], and so on. Most of the gathered evidences indicate that it is extremely difficult to induce mycobactericidal activity in purified populations of phagocytes. Therefore some more complex models arose, for instance, co-culture of immune cells [122], whole blood [130], and microenvironment comprising epithelial and endothelial cells [131] as well as methods containing diverse stimuli (cytokines, vitamins, lipids, nucleotides, and so on [132-135]).

Nonetheless, these large variations of results make it difficult to arrive at definite conclusions. In addition, recent studies have suggested that the nature of the infecting bacilli also contributes to the outcome of infection [136, 137]. The exact mechanism underlying mycobacteria dependent differential response is, however, not fully understood.

Hence, it would be valuable to establish a more meaningful model for mycobacterial infection, in which cross-talk between human host and infectious agent can be examined, which maintained the normal architecture of the lung including all cell types, and which allows a comparison of virulent and non-virulent strains.

One of such a model is the *ex vivo* STST (Short-Term Stimulation of Tissues) model, which was established in our group a few years ago [138]. Like another commonly used *ex vivo* model, the precision-cut lung slices (PCLS), the STST closely resembles the morphology and functionality of the intact respiratory tract, and thus bridge the gap between cell culture and animal models [139, 140]. Moreover, both models have been used to investigate the immune response to immunomodulators as well as bacterial or adenoviral infection in the context of respiratory diseases including pneumonia, COPD, or asthma [141, 142]. Especially the STST model has successfully been used with human lung tissue to obtain valuable information of early pathogenesis for several infectious agents of lung diseases, including *Legionella pneumophila*, *Pseudomonas aeruginosa*, *Streptococcus pneumoniae*, *Chlamydia pneumoniae*, *Haemophilus influenzae* since there is no agarose like in the PCLS which might affect the infection [143-147]. Although mycobacteria can affect any organ in the body, 85% of all cases develop the disease exclusively in the lungs. Thus, in the presented study, human lung tissue was used in the STST model and infected with 3 species of mycobacteria, respectively. The achievements of establishment of the model were verified by two main criteria. Firstly, the viability of the tissues was assessed via histopathological analysis, as well as, viability assays (MTT and TUNEL). Secondly, the infection of the tissues was detected via histo- and molecular-pathological methods.

Since the viability of the tissue is a crucial aspect of the study, we determined the viabilities in multiple variations. Throughout histopathological examination, mycobacteria-infected, non-infected, and fresh lung tissues did not noticeably differ, leading to viability assays, which could give numerical measurements. In contrast to mycobacterial infection, the study about *Legionella pneumophila* infection in *ex vivo* model by Jager J et al. observed tissue damages and epithelial delaminations owing to adhesions of the bacteria. The authors concluded that this harmful extracellular adhesion of *L. pneumophila* facilitates bacterial invasion and replication in recruited macrophages [143]. According to both MTT and TUNEL assays in the presented study, all measurements from the *ex vivo* tissues ranged between positive and negative controls, thus, it can be believed that viability of tissues was quite acceptable after overnight incubation. Likewise, the MTT colorimetric assay allowed us to calculate suitable incubation conditions depending on the amounts of tissues per number of pieces per well and volume of medium. In conclusion, 1 piece of tissue (~30 mg) was optimal for the *ex vivo* STST model either in 2 ml or 3 ml medium.

Regarding to TUNEL assay, all *ex vivo* STST samples after an incubation time of 16 h had approximately 7.15% apoptotic cells. Furthermore, the area per nucleus of living cells was larger than dead cells, indicating nuclear shrinkage of apoptosis. Feng Xu et al studied the inflammatory response to *Streptococcus pneumoniae* in the same model system and also performed measurements of apoptosis in lung specimens via TUNEL [148]. After pneumococcal infection, a time-dependent increase of apoptosis in macrophages was observed as compared with the control group (30–50% versus 4–8% [24 h], 40–70% versus 10–15% [48 h]) [148]. Interestingly, the measurements of their control groups are in line with our *ex vivo* samples, but their pneumococci-infected samples revealed much more apoptosis than our presented mycobacterial cases. Among the above cited studies, different incubation times were used, additionally to our 16 h, they performed 2 h, 4 h, 8 h, 24 h, and 48 h time points. Moreover, the size of the lung specimens was up to 1.6 times bigger (0.8-1 cm³) compared to ours. Despite the longer incubation time and bigger tissue samples, they assumed the viability of their tissues to be acceptable. On the other hand, these larger ranges of time points demanding on the generation time of those pathogens, which are more rapid than mycobacteria.

In order to detect mycobacterial infection and other bacterial contaminations, all infected samples were stained with ZN and gram in parallel. We optimized the cold ZN technique/Kinyoun staining by adding Mayer's hemalum for HOPE-fixed, paraffin-embedded tissues. The modification of staining allowed us to receive a good counter-staining, and even gave a chance to distinguish between different infected cells types. As a consequence, all cases of positive ZN staining verified a successful infection. Whereas, all gram-stainings were negative, indicating that the growth of other bacteria could be prevented via the BBL™ MGIT™ PANTA™ antibiotic mixture. During the detection of mycobacteria in all cases, some micro clumps have been found which did not interrupt the successful infection of the *ex vivo* STST model systematically. For further studies, the suspensions of mycobacteria should be better dispersed by adding detergents (like Tween-50 or nonhydrolyzable tyloxapol [149]), or by vortexing with glass beads, or by passing several times through a 25-gauge needle [28]. The molecular-pathological methods, including PCR, real time PCR, and sequencing detected the genetic material of infectious agents in the *ex vivo* tissues.

Once the *ex vivo* model of mycobacterial infection was established successfully, we encountered an interesting question: Since the mycobacteria are non-motile, how deep could the infectious agents infiltrate into the tissues? To address this question, mycobacteria were counted in the different layers of a whole tissue block (~500 µm). The frequency of infected cells in the peripheral slides was comparable lower than in the central parts. It was a kind of surprise, since in fact the peripheral part of the tissues had more contact with the mycobacterial suspension, so there should have been more infected cells. Some possible reasons might be: (1) the infected cells in the peripheral part have been washed away during tissue processing, or (2) there were different sizes of layers

(peripheral apex parts are narrower than middle part), or (3) the phagocytes dispersed into the supernatant owing to chemotaxis. Therefore, supernatants from *ex vivo* stimulation were stored at -20°C for further analysis of chemokines. It would be a subject of following studies. The results might contain a lot of interesting information about the host-pathogen interaction, as well as unknown humoral factors. Previous studies on *ex vivo* infection models have already discovered new mechanism of the early steps of infection by evaluating supernatants [143-147].

Kolja V et al. injected 200 µl of infectious suspensions per 100 mg tissues in order to stimulate lung specimens without destructing the unique lung structures [145]. According to our infectious methodology, the infectious invasion was enough to infiltrate deep into of the tissues. However, we assume that this might also be a promising approach to increase the mycobacterial infection and to reduce the required amount of mycobacterial suspension for further studies. Since there are pores of Kohn, which are 1-12 µm in diameter and permit the communication between adjacent alveoli, slow injection would not be harmful for the microstructure of the lung.

4.2. Findings using the *ex vivo* STST model for mycobacteria

According to the WHO, tuberculosis is still a global public health problem and is estimated to affect 1.7 billion individuals worldwide. Of these latent individuals, only 5–10% will develop active tuberculosis disease in their lifetime. In 2012 about 8.6 million people were affected [12]. On average, one person with smear-positive tuberculosis can infect 10–14 people per year (Tuberculin skin test, TST+), of which 0.6–1.2 individuals develop active tuberculosis. From an immunological point of view, there are some factors related with host factor that determine why some individuals are protected from the infection while others proceed to develop the disease. Epidemiological studies showed that only 20 – 50% of people with latent tuberculosis exhibit a positive TST skin reaction [26, 150-152]. These TST non-responders suggest two alternatives: 1) the individuals were uninfected because of the host resistance, or 2) the infection might have been cleared by the innate immune system.

We are more convinced of the idea about the elimination of mycobacterial infection by the innate immunity. Unfortunately, the power of innate immunity upon mycobacterial infection is usually underestimated because of several reasons. Herein, molecular epidemiological evidence suggests that the original infecting strain can lead to reactivation of TB up to 30 years after the initial infection [153]. Retrospective studies of innate immunity upon mycobacterial infection are, however, not possible, because nobody knows exactly on which day the bacilli have been inhaled. Also, primary and acquired immunodeficiencies (especially HIV infection) had dramatically shown the importance of cellular immunity in tuberculosis. Interestingly, the burden of the TB pandemy lies squarely in the same regions as the HIV pandemy [154]. Mycobacteria cause

granulomatous diseases, which are distinct patterns of chronic inflammation involving delayed type-hypersensitivity (DTH) and cell mediated immune response [92]. Besides of these disease characteristics, many researchers focus on T-cell mediated immunity to create novel vaccines.

There are several lines of epidemiological evidences supporting a role for innate immunity and revealing the mysteries related with innate immunity in tuberculosis. For instance, it is well known that BCG vaccination does not prevent from initial pulmonary infection, but it usually prevents from the progressive disease in children [9, 155]. Also a report by Kagina et al. verified that during BCG vaccination of newborns, the frequency and cytokine profile of the mycobacteria-specific T cell response did not correlate with protection from or susceptibility to the development of TB [156]. Historically in the Lübeck disaster (1929), a virulent strain of *Mycobacterium tuberculosis* was inadvertently inoculated to about 200 newborns instead of the BCG vaccine. The fact that 54% of the infected babies who suffered from the disease and recovered, provided evidence for a potential innate immune response [157]. Obviously, this early infection in neonates cannot be attributed to T-cell mediated immunity since their adaptive immune responses have not yet developed properly. On the other hand, active TB results from either reactivation or reinfection. If the acquired T-cell immunity would be the crucial protective elements against active TB, it could have prevented from an exogenous reinfection [158]. Nowadays, this phenomenon of the removal of mycobacteria by innate immunity is still controversial discussed due to the lack human studies. Hence, with the hypothesis that the innate immune system eliminates mycobacteria, we pointed out functional studies on the initial phase of mycobacterial infection in human lung tissues by using the *ex vivo* STST model. Moreover, since the *ex vivo* STST model represents the complex and proper structural organization of the lung, it is a promising opportunity to explore innate immune response upon mycobacterial infection, and interaction of the cells. Furthermore, it may help to uncover new antimycobacterial mechanisms and unknown humoral factors.

Firstly, all collected lung specimens of patients were infected and showed that the initial host defense mechanism is actively working via phagocytosis without any additional stimulation, unlike *in vitro* experiments [28].

Secondly, we observed that different cell types were infected, including macrophages, neutrophils, monocytes, and type II pneumocytes. The internalization of mycobacteria into neutrophils and type II pneumocytes was a kind of surprise. Because the majority of literature about infectious diseases describe that the inhaled tubercle bacilli engulfed primarily by alveolar resident macrophages followed by interaction between T-cell and macrophages. Personally, I assumed that the main target of mycobacteria are macrophages owing to the rule of infectious diseases “special agent affects on special target” [2, 4, 9, 92].

4.2.1. Monocytes and macrophages

In the presented study, as totally 900 infected cells were counted in each mycobacterial species, macrophages and monocytes were predominantly infected ($85.31 \pm 3.1\%$ and $6.44 \pm 1.1\%$) regardless of the mycobacterial strains ($p=0.539$ and $p=0.761$). This is in line with the literature since mycobacteria are mainly engulfed by macrophages where they circumvent cellular defense mechanisms and replicate. However, the correspondence analysis showed that monocytes had the tendency to be more associated with AB1 and AB2 strains. Therefore, it can be predicted that strains of *M. abscessus* cause acute inflammation with a higher recruitment of leukocytes. Furthermore, we observed some cellular changes induced by mycobacteria in phagocytes (here we do not know the exact origins of the cells whether macrophages, monocytes or neutrophils), including karyopyknosis, karyolysis, and karyorrhexis. Based on statistical performances, we concluded that *M. avium* strains cause significantly more cell injuries. Likewise, a factorial ANOVA for TUNEL assay verified that the AV strains induced more apoptosis. This observation is in accordance with a previous study by Agdestein et al., who characterized the gene expression program triggered by two strains of *M. avium* in human primary macrophages. They demonstrated the induction of pro-apoptotic genes, such as RIPK2, BID, and tBID after infection. Additionally, these two strains induced a strong activation of macrophages and the innate immune responses on the transcriptional level [159]. In general, the mycobacterial virulence depends on the ability of these bacteria to invade, persist, and replicate within macrophages [160]. Likewise, the correlation between apoptosis and virulence of mycobacterial strains is debated [161]. Particularly, even in comparison among Mtb strains, Keane et al. determined that attenuated variants of *M. tuberculosis* are associated with macrophage apoptosis, whereas virulent strains inhibit apoptosis [162]. Thus, we conclude that strains of *M. avium* are less virulent than *M. tuberculosis* based on the induction of apoptosis.

Here, monocytes were recognized only by cellular morphology (size, location and shape of nucleus) and not distinguished from macrophages via molecular pathological methods, which was an inherent limitation of our study. It had been investigated that monocytes phagocytizing *M. tuberculosis* secrete pro-inflammatory cytokines and chemokines, such as IL-1 β , TNF- α , or IL-8 [163-166]. Since monocytes are freshly recruited host defense cells, these events are obvious contributions to an immune reaction. But impressive findings were observed by Shaw et al. about the secretion of IL-10 after phagocytosis of Mtb by human monocytes without blocking autologous IL-8 secretion. The authors concluded that phagocytosis of Mtb by human monocytes displays a specific stimulus to IL-10 secretion [167]. So, it seems that successful removal of mycobacterial infection is terminated by an early anti-inflammatory activity of monocytes to prevent host tissue injury, where adaptive responses have not involved yet.

These hypothesis would solve the following assumptions: 1) generally, once the infection is controlled, it is important that pro-inflammatory responses are down-regulated

to minimize host tissue destruction, in which T cells take place, especially Th2 CD4+ lymphocytes [168], 2) epidemiologically, in the majority of cases within immunocompetent hosts the initial mycobacterial infection is controlled and regressed, leaving behind little to no evidence of past encounter with mycobacteria [8], and 3) an active mycobacterial disease causes certain characteristic lesions [39, 92]. It is clear that these tissue damages are not a direct result of bacterial toxicity, but is largely an immunopathological affects associated with strong immune responses, including DTH and cell-mediated immunity [92].

Needless to say that macrophages were infected by mycobacteria. Instead, it is worth to discuss about the capacity of killing mycobacteria by macrophages, or to use macrophages as positive controls for other professional and non-professional phagocytes, or investigate all of these cell types interactions and co-operations upon mycobacterial infection. We are convinced that tuberculocidal activity of the innate immunity is based on phenomenon that humans are not uniformly susceptible to mycobacterial infection, which may operate independently of acquired immunity. Perhaps, there is a potential of macrophages behind this phenomenon, since they are main target cells. The findings of the presented study support this assumption, which will be separately discussed below in “self-split cell death” part (4.3).

4.2.2. Neutrophils

Among the six mycobacterial strains, overall incidences of infected neutrophils were $4.68 \pm 1.58\%$ in 900 cells. Moreover, correspondence analysis showed that neutrophils were more associated with ABs, indicating AB strains likely induced more neutrophil's migration. Neutrophils -an essential member of the innate immune system- represent the most abundant type of white blood cells (40-75%), however, we observed that the average numbers of infected neutrophils were less than macrophages and monocytes among all mycobacterial strains [169]. Here we have three presumptions: 1) since they are highly motile (recruited to the site within minutes [169]), the majority of them might have dispersed into supernatant; 2) after phagocytosis they have been cleared by apoptosis during overnight incubation (about 16h), which is a nature of neutrophils after competing any pathogen [92], or 3) some of the infected neutrophils have already been counted as karyopyknotic cells in addition to macrophages. Also we previously concluded that AV strains induced more apoptosis and the incidences of infected neutrophils were significantly less in cases of AV strains ($p=0.007$), so it is possible, that neutrophils have been reduced more in the AV cases due to apoptosis during incubation.

Wolbers et al. reviewed that apoptosis is a dynamic process of variable length depending upon a wide variety of factors, such as the cell type, nature of the inducing agent (i.e., intensity, exposure time), an involved pathway of apoptosis and the measured parameters [170]. For instance, the average duration of a single retinal cell undergoing apoptosis, as judged by the duration of annexin 5 labeling, was around 60 min, ranging

from 30 to 100 min [171]. In the Jurkat T cell model, apoptosis has been initiated after 4 h treatment and was conspicuous between 6 and 20 h [172]. We don't know the exact duration time of apoptosis in neutrophils induced by phagocytizing mycobacteria. It should, however, be quicker than overnight, but should be elucidated in a further separate *in vitro* study.

Theoretically it is well known that neutrophils have a short lifetime (in tissues 1–2 days) and are inherently pre-programmed to die by constitutive apoptosis in order to minimize intracellular propagation and parasitize of pathogens [173, 174]. Therefore, it seems that the mycobacterial strategy to survive within host cells by inhibiting apoptosis does not work in neutrophils. Unlike neutrophils, macrophages exhibit a long life span and provide a nice opportunity for mycobacteria to shelter. Here is the mystery of innate immune system upon mycobacteria based on nature of neutrophils. On the other hand, it has been observed that mycobacteria in apoptotic bodies were eliminated, since they were not able to inhibit the phagolysosome fusion from the inside, when they are engulfed by fresh phagocytes [175]. In order to verify this hypothesis, a co-culture of neutrophils and macrophages or a step-by-step culture (first neutrophils, then macrophages) infected with mycobacteria followed by a mycobacterial viability assay should be performed in further studies.

Besides of apoptosis, there are some evidences showing intrinsic mycobactericidal capacity of neutrophils. However, most of the available knowledge regarding mycobacteria has been gained by studying macrophages. It is still little known how the neutrophils act upon mycobacteria. Generally, neutrophils are primary responders in host defense against any invading pathogens and destroy them by both oxidative and non-oxidative mechanisms, either through phagocytosis of the microorganisms itself or through extracellular release of microbicidal granules [176].

Yang CT and co-workers established an optical transparency zebrafish model to monitor neutrophil behavior upon mycobacterial infection. The obtained results provided that neutrophils rapidly kill the internalized mycobacteria through a NADPH oxidase-dependent mechanism [177] and the NADPH oxidase complex assembles on the phagosomal and plasma membranes and initiate ROS cascade [178, 179]. On the other hand, the importance of oxidative mechanisms in neutrophils is clearly seen in chronic granulomatous disease (CGD), also known as Bridges–Good syndrome. This disease is caused by mutations rendering the NADPH oxidase nonfunctional, which results in a poor ability of neutrophils to kill any microbes and thus makes these patients susceptible to many infections including tuberculosis and autoinflammation [180].

Likewise, after using free-radical inhibitors, Jones et al. demonstrated that neutrophils could eliminate *Mycobacterium tuberculosis* independent of the oxygen metabolic burst (a nonoxidative process) [181]. This observation associated with nonoxidative processes is in accordance with a study by Kisich et al., who reported that defensins – cationic antimicrobial proteins – are important to eliminate intracellular mycobacteria in neutrophils. This leads to the conclusion that human neutrophils are

potential defense mechanisms against mycobacterial infection [182]. In microbiological media, the human neutrophil isolated peptides (HNPs) 1–3 killed *M. tuberculosis*. Moreover, the purified neutrophil cathelicidin LL-37 and lipocalin 2 restricted the growth of the mycobacteria [183]. A study by Majeed et al., indicated that neutrophil-mediated killing of mycobacteria is a Ca^{2+} -dependent process [184].

In our point of view, these variabilities in mechanisms are associated to the receptors used for recognition and phagocytosis triggering different intracellular cascades. Nevertheless, any of these mechanisms seem to be adequate in order to eliminate mycobacteria unlike macrophages. In case of macrophages, the fate of engulfed mycobacteria depends on receptors involved in phagocytosis and recognitions. For instance, survival of *M. tuberculosis* after binding to complement receptor-1 (CR1) is better than after binding to CR3 or CR4 [127, 185]. Epidemiological reports reflected that neutrophils contribute substantially to the innate resistance of TB infections. Particularly, the prevalence of tuberculosis among blacks is known to be about twice that among whites [186]. Because they have lower neutrophil counts and lower circulating concentrations of HNP1–3 and lipocalin 2 than south Asian and white people, showing the great importance of neutrophils for the prevention of TB [183].

Even later in the period of acquired immunity, it is recently noticed that neutrophils play an active role in active TB patients based on infected neutrophils found in lung surgery material, bronchoalveolar lavage specimens, and advanced cavitory lesions obtained by post-mortem examination [187, 188]. Consistent with these histological findings Berry and colleagues have identified 393 transcript signatures for active TB in whole-blood. Their modular and pathway analysis revealed a dominant neutrophil-driven interferon (IFN)-inducible gene profile [189]. Next question would be how or why innate immune cells are recruited so late. On the other hand, interaction of tubercle bacilli with pulmonary epithelial cells and monocytes resulted in a rapid influx of neutrophils [182, 190-192].

We suppose that the main mechanism is interleukin 8 (IL-8), which is a potent neutrophil attractant. It is also known as *neutrophil chemotactic factor*, and induces chemotaxis, phagocytosis, as well as series of physiological responses in neutrophils (increases in intracellular Ca^{2+} , exocytosis, and respiratory burst) [7]. Since IL-8 can be secreted by any cell with toll-like receptors (TLR), macrophages can also contribute to IL-8 levels during mycobacterial infection, because: 1) they recognize mycobacteria by TLR2, TLR4, TLR9, and 2) they participate during whole mycobacterial infection. We assume that this is the reason why neutrophils participate still in the late period in mycobacterial lifelong infection, because of prolonged production of IL-8 from macrophages. Interestingly, following antituberculous treatment, concentrations of IL-8 remain elevated in alveolar lavage fluid and serum for months [193, 194]. Therefore, it can be predicted that these potential killer of mycobacteria makes an impact on a successful therapy in addition to the main therapeutic mechanism.

4.2.3. Pneumocytes-II

It is always described that inhaled infected droplets with mycobacteria reach eventually the alveolar space, where engulfed by alveolar macrophages developing disease. In fact, the chance that mycobacteria encounter an alveolar epithelial cell (account for 60% of the alveolar lining cells [176]) is significantly greater than an alveolar macrophage (50-100 macrophages per alveolus [195]). Moreover, Bermudez et al. calculated that the number of pneumocytes type II surpasses up to 30 times the number of macrophages [131]. From this fact arose the hypothesis that mycobacteria can contact to pneumocytes type II upon arrival into alveolar space. This hypothesis had been claimed successfully via *in vitro* infection models with cell lines (i.e., HeLa cells [196], A549 [91]).

In our *ex vivo* study, infection of pneumocytes-II exhibited $3.53 \pm 2.25\%$ in a total of 900 infected cells among six mycobacterial strains. Infected pneumocytes-II were more common in TB strains as demonstrated by correspondence analysis. We are in doubt with the following variations regarding frequency of differences associated with strains: 1) perhaps, during overnight incubation, AB and AV strains induced more cell death to pneumocytes-II, 2) perhaps, the features of TB strain's cell walls are more affinity to the receptors in pneumocytes than AB, AV strains' cell wall, which facilitate phagocytosis. On the other hand, Feng Xu et al., studied the inflammatory response of *Streptococcus pneumoniae* in the same model system and observed that after 24 hours incubation, *S. pneumoniae* was predominantly detected in alveolar macrophages compared to pneumocytes-II [80-90% versus 15-30%]. Interestingly the authors also noticed that 48 hour-stimulation increased the infection rates of pneumocytes-II [148]. It seems to be that the internalizations of pneumocytes-II are slow, since they are considered as non-professional phagocytes. Of this special interest, we infected non-professional phagocytes (primary pneumocytes-II) and compared them to professional phagocytes (primary alveolar macrophages) *in vitro* by H37Rv, respectively, in order to see the capacity and rate of internalization, as well as, to compare the replication of mycobacteria within these cells.

Regarding the initial invasion (4 hours), macrophages engulfed about 5.5 times more mycobacteria than pneumocytes-II both at MOIs of 1:1 and 3:1. On the contrary, with a MOI of 10:1, mycobacteria up-taked by both cell types almost equally (macrophages $2.82 \pm 1.1\%$, pneumocytes $2.6 \pm 0.08\%$). Here we were faced with some drawbacks: 1) we don't know whether a single cell engulfed single bacilli or several bacilli, 2) we don't know whether either apical or basolateral domains of pneumocytes-II membrane was used to connect with bottom part of wells, because they are polarized cells. If the apical part, which is more active for endocytosis and exocytosis facing to alveolar lumen, participated for seeding, then endocytosis can be limited.

Also in the further studies, after inoculation the wells should be centrifuged at low speed for few minutes to increase the contact between pathogen and pneumocytes-II by settling to the bottom. We assume that low concentration of bacilli can be still dispersed

into suspension and float during stimulation, whereas cells are already connected with the bottom of the wells and diameter of pneumocytes are smaller than macrophages [$\sim 10\mu\text{m}$ versus $12\text{-}40\mu\text{m}$ [195, 197]. Therefore, if during incubation the bacilli were not able to encounter with pneumocytes-II properly, the comparison of phagocytosis activity of these cell types may not be accurate. In our study with a MOI of 10:1, mycobacteria invaded into pneumocytes-II with an efficiency of $2.6\pm 0.08\%$, which correlates well with a study by Bermudez et al. Here, they reported that *M. tuberculosis* invaded A549, a “type II-like” alveolar cell line, with an efficiency of 2-3% [131].

In their previous study, however, the infectious efficiency of the virulent strain (H37Rv) was $4.7\pm 1.0\%$, which was higher than the non-virulent strain (H37Ra) as well as *M. avium* [$3.1\pm 0.8\%$ and $2.1\pm 0.9\%$], even after 2 hours [91]. Perhaps it depends on protocols, likewise, it is the clue why we observed less infection of pneumocytes in AV and AB strains than TB strains. Sato K and coworkers analogized infection of *M. tuberculosis* and *M. avium* to A549 cells, and concluded that the invasiveness into alveolar epithelial cells was in order of the virulence [198]. Interestingly, in the previous study by Bermudez et al., a MOI of 100:1 in addition to MOI of 10:1 was used. However, the amounts of intracellular bacilli were not well comparable [$5.7\pm 1.6\%$ versus $4.7\pm 1.0\%$]. Thus, we presume that the capacity of phagocytosis in pneumocytes-II might be limited because of their main secretory function. Particularly, each pneumocyte-II contains about 150 lamellar bodies, which have a mean diameter of $1\ \mu\text{m}$ [195]. As comparing differences between MOIs, more intracellular bacilli were counted at MOI 3:1 than MOI 10:1 within pneumocytes-II. Thus, if pneumocytes-II have any limitation of endocytosis, the threshold can exist between concentration of 3:1 and 10:1.

About the replication of intracellular bacilli within these cell types, at the beginning we focused on a MOI of 10:1, where no differences in engulfment between cells were detectable. Mycobacteria decreased within pneumocytes-II, but increased about 3 times within macrophages after 7 days, as well as, Chi square test verified high association between cell type and bacterial growth. As concerning all MOIs, intracellular mycobacteria decreased in pneumocytes-II in all cases. Whereas in case of macrophages, finally all MOIs exhibited increase of bacilli though [7 days], at low MOIs (1:1 and 3:1) intracellular bacilli decreased initially [3 days] in accordance with Lurie’s fundamental studies in rabbits [199]. So, our results suggest that 1) intrinsic mycobactericidal capacity might be enough in both cell types when they encounter single bacteria or few bacilli, 2) the mycobacterial survival strategies do not work in pneumocytes properly, and 3) after 7 days, there was an abrupt decrease of intracellular bacilli within pneumocytes [MOI 10:1], suggesting association between viability of cell and mycobacterial growth. Therefore, in subsequent studies, multi-viability assays should be performed daily for both host cells and pathogens in order to determine whether death of pneumocytes-II (either due to mycobacteria or other causes, i.e., age, inability of adaptation to *in vitro* environment) can influence the survival of intracellular mycobacteria. Moreover, there is a controversial

issue about isolation and culture of type II pneumocytes, which should be considered in the further studies. In particular, it is said that the *in vitro* environment triggers the differentiation of pneumocytes-II to pneumocytes-I [200], whereas, some authors reported that pneumocytes-II undergo cytoarchitectural change *in vitro*, therefore, culturing on Engelbreth-Holm-Swarm tumor basement membrane or contracted collagen gel maintains the cuboidal shape the cells [201, 202]. However, in a following study the counted intracellular bacilli should be compared with the concrete generation time in order to elucidate whether there is any certain balance between bacterial growth and host defense. Also only mycobacteria, which are in log phase (also known as exponential phase of bacterial growth), should be used for studying replication within these cells.

Danelishvili and coworkers carried out an apoptosis pathway-specific cDNA microarray analysis of “type II-like” alveolar epithelial cells (A549) after mycobacterial infection [128]. They concluded that the cytotoxicity of these cells was the result of necrosis, not apoptosis [59% versus 14%]. This research team also examined the influences of apoptosis by using staurosporine and rifampicin to block protein synthesis. In conclusion, virulent *M. tuberculosis* blocks staurosporine-induced apoptosis. Moreover, when the protein synthesis of bacilli was inhibited via rifampicin, the host cells’ apoptosis increased. On the other hand, Dobos et al. demonstrated that cytotoxicity of pneumocytes-II is specific to virulent mycobacterial infection leading to cellular necrosis, which is characterized by cell permeation [194]. Also inactivated bacilli or its subcellular fractions did not result in this necrosis. Likewise, this mycobacterium-induced necrosis did not correlate to higher levels of growth (both intracellular and extracellular) or the expression of host cell factors [203]. It is likely that the inhibition of apoptosis is an active process of mycobacteria and that an induction of necrosis results in the release of viable mycobacteria. This is not regarded as a host defense mechanism but as a means of the pathogen to induce maximal pathology to allow transmission.

Puzzled by this phenomenon, the question rises whether there is any benefit for mycobacteria to destroy their shelters. Is it a kind of amensalism leading to extracellular transmission for exchanging short-aged cells or to disseminate hematogenously after destroying the intact alveolar wall? Or is it a kind of synnecrosis because of inadequate endosymbiont? Perhaps it would become clear after distinguishing which kind of necrosis happens and performing parallel determination of viability assay for both host cells and pathogens.

Next unclear questions are which mechanisms of endocytosis are responsible for the mycobacterial internalization into pneumocytes-II? How many mechanisms associated with mycobacterial ligands and pneumocytes’ recognitions are available? If there are some, do they influence intracellular mycobacterial occurrence? Because mycobacterial fate within macrophages somehow depends on receptors linked to intracellular pathways [127]. Bermudez et al. reported that the internalization process was performed by vitronectin and β -1 integrin receptors, following actin microfilaments and microtubules-mediated

mechanism. In addition, usage of caffeine -an inhibitor of pinocytosis- verified pinocytosis was not involved as a mechanism of internalization. In our point of view, it is obvious, since the size of mycobacteria is larger than 150 nm, which is possible for pinocytosis [176]. Anyway, after complete discovery of all interaction mechanisms between pneumocytes-II and mycobacteria, it would be worthy to discuss intrinsic capacity of tuberculocidal activity in pneumocytes.

On the other hand, undoubtedly their secretory contribution can be valuable upon mycobacterial infection, once their cytoplasm rich in lamellar bodies (containing many surfactant proteins, lysosomal enzymes, cytokines, and chemokines), that's why they were originally called "granular pneumocytes" in former time [169, 176, 195, 204]. Therefore, we performed real time-PCR in order to evaluate secretion of some pro- and antiinflammatory factors (Wnt3a, MCP-1, TNF- α , VEGF-A, CCL4, hIL6, CXCL10, LNC2/ NGAL). Although some of them were consistent with previous studies results [192, 198, 203, 205], we considered repetitions of the experiments due to high variance of data. Personally we appreciated a great idea of Sato and coworkers who infected macrophages and A549 cells in dual-chamber culture system separated by Millipore filter. Their results dramatically showed that modulatory humoral effects of infected pneumocytes-II activated sufficiently macrophages to eliminate their intracellular mycobacteria [198].

4.2.4. Other cell types

The structural complexity of the *ex vivo* STST model is not limited by the above mentioned cell types. Some researchers studied the roles of thrombocytes, eosinophils, endothelia, and fibroblasts in mycobacterial infection, respectively. Since our model system contains all these components, they should not be overlooked in further studies. For instance, Khechinashvili et al. hold the view that platelets are involved in the immune processes, particularly in case of tuberculosis. They compared the ultrastructures of thrombocytes in three groups of people, including acute tuberculosis, chronic tuberculosis, and healthy subjects. The authors concluded that acute and chronic forms of pulmonary tuberculosis were associated with different changes in the platelet morphology, resulting in a different functional activity [206]. According to the nature of platelets, after loss of integrity of blood vessels they immediately activate changing their own characteristics drastically and perform multi-functions [207]. Thus, the three dimensional cut *ex vivo* model of human tissue can contain activated thrombocytes, which might contribute to immune response upon mycobacterial infection and should be considered in future studies. Furthermore, there are accumulating incidences that eosinophils are also involved in the mycobacterial infection in a different number of ways. Herein, cell composition of granuloma formation in response to *M. tuberculosis* infection includes eosinophils in addition to macrophages and lymphocytes. The peripheral blood of patients with pulmonary tuberculosis often contains excessive amounts of eosinophils [208]. It was shown that eosinophils present TLR-2 on their surface, through which these cells interact

with *M. tuberculosis* resulting in the release of α -defensins and eosinophilic peroxidase. These enzymes initiate cell wall injury and lysis of mycobacteria [209]. Additionally, Hernandez-Pando et al., found mycobacterial DNA from non-phagocytic cells, including epithelial, endothelial, and fibroblasts from latent individuals who died due to other circumstances [210].

4.3. “A self-split cell death” is a potential host defense mechanism of eliminating mycobacteria

In the presented findings, one of the infected cell types – counted as lymphocytes – could not be proved via serial and double stainings. Therefore, it was presumed that they represent the progressive cellular shrinkage of phagocytes. We also observed that among all types of cellular changes, some infected cells underwent measurable shrinkage, which was characterized by a round shape without blebbing and nuclear fragmentation (unlike apoptosis), high condensation of cytoplasm and nucleus. Their cytoplasmic and nuclear diameters were approximately 1.69 times and 1.75 times smaller (Mann-Whitney U test, $p < 0.001$), respectively, than non-infected normal cellular measurements. Furthermore, light density of these pyknotic cells was 4.15 times darker than the normal cells (Mann-Whitney U test, $p < 0.001$) differing from cellular swelling or vacuolar degeneration. While N/C (nucleus:cytoplasm ratio) of infected and non-infected cells did not differ ($p = 0.642$), the cellular shrinkage involved both compartments – nucleus and cytoplasm.

The observation of progressive shrinkage of infected cells with high density supports the assumption that this cellular morphological change can be a kind of cell death induced by mycobacteria. So far, around 15 kinds of cell deaths have been identified. Among these, the above described cellular morphology is in accordance with a self-split cell death, also known as autoschizis. With the assumption that these morphological changes are related to autoschizis, we verified that alveolar macrophages demise via self-split mechanism by using combinations of vitamin C (VC) and K_3 (VK) at their 90% level of cytotoxic dose. Although, VC and VK are traditionally perceived as antioxidants, they can act as pro-oxidants [211, 212].

Autoschizis was initially observed by Gilloteaux J et al. [213], but it remained without a name until Gilloteaux created the term “autoschizis” since the cells seem to cut themselves [214]. As in case of apoptosis, the various stages in autoschizic cell death were initially determined by light microscopy [215]. Thereupon, the ultrastructural features and molecular mechanisms have been described in detail by further studies [213, 214, 216, 217]. Briefly, the main mechanism of self-split cell death is oxidative stress. Thus, the morphological changes are characterized by membrane damage due to lipid peroxidation. Therefore, organelle-free cytoplasm progressively diminishes through a series of self-excisions until one-half to one-third of the cells’ original size. Also the nucleus becomes smaller; most organelles surround a small intact nucleus in a narrow rim of cytoplasm.

Likewise, the authors illustrated six sequential steps in autschizis based on ultrastructure [214, 216, 218].

This was also observed in our presented measurements (Spearman's correlation matrix), showing a significant correlation of nuclear and cytoplasmic size changes with the nuclear ($\rho=0.628$, $p<0.0001$) and cytoplasmic light densities ($\rho=0.234$, $p<0.001$), as well size changes of nucleus and cytoplasm together ($\rho=0.894$, $p<0.0001$). Furthermore, the linear regression equations of these correlations were calculated. Herein, the equation for cytoplasmic size and its light density (LD) was $\hat{Y}=-1.581E-016+0.214*X+0.069$, for nuclear size and nuclear LD was $\hat{Y}=1.045E-015+0.601*X+0.057$, and for cytoplasmic size and nuclear size was $\hat{Y}=1.247E-015+0.846*X+0.53$. With these equations stages of shrinkage can be calculated, as well as the degree of cytoplasmic density.

Up to now, the majority of studies concerning autschizis deal with neoplastic cells, such as melanoma cells [219], neuroblastoma cells [220], oral tumor cell lines [212], prostatic carcinoma cells [215] or, ovarian carcinoma cells [221], which leads to the suggestion that this type of cell death might be interesting for novel antitumor therapies. Besides, the self-split cell death also has been found in normal cell, such as platelets [222], pancreatic acinar cells [223], neuroectodermal cell line [211], hepatocytes [224], leukemic cells [225, 226], endothelial cells [218], nerve tissue [227], and synovial cells. On accounts of these studies, cytotoxic doses of the vitamin combinations (at 100:1 ratio of VC:VK) were lower than 6000 μM :60 μM for normal cells, and even lower < 500 μM :5 μM for tumor cells. Unlikely, in our study the cytotoxic dose of the vitamin combination was 8313 μM :83.13 μM for primary alveolar macrophages. We assumed that these higher concentrations for primary professional phagocytes depended on their enzymatic system. For example in case of tumor cells, it is known that they have deficiencies in detoxifying enzymes owing to their low differentiation [228, 229].

Moreover, as reviewed in the citation [230] there are increasing evidences that oxidative stress is involved in several human diseases, including atherosclerosis and related vascular diseases, degenerative diseases, immunologic disorders, cellular storage diseases, and even the aging process. Infectious diseases are also associated with oxidative stress in a number of ways. As confirmed by Phanka and colleagues [231], the reactive oxygen species (ROS) display a host defense mechanism to kill pathogens (as an actively initiated process) though, some infectious agents can attribute to generate reactive species (as an unwanted process). It is noteworthy that ROS created via both pathways can be further propagated as an uncontrolled process leading to oxidative stress. Especially the peroxidation of lipids is the most relevant process of ROS propagation. [232]. Depending on the level of reactive oxygen and lasting oxidative stress, it can cause cell death (apoptosis, necrosis, pyroptosis, necroptosis, and autschizis), and tissue damage [233-236].

Virulent mycobacteria have the ability to survive within macrophages using diverse strategies. Crucial is the inhibition of apoptosis of macrophages due to protect their replicative niche. Inhibition of maturation of phagosome-lysosome is a further strategy [237]. Apoptosis is an innate defense mechanism against intracellular bacilli, however, Lee

et al. induced apoptosis in infected macrophages via TNF- α and demonstrated a reduction of viability of virulent mycobacteria [129]. Whereas the elimination of attenuated mycobacterial strains during host cell's apoptosis is well documented [128]. Further, Lee and colleagues found a special kind of cell death induced when infecting macrophages with a high MOI of virulent mycobacteria (>20 mycobacteria per macrophage) [238]. They elucidated all features of the cell death and differentiated from other types of cell death. Their scanning and transmission electron microscopic outcomes were similar to autschizic changes demonstrated in tumor cells by Jamison et al. [239]. The authors also demonstrated that lysosomal membrane permeabilization followed by widespread destruction of lipid bilayers and concomitant degradation of several phospholipid species preceded the macrophages' cell death. Moreover, the cytosolic pH decreased, cytochrome C levels increased, and the dying cells were positive for propidium iodide (PI). The discrimination from other cell types was verified by absence of caspase-1, activated cathepsin B (indicate no pyroptosis), TNF- α and caspases (indicate no apoptosis). In addition, ultrastructural features differed from classical necrosis, including no cell swelling, osmotic lysis and pore formations [239]. On the other hand, Ervin E et al. [240] worked on co-incubation of tumor cells with an annexin V-FITC/PI mixture following exposure of vitamin combinations. As a result, the dual-labeled cells are the necrotic cells, the annexin-labeled cells displayed the apoptotic cells, and PI-labeled cells represented the autschizic cells. Hence, all findings of atypical cell death induced by mycobacteria hold autschizic characteristics. But the authors referred these as an atypical death because of exclusion of apoptosis, necrosis, and pyroptosis. They also predicted that this cell death might provide a mechanism for viable bacilli to exit host macrophages for spreading. In our point of view, the host cell's death, in which oxidative stress involves overall the cell, could be high efficient to kill intracellular bacilli. There are several lines of evidences which indicate that killing of mycobacteria via single members of ROS (herein, nitric oxide [241], peroxide [242] and reactive nitrogen intermediates [243]). Even, Bocchino M et al. have shown that mycoacteria in apoptotic bodies were eliminated, when they are engulfed by fresh phagocytes [175]. It is remarkable evidence, showing that mycobacteria can be killed within macrophages, when they can not inhibit phagolysosome fusion. In future studies, the induction of autschizis with vitamin combinations (at 100:1 ratio of VC:VK) in infected macrophages followed by a viability assessment of intracellular mycobacteria, should be investigated.

On the other hand, curing TB requires a prolonged combination of antibiotherapeutics. Antibiotics as well as antiviral drugs are metabolized by the cytochrome P450 system, which is an important source of hydrogen peroxide [244]. The resulting overproduction of hydrogen peroxide significantly leads to the development of oxidative stress. Therefore, it can be predicted that the oxidative stress induced by multi-drug treatment upon mycobacteria has an impact on the successful therapy in addition to the main therapeutic mechanism.

Likewise, Deshmane et al., [245] firstly revealed a link between AIDS and oxidative stress via the hypoxia-inducible factor 1. Thereupon, other researchers reported

some diseases in which hypoxia takes place, herein, atherosclerosis, autoimmune diseases, malignant tumors, as well as some infectious diseases, including influenza, viral hepatitis, and tuberculosis. In tuberculosis cases, Nickel and colleagues concluded that a hypoxic microenvironment, which is characteristic for infected tissue, supports the efficacy of antimicrobial immunity by the regulation of the antimicrobial peptide human β -defensin-2 (HBD-2) [246]. Several lines of evidence indicate that oxygen restriction is beneficial for the clinical outcome of tuberculosis. For example, the infection in rabbits with low oxygen supply was markedly mild in comparison with the control animals maintained in open cages [247]. Interestingly, the prevalence of tuberculin skin test positivity in humans was reduced in mountain villages compared with control villages at sea level, indicating that innate immune responses cleared the pathogen more efficiently in a hypoxic environment [248]. Thus, it can be supposed, that this is the reason of mycobacterial lesions found in the highly oxygenized apex of the human lung.

Firstly, the *ex vivo* STST model had a reflection of oxidative stress, which was cellular change. Secondly, although it needs to be proven in further studies, the model might be feasible to assume a hypoxic microenvironment owing to some reasons. Herein, 1) less oxygen exchange during incubation with 5-10% CO₂ in closed wells, while air has 0.04% of CO₂, 2) we incubated tissues in liquid, it is well known that oxygen levels are much lower in water [7], 3) the transport of oxygen from air to liquid is required certain partial pressure, which is not involved in the incubation condition. Thus, by using *ex vivo* STST model the biomarkers for killing of intracellular mycobacteria can be explored.

When oxidative stress is actively initiated, the expression of some enzymes is up-regulated such as myeloperoxidase, NADPH oxidase, and nitric oxide synthase. Also reactive species can be generated among others, by cytochrome P450, some metals, and xanthine oxidase. Sanchez-Lopez et al. studied on cross-link between oxidative stress and inflammation biomarkers in the blood of patients with Huntington's disease [249]. As a consequence, the authors concluded that the expression of myeloperoxidase, NADPH oxidase, and nitric oxide synthase enzymes serves as a suitable marker for inflammation which involves oxidative stress. Also other biomarkers associated with anti- and pro-oxidant status are ascorbic acid, malondialdehyde, 8-OHdG and so on [250, 251]. In hope that there were appropriate or validated biomarkers of protective immunity to tuberculosis which may help us in the development of new vaccines or treatment regimens. So we would like to recommend that after successful therapy of mycobacterial infection or after inducing primary infection in experimental animals or for searching tuberculocidal activity of host defense, these markers should be checked in the future.

Summary

Research on mycobacterial infections is limited by the models available. Particularly, many different species of animals had been involved since Robert Koch's period, however, all existing animal models fail to mimic the human disease perfectly. Hence, *in vitro* studies with human cells had been established. Unfortunately, optimization of *in vitro* infection protocols has been difficult due to biosafety concerns and manipulations of mycobacteria. As a consequence, there are large variations in the methodology that make it hard to summarize the results obtained by different research groups. Likewise, the majority of the experiences faced with the problem of difficulties to induce mycobactericidal activity in purified populations of phagocytes.

On the other hand, until clinical manifestations of tuberculosis is present it lasts up to 30 years after primary infection. That's why early stage of mycobacterial infection is still unclear in humans. There are several lines of epidemiological evidences supporting the role of innate immunity, which may prevent from mycobacterial infection.

Therefore, the purpose of the study was to establish a human *ex vivo* tissue culture model for the initial phase of mycobacterial infection. We are convinced that this novel model allows to explore: 1) cross-talk between human host and infectious agent, 2) since tissue specimens contain normal architecture of the lung, all cell types' interactions and co-operations upon mycobacterial infection can be elucidated, 3) usage of 3 different mycobacterial species may help to compare more virulent and more avirulent strains, 4) our model allows us to characterize the early innate immune response to mycobacterial infection, 5) short-term stimulated vital lung tissue fixed by the HOPE technology gives a chance to obtain high quality of nucleic acids and to investigate genes on mRNA level from a genome-wide expression profile upon mycobacterial infection.

The achievements of establishing the model were verified by two main criteria, including the viability and infection of the tissues. All collected patients' lung specimens were infected, indicating an initial host defense mechanism that is actively working without any additional stimulations. We observed that infections of different cell types (macrophages, monocytes, neutrophils, and pneumocytes-II) and some cellular changes (karyopyknosis, karyrrhexis, and karyolysis) are induced by mycobacteria. Furthermore, cell injuries and exposure of cell types were significantly dependent on mycobacterial strains significantly.

While inspecting gene expression patterns of tissue responses upon mycobacterial infection, the differences in upregulated genes associated with mycobacterial strains were found and the identified candidate genes are currently being validated.

Bibliography

1. EUZÉBY, J.P. *LPSN (List of Prokaryotic Names with Standing in Nomenclature)*. 24 September 2013 [cited 1998 28 January]; Available from: <http://www.bacterio.net>.
2. Gandadharam PRJ, J.P., *Mycobacteria: Basic aspects, Chapman & Hall Medical microbiology series*. 1998, New York, USA: International Thomson Publishing.
3. Tortoli, E., *The new mycobacteria: an update*. FEMS Immunol Med Microbiol, 2006. **48**(2): p. 159-78.
4. Kenneth Ryan, C.G.R., Nafees Ahmad, W. Lawrence Drew, James Plorde *Sherris Medical Microbiology, 5th editon*. fifth ed. 2010.
5. Patrick R.Mirrya, Ken S.Rosenthal, M.A.P., *Medical microbiology 5th edition*. 5th edition ed. Vol. 1. 2005, USA: Elsevier's Health Science.
6. Lundberg, D.G.D. owner WebMD, *Medscape*. Updated: Mar 14, 2014 [cited May 1995; available at <http://www.medscape.com>].
7. Wikipedia. *The Free Encyclopedia* Available from: <http://www.wikipedia.org/>.
8. Actor, J., R. Hunter, Jr., and C. Jagannath, *Immunopathology of Tuberculosis*, in *Molecular Pathology of Lung Diseases*, D. Zander, et al., Editors. 2008, Springer New York. p. 419-428.
9. Gerald L. Mandell, J.E.B., Raphael Dolin *Principles and practice of infectious diseases, 7th edition*. Vol. 2. 2010: Elsevier.
10. Gengenbacher, M. and S.H. Kaufmann, *Mycobacterium tuberculosis: success through dormancy*. FEMS Microbiol Rev, 2012. **36**(3): p. 514-32.
11. Vinay Kumar, A.K.A., Nelson Fausto, Jon Aster, *Robbins and Cotran: Pathologic Basis of Disease* 8th ed. 2010.
12. *Global tuberculosis report 2013*, in *WHO/HTM/TB/2013.11*. 2013, WHO Press: France.
13. Ernst, J.D., G. Trevejo-Nunez, and N. Banaiee, *Genomics and the evolution, pathogenesis, and diagnosis of tuberculosis*. J Clin Invest, 2007. **117**(7): p. 1738-45.
14. Montali, R.J., S.K. Mikota, and L.I. Cheng, *Mycobacterium tuberculosis in zoo and wildlife species*. Rev Sci Tech, 2001. **20**(1): p. 291-303.
15. Oh, P., et al., *Human exposure following Mycobacterium tuberculosis infection of multiple animal species in a Metropolitan Zoo*. Emerg Infect Dis, 2002. **8**(11): p. 1290-3.
16. Evans, J.T., et al., *Cluster of human tuberculosis caused by Mycobacterium bovis: evidence for person-to-person transmission in the UK*. Lancet, 2007. **369**(9569): p. 1270-6.
17. Frampton, M.W., *An outbreak of tuberculosis among hospital personnel caring for a patient with a skin ulcer*. Ann Intern Med, 1992. **117**(4): p. 312-3.
18. Templeton, G.L., et al., *The risk for transmission of Mycobacterium tuberculosis at the bedside and during autopsy*. Ann Intern Med, 1995. **122**(12): p. 922-5.
19. Murray, J.F., *A century of tuberculosis*. Am J Respir Crit Care Med, 2004. **169**(11): p. 1181-6.
20. Edlin, B.R., et al., *An outbreak of multidrug-resistant tuberculosis among hospitalized patients with the acquired immunodeficiency syndrome*. N Engl J Med, 1992. **326**(23): p. 1514-21.
21. Hoge, C.W., et al., *Risk factors for transmission of Mycobacterium tuberculosis in a primary school outbreak: lack of racial difference in susceptibility to infection*. Am J Epidemiol, 1994. **139**(5): p. 520-30.
22. Mosher, C.B., et al., *Unusually aggressive transmission of tuberculosis in a factory*. J Occup Med, 1987. **29**(1): p. 29-31.
23. Curtis, A.B., et al., *Analysis of Mycobacterium tuberculosis transmission patterns in a homeless shelter outbreak*. Int J Tuberc Lung Dis, 2000. **4**(4): p. 308-13.
24. Valway, S.E., et al., *Outbreak of multi-drug-resistant tuberculosis in a New York State prison, 1991*. Am J Epidemiol, 1994. **140**(2): p. 113-22.
25. Bates, J.H. and W.W. Stead, *The history of tuberculosis as a global epidemic*. Med Clin North Am, 1993. **77**(6): p. 1205-17.
26. Styblo, K., *Recent advances in epidemiological research in tuberculosis*. Adv Tuberc Res, 1980. **20**: p. 1-63.
27. Ugarte-Gil, C. and D.A. Moore, *[Tuberculosis and diabetes co-morbidity: An unresolved problem]*. Rev Peru Med Exp Salud Publica, 2014. **31**(1): p. 137-42.
28. Rivero-Lezcano, O.M., *In vitro infection of human cells with Mycobacterium tuberculosis*. Tuberculosis (Edinb), 2013. **93**(2): p. 123-9.
29. Lee, P.H., et al., *Diabetes and risk of tuberculosis relapse: nationwide nested case-control study*. PLoS One, 2014. **9**(3): p. e92623.

30. Raghuraman, S., et al., *Prevalence of Diabetes Mellitus among Tuberculosis Patients in Urban Puducherry*. N Am J Med Sci, 2014. **6**(1): p. 30-4.
31. Hill, A.V., *Aspects of genetic susceptibility to human infectious diseases*. Annu Rev Genet, 2006. **40**: p. 469-86.
32. Cardona, P.J. and J. Ruiz-Manzano, *On the nature of Mycobacterium tuberculosis-latent bacilli*. Eur Respir J, 2004. **24**(6): p. 1044-51.
33. Cardona, P.J., *New insights on the nature of latent tuberculosis infection and its treatment*. Inflamm Allergy Drug Targets, 2007. **6**(1): p. 27-39.
34. Gomez, J.E. and J.D. McKinney, *M. tuberculosis persistence, latency, and drug tolerance*. Tuberculosis (Edinb), 2004. **84**(1-2): p. 29-44.
35. Vinay Kumar, A.K.A., Nelson Fausto, Richard Mitchell., *Robbins Basic Pathology With STUDENT CONSULT Online Access*. 8th ed. Vol. 1. 2007, China Elsevier
36. Tollefson, D., et al., *Burden of tuberculosis in indigenous peoples globally: a systematic review*. Int J Tuberc Lung Dis, 2013. **17**(9): p. 1139-50.
37. Philips, J.A. and J.D. Ernst, *Tuberculosis pathogenesis and immunity*. Annu Rev Pathol, 2012. **7**: p. 353-84.
38. Dannenberg, A.M., Jr., *Delayed-type hypersensitivity and cell-mediated immunity in the pathogenesis of tuberculosis*. Immunol Today, 1991. **12**(7): p. 228-33.
39. Peter DO Davies, P.F.B., Stephen B Gordon, *Clinical Tuberculosis, Fourth edition*. Vol. 1. 2008, London, UK: Hodder & Stoughton Ltd.
40. North, R.J. and Y.J. Jung, *Immunity to tuberculosis*. Annu Rev Immunol, 2004. **22**: p. 599-623.
41. Smith, I., *Mycobacterium tuberculosis pathogenesis and molecular determinants of virulence*. Clin Microbiol Rev, 2003. **16**(3): p. 463-96.
42. Slavin, R.E., *Late generalized tuberculosis: a clinical and pathologic analysis of a diagnostic puzzle and a changing pattern*. Pathol Annu, 1981. **16 Pt 1**: p. 81-99.
43. Slavin, R.E., T.J. Walsh, and A.D. Pollack, *Late generalized tuberculosis: a clinical pathologic analysis and comparison of 100 cases in the preantibiotic and antibiotic eras*. Medicine (Baltimore), 1980. **59**(5): p. 352-66.
44. Raviglione, M.C. and M.W. Uplekar, *WHO's new Stop TB Strategy*. Lancet, 2006. **367**(9514): p. 952-5.
45. Castell, S., et al., *[International Standards of Tuberculosis Care (ISTC)--comments from the German point of view]*. Pneumologie, 2012. **66**(4): p. 240-9.
46. Wikipedia. *Nontuberculous mycobacteria*, available at http://en.wikipedia.org/wiki/Nontuberculous_mycobacteria This page was last modified on 2 February 2014 at 07:34.
47. van Ingen, J., et al., *Clinical relevance of non-tuberculous mycobacteria isolated in the Nijmegen-Arnhem region, The Netherlands*. Thorax, 2009. **64**(6): p. 502-6.
48. Griffith, D.E., et al., *An official ATS/IDSA statement: diagnosis, treatment, and prevention of nontuberculous mycobacterial diseases*. Am J Respir Crit Care Med, 2007. **175**(4): p. 367-416.
49. Clinic, C. *Center for Continuing Education*. 2000 03/18/2009; Available from: <http://www.clevelandclinicmeded.com/medicalpubs/diseasemanagement/infectious-disease/nontuberculous-mycobacterial-disorders/>.
50. Ioachimescu, O.C. and J.W. Tomford. *"The Cleveland Clinic" Center for Continuing Education*. Published: August, 2010; available at <http://www.clevelandclinicmeded.com/medicalpubs/diseasemanagement/infectious-disease/nontuberculous-mycobacterial-disorders/#cetable1>.
51. *Mycobacterium avium Complex*, Centers for Disease Control and Prevention. 2011 August 15, 2011; available at http://www.cdc.gov/ncidod/dbmd/diseaseinfo/mycobacteriumavium_t.htm.]
52. Ogawa, K. and C. Sano, *[Strategies for Mycobacterium avium complex infection control in Japan: how do they improve the present situation?]*. Kekkaku, 2013. **88**(3): p. 355-71.
53. Maugein, J., et al., *Sentinel-site surveillance of Mycobacterium avium complex pulmonary disease*. Eur Respir J, 2005. **26**(6): p. 1092-6.
54. Debrunner, M., et al., *Epidemiology and clinical significance of nontuberculous mycobacteria in patients negative for human immunodeficiency virus in Switzerland*. Clin Infect Dis, 1992. **15**(2): p. 330-45.
55. Liandris, E., et al., *Evaluation of the microbial safety of child food of animal origin in Greece*. J Food Sci, 2014. **79**(3): p. M362-8.
56. Han, X.Y., et al., *Clinical significance and epidemiologic analyses of Mycobacterium avium and Mycobacterium intracellulare among patients without AIDS*. J Clin Microbiol, 2005. **43**(9): p. 4407-12.

57. Reichenbach, J., et al., *Mycobacterial diseases in primary immunodeficiencies*. *Curr Opin Allergy Clin Immunol*, 2001. **1**(6): p. 503-11.
58. Sexton, P. and A.C. Harrison, *Susceptibility to nontuberculous mycobacterial lung disease*. *Eur Respir J*, 2008. **31**(6): p. 1322-33.
59. Winter, S.M., et al., *Humoral response to disseminated infection by Mycobacterium avium-Mycobacterium intracellulare in acquired immunodeficiency syndrome and hairy cell leukemia*. *J Infect Dis*, 1985. **151**(3): p. 523-7.
60. Nishiuchi, Y., et al., *The recovery of Mycobacterium avium-intracellulare complex (MAC) from the residential bathrooms of patients with pulmonary MAC*. *Clin Infect Dis*, 2007. **45**(3): p. 347-51.
61. Reed, C., et al., *Environmental risk factors for infection with Mycobacterium avium complex*. *Am J Epidemiol*, 2006. **164**(1): p. 32-40.
62. Esteban, J., et al., *Current treatment of nontuberculous mycobacteriosis: an update*. *Expert Opin Pharmacother*, 2012. **13**(7): p. 967-86.
63. Brown-Elliott, B.A. and R.J. Wallace, Jr., *Clinical and taxonomic status of pathogenic nonpigmented or late-pigmenting rapidly growing mycobacteria*. *Clin Microbiol Rev*, 2002. **15**(4): p. 716-46.
64. Wilson, R.W., et al., *Mycobacterium immunogenum sp. nov., a novel species related to Mycobacterium abscessus and associated with clinical disease, pseudo-outbreaks and contaminated metalworking fluids: an international cooperative study on mycobacterial taxonomy*. *Int J Syst Evol Microbiol*, 2001. **51**(Pt 5): p. 1751-64.
65. Griffith, D.E., W.M. Girard, and R.J. Wallace, Jr., *Clinical features of pulmonary disease caused by rapidly growing mycobacteria. An analysis of 154 patients*. *Am Rev Respir Dis*, 1993. **147**(5): p. 1271-8.
66. Winthrop, K.L., et al., *An outbreak of mycobacterial furunculosis associated with footbaths at a nail salon*. *N Engl J Med*, 2002. **346**(18): p. 1366-71.
67. Dioni, E., et al., *Central vascular catheters and infections*. *Early Hum Dev*, 2014. **90s1**: p. S51-s53.
68. Soper, F.L., *Problems to be solved if the eradication of tuberculosis is to be realized*. *Am J Public Health Nations Health*, 1962. **52**: p. 734-48.
69. Lonnroth, K., et al., *Tuberculosis control and elimination 2010-50: cure, care, and social development*. *Lancet*, 2010. **375**(9728): p. 1814-29.
70. Velayati, A.A., et al., *Emergence of new forms of totally drug-resistant tuberculosis bacilli: super extensively drug-resistant tuberculosis or totally drug-resistant strains in iran*. *Chest*, 2009. **136**(2): p. 420-5.
71. Beverley, P.C., et al., *Harnessing local and systemic immunity for vaccines against tuberculosis*. *Mucosal Immunol*, 2014. **7**(1): p. 20-6.
72. Jeffrey K. Actor, R.L.H.J., Chinnaswamy Jagannath, *Immunopathology of Tuberculosis*, in *Molecular Pathology of Lung Diseases*, H.H.P. Dani S. Zander, Jaishree Jagirdar, Abida K. Haque, , Editor. 2008, Springer New York.
73. Group., T.A., *Report on tuberculosis research funding trends, 2005–2008*. 2009: New York: Treatment Action Group,.
74. Flynn, J.L. and J. Chan, *Immunology of tuberculosis*. *Annu Rev Immunol*, 2001. **19**: p. 93-129.
75. Cegielski, J.P. and D.N. McMurray, *The relationship between malnutrition and tuberculosis: evidence from studies in humans and experimental animals*. *Int J Tuberc Lung Dis*, 2004. **8**(3): p. 286-98.
76. Browning, C.H. and R. Gulbransen, *Studies on Experimental Tuberculosis in Mice: The susceptibility of Mice to Inoculation with Tubercle Bacilli*. *J Hyg (Lond)*, 1926. **25**(3): p. 323-32.
77. Singhal, A., et al., *BCG induces protection against Mycobacterium tuberculosis infection in the Wistar rat model*. *PLoS One*, 2011. **6**(12): p. e28082.
78. Lurie, M.B., P. Zappasodi, and C. Tickner, *On the nature of genetic resistance to tuberculosis in the light of the host-parasite relationships in natively resistant and susceptible rabbits*. *Am Rev Tuberc*, 1955. **72**(3): p. 297-329.
79. Walsh, G.P., et al., *The Philippine cynomolgus monkey (Macaca fascicularis) provides a new nonhuman primate model of tuberculosis that resembles human disease*. *Nat Med*, 1996. **2**(4): p. 430-6.
80. Jeevan, A., et al., *Differential expression of gamma interferon mRNA induced by attenuated and virulent Mycobacterium tuberculosis in guinea pig cells after Mycobacterium bovis BCG vaccination*. *Infect Immun*, 2003. **71**(1): p. 354-64.
81. Flynn, J.L., *Lessons from experimental Mycobacterium tuberculosis infections*. *Microbes and Infection*, 2006. **8**(4): p. 1179-1188.

82. Ottenhoff, T.H., et al., *Control of human host immunity to mycobacteria*. Tuberculosis (Edinb), 2005. **85**(1-2): p. 53-64.
83. Mackaness, G.B., *The growth of tubercle bacilli in monocytes from normal and vaccinated rabbits*. Am Rev Tuberc, 1954. **69**(4): p. 495-504.
84. Peterson, P.K., et al., *CD14 receptor-mediated uptake of nonopsonized Mycobacterium tuberculosis by human microglia*. Infect Immun, 1995. **63**(4): p. 1598-602.
85. Steele, J., et al., *Inhibition of virulent Mycobacterium tuberculosis by murine peritoneal macrophages and human alveolar lavage cells: the effects of lymphokines and recombinant gamma interferon*. Tubercle, 1986. **67**(4): p. 289-94.
86. Brown, A.E., T.J. Holzer, and B.R. Andersen, *Capacity of human neutrophils to kill Mycobacterium tuberculosis*. J Infect Dis, 1987. **156**(6): p. 985-9.
87. Stokes, R.W. and D. Doxsee, *The receptor-mediated uptake, survival, replication, and drug sensitivity of Mycobacterium tuberculosis within the macrophage-like cell line THP-1: a comparison with human monocyte-derived macrophages*. Cell Immunol, 1999. **197**(1): p. 1-9.
88. Rockett, K.A., et al., *1,25-Dihydroxyvitamin D3 induces nitric oxide synthase and suppresses growth of Mycobacterium tuberculosis in a human macrophage-like cell line*. Infect Immun, 1998. **66**(11): p. 5314-21.
89. Wei, J., et al., *Identification of a Mycobacterium tuberculosis gene that enhances mycobacterial survival in macrophages*. J Bacteriol, 2000. **182**(2): p. 377-84.
90. Shepard, C.C., *Growth characteristics of tubercle bacilli and certain other mycobacteria in HeLa cells*. J Exp Med, 1957. **105**(1): p. 39-48.
91. Bermudez, L.E. and J. Goodman, *Mycobacterium tuberculosis invades and replicates within type II alveolar cells*. Infect Immun, 1996. **64**(4): p. 1400-6.
92. Vinay Kumar, A.K.A., Nelson Fausto, Jon Aster, *Robbins and Cotran: Pathologic Basis of Disease*. 8th ed. 2010.
93. Morrison, J., M. Pai, and P.C. Hopewell, *Tuberculosis and latent tuberculosis infection in close contacts of people with pulmonary tuberculosis in low-income and middle-income countries: a systematic review and meta-analysis*. Lancet Infect Dis, 2008. **8**(6): p. 359-68.
94. Wikipedia. *Ex vivo*, available at http://en.wikipedia.org/wiki/Ex_vivo. This page was last modified on 30 April 2014 at 22:11.
95. Allen, T. and P. Cagle, *Bioinformatics and Omics*, in *Molecular Pathology of Lung Diseases*, D. Zander, et al., Editors. 2008, Springer New York. p. 65-69.
96. Goldmann, T., et al., *Tissue microarrays from HOPE-fixed specimens allow for enhanced high throughput molecular analyses in paraffin-embedded material*. Pathol Res Pract, 2005. **201**(8-9): p. 599-602.
97. Goldmann, T., et al., *Enhanced molecular analyses by combination of the HOPE-technique and laser microdissection*. Diagn Pathol, 2006. **1**: p. 2.
98. Olert, J., et al., *HOPE fixation: a novel fixing method and paraffin-embedding technique for human soft tissues*. Pathol Res Pract, 2001. **197**(12): p. 823-6.
99. Goldmann, T., E. Vollmer, and J. Gerdes, *What's cooking? detection of important biomarkers in HOPE-fixed, paraffin-embedded tissues eliminates the need for antigen retrieval*. Am J Pathol, 2003. **163**(6): p. 2638-40.
100. Shevchuk, O., et al., *HOPE-Fixation of Lung Tissue Allows Retrospective Proteome and Phosphoproteome Studies*. J Proteome Res, 2014.
101. Marwitz, S., et al., *The tissue is the issue: improved methylome analysis from paraffin-embedded tissues by application of the HOPE technique*. Lab Invest, 2014.
102. Pedersen, F., et al., *HOPE-preservation of paraffin-embedded sputum samples--a new way of bioprofiling in COPD*. Respir Med, 2013. **107**(4): p. 587-95.
103. Marwitz, S., et al., *HOPE-BAL: improved molecular diagnostics by application of a novel technique for fixation and paraffin embedding*. J Histochem Cytochem, 2011. **59**(6): p. 601-14.
104. Greer, C.E., et al., *PCR amplification from paraffin-embedded tissues. Effects of fixative and fixation time*. Am J Clin Pathol, 1991. **95**(2): p. 117-24.
105. Schewe, C., et al., *Inter-laboratory validation of PCR-based detection of Mycobacterium tuberculosis in formalin-fixed, paraffin-embedded tissues*. Virchows Arch, 2005. **447**(3): p. 573-85.
106. Coutlee, F., et al., *An important proportion of genital samples submitted for Chlamydia trachomatis detection by PCR contain small amounts of cellular DNA as measured by beta-globin gene amplification*. J Clin Microbiol, 2000. **38**(7): p. 2512-5.
107. Edwards, U., et al., *Isolation and direct complete nucleotide determination of entire genes. Characterization of a gene coding for 16S ribosomal RNA*. Nucleic Acids Res, 1989. **17**(19): p. 7843-53.

108. Boddingtonhaus, B., et al., *Detection and identification of mycobacteria by amplification of rRNA*. J Clin Microbiol, 1990. **28**(8): p. 1751-9.
109. Richter, E., et al., *Assessment of mycobacterial DNA in cells and tissues of mycobacterial and sarcoid lesions*. Am J Respir Crit Care Med, 1996. **153**(1): p. 375-80.
110. Arnoldi, J., et al., *Species-specific assessment of Mycobacterium leprae in skin biopsies by in situ hybridization and polymerase chain reaction*. Lab Invest, 1992. **66**(5): p. 618-23.
111. Motulsky, D.H. *GraphPad Software*. Available from: <http://www.graphpad.com/quickcalcs/Molarityform.cfm>.
112. Creative Research Systems. 1982 Available from: <http://www.surveysystem.com/sscalc.htm>.
113. Herzmann, C. and C. Lange, [Infections with non-tuberculous mycobacteria and HIV]. Dtsch Med Wochenschr, 2010. **135**(23): p. 1192-7.
114. Kaufmann, S.H., *Tuberculosis vaccine development: strength lies in tenacity*. Trends Immunol, 2012. **33**(7): p. 373-9.
115. Young, D.B., et al., *Confronting the scientific obstacles to global control of tuberculosis*. J Clin Invest, 2008. **118**(4): p. 1255-65.
116. Dye, C., et al., *Targets for global tuberculosis control*. Int J Tuberc Lung Dis, 2006. **10**(4): p. 460-2.
117. Gupta, U.D. and V.M. Katoch, *Animal models of tuberculosis*. Tuberculosis (Edinb), 2005. **85**(5-6): p. 277-93.
118. Ulrichs, T. and S.H. Kaufmann, *Mycobacterial persistence and immunity*. Front Biosci, 2002. **7**: p. d458-69.
119. Shen, Y., et al., *Adaptive immune response of Vgamma2Vdelta2+ T cells during mycobacterial infections*. Science, 2002. **295**(5563): p. 2255-8.
120. Shi, L., et al., *Isolation and purification of Mycobacterium tuberculosis from H37Rv infected guinea pig lungs*. Tuberculosis (Edinb), 2014.
121. Flynn, J.L., *Lessons from experimental Mycobacterium tuberculosis infections*. Microbes Infect, 2006. **8**(4): p. 1179-88.
122. Crowle, A.J. and M. May, *Preliminary demonstration of human tuberculoimmunity in vitro*. Infect Immun, 1981. **31**(1): p. 453-64.
123. Caccamo, N., et al., *Identification of epitopes of Mycobacterium tuberculosis 16-kDa protein recognized by human leukocyte antigen-A*0201 CD8(+) T lymphocytes*. J Infect Dis, 2002. **186**(7): p. 991-8.
124. Suter, E., *The multiplication of tubercle bacilli within normal phagocytes in tissue culture*. J Exp Med, 1952. **96**(2): p. 137-50.
125. Patterson, R.J. and G.P. Youmans, *Multiplication of Mycobacterium tuberculosis Within Normal and "Immune" Mouse Macrophages Cultivated With and Without Streptomycin*. Infect Immun, 1970. **1**(1): p. 30-40.
126. Lamhamedi-Cherradi, S., C. de Chastellier, and J.L. Casanova, *Growth of Mycobacterium bovis, Bacille Calmette-Guerin, within human monocytes-macrophages cultured in serum-free medium*. J Immunol Methods, 1999. **225**(1-2): p. 75-86.
127. Ernst, J.D., *Macrophage receptors for Mycobacterium tuberculosis*. Infect Immun, 1998. **66**(4): p. 1277-81.
128. Danelishvili, L., et al., *Mycobacterium tuberculosis infection causes different levels of apoptosis and necrosis in human macrophages and alveolar epithelial cells*. Cell Microbiol, 2003. **5**(9): p. 649-60.
129. Lee, J., et al., *Macrophage apoptosis in response to high intracellular burden of Mycobacterium tuberculosis is mediated by a novel caspase-independent pathway*. J Immunol, 2006. **176**(7): p. 4267-74.
130. Wallis, R.S., S. Vinhas, and E. Janulionis, *Strain specificity of antimycobacterial immunity in whole blood culture after cure of tuberculosis*. Tuberculosis (Edinb), 2009. **89**(3): p. 221-4.
131. Bermudez, L.E., et al., *The efficiency of the translocation of Mycobacterium tuberculosis across a bilayer of epithelial and endothelial cells as a model of the alveolar wall is a consequence of transport within mononuclear phagocytes and invasion of alveolar epithelial cells*. Infect Immun, 2002. **70**(1): p. 140-6.
132. Bonay, M., et al., *Effect of stimulation of human macrophages on intracellular survival of Mycobacterium bovis Bacillus Calmette-Guerin. Evaluation with a mycobacterial reporter strain*. Am J Respir Crit Care Med, 1999. **159**(5 Pt 1): p. 1629-37.
133. Martineau, A.R., et al., *IFN-gamma- and TNF-independent vitamin D-inducible human suppression of mycobacteria: the role of cathelicidin LL-37*. J Immunol, 2007. **178**(11): p. 7190-8.
134. Garg, S.K., et al., *Sphingosine 1-phosphate induces antimicrobial activity both in vitro and in vivo*. J Infect Dis, 2004. **189**(11): p. 2129-38.

135. Kusner, D.J. and J. Adams, *ATP-induced killing of virulent Mycobacterium tuberculosis within human macrophages requires phospholipase D*. J Immunol, 2000. **164**(1): p. 379-88.
136. Nicol, M.P. and R.J. Wilkinson, *The clinical consequences of strain diversity in Mycobacterium tuberculosis*. Trans R Soc Trop Med Hyg, 2008. **102**(10): p. 955-65.
137. Caws, M., et al., *The influence of host and bacterial genotype on the development of disseminated disease with Mycobacterium tuberculosis*. PLoS Pathog, 2008. **4**(3): p. e1000034.
138. Lang, D.S., et al., *A novel human ex vivo model for the analysis of molecular events during lung cancer chemotherapy*. Respir Res, 2007. **8**: p. 43.
139. Wiles, S., et al., *Modelling infectious disease - time to think outside the box?* Nat Rev Microbiol, 2006. **4**(4): p. 307-12.
140. Holmes, A.M., R. Solari, and S.T. Holgate, *Animal models of asthma: value, limitations and opportunities for alternative approaches*. Drug Discov Today, 2011. **16**(15-16): p. 659-70.
141. Booth, J.L., et al., *Adenovirus type 7 induces interleukin-8 in a lung slice model and requires activation of Erk*. J Virol, 2004. **78**(8): p. 4156-64.
142. Switalla, S., et al., *Natural innate cytokine response to immunomodulators and adjuvants in human precision-cut lung slices*. Toxicol Appl Pharmacol, 2010. **246**(3): p. 107-15.
143. Jager, J., et al., *Human lung tissue explants reveal novel interactions during Legionella pneumophila infections*. Infect Immun, 2014. **82**(1): p. 275-85.
144. Harrison, F., et al., *Development of an ex vivo porcine lung model for studying growth, virulence, and signaling of Pseudomonas aeruginosa*. Infect Immun, 2014. **82**(8): p. 3312-23.
145. Szymanski, K.V., et al., *Streptococcus pneumoniae-induced regulation of cyclooxygenase-2 in human lung tissue*. Eur Respir J, 2012. **40**(6): p. 1458-67.
146. Rupp, J., et al., *Alveolar epithelial cells type II are major target cells for C. pneumoniae in chronic but not in acute respiratory infection*. FEMS Immunol Med Microbiol, 2004. **41**(3): p. 197-203.
147. Dromann, D., et al., *The TGF-beta-pseudoreceptor BAMBI is strongly expressed in COPD lungs and regulated by nontypeable Haemophilus influenzae*. Respir Res, 2010. **11**: p. 67.
148. Xu, F., et al., *Modulation of the inflammatory response to Streptococcus pneumoniae in a model of acute lung tissue infection*. Am J Respir Cell Mol Biol, 2008. **39**(5): p. 522-9.
149. Dubos, R.J. and B.D. Davis, *Factors affecting the growth of tubercle bacilli in liquid media*. J Exp Med, 1946. **83**: p. 409-23.
150. O'Garra, A., et al., *The immune response in tuberculosis*. Annu Rev Immunol, 2013. **31**: p. 475-527.
151. Jereb, J., et al., *Tuberculosis contact investigations: outcomes in selected areas of the United States, 1999*. Int J Tuberc Lung Dis, 2003. **7**(12 Suppl 3): p. S384-90.
152. Marks, S.M., et al., *Outcomes of contact investigations of infectious tuberculosis patients*. Am J Respir Crit Care Med, 2000. **162**(6): p. 2033-8.
153. Lillebaek, T., et al., *Stability of DNA patterns and evidence of Mycobacterium tuberculosis reactivation occurring decades after the initial infection*. J Infect Dis, 2003. **188**(7): p. 1032-9.
154. *AIDS and Tuberculosis*. 2009, Federal Republic of Germany: WILEY-VCH Verlag GmbH & Co. KGaA, Weinheim.
155. Colditz, G.A., et al., *Efficacy of BCG vaccine in the prevention of tuberculosis. Meta-analysis of the published literature*. Jama, 1994. **271**(9): p. 698-702.
156. Kagina, B.M., et al., *Specific T cell frequency and cytokine expression profile do not correlate with protection against tuberculosis after bacillus Calmette-Guerin vaccination of newborns*. Am J Respir Crit Care Med, 2010. **182**(8): p. 1073-9.
157. Sakula, A., *BCG: who were Calmette and Guerin?* Thorax, 1983. **38**(11): p. 806-12.
158. van Rie, A., et al., *Exogenous reinfection as a cause of recurrent tuberculosis after curative treatment*. N Engl J Med, 1999. **341**(16): p. 1174-9.
159. Agdestein, A., et al., *Intracellular growth of Mycobacterium avium subspecies and global transcriptional responses in human macrophages after infection*. BMC Genomics, 2014. **15**: p. 58.
160. Sturgill-Koszycki, S., U.E. Schaible, and D.G. Russell, *Mycobacterium-containing phagosomes are accessible to early endosomes and reflect a transitional state in normal phagosome biogenesis*. Embo j, 1996. **15**(24): p. 6960-8.
161. Lee, J., M. Hartman, and H. Kornfeld, *Macrophage apoptosis in tuberculosis*. Yonsei Med J, 2009. **50**(1): p. 1-11.
162. Keane, J., H.G. Remold, and H. Kornfeld, *Virulent Mycobacterium tuberculosis strains evade apoptosis of infected alveolar macrophages*. J Immunol, 2000. **164**(4): p. 2016-20.
163. Wallis, R.S., M. Amir-Tahmasseb, and J.J. Ellner, *Induction of interleukin 1 and tumor necrosis factor by mycobacterial proteins: the monocyte western blot*. Proc Natl Acad Sci U S A, 1990. **87**(9): p. 3348-52.

164. Zhang, Y., et al., *Mechanisms of stimulation of interleukin-1 beta and tumor necrosis factor-alpha by Mycobacterium tuberculosis components*. J Clin Invest, 1993. **91**(5): p. 2076-83.
165. Fulton, S.A., et al., *Regulation of interleukin-12 by interleukin-10, transforming growth factor-beta, tumor necrosis factor-alpha, and interferon-gamma in human monocytes infected with Mycobacterium tuberculosis H37Ra*. J Infect Dis, 1998. **178**(4): p. 1105-14.
166. Friedland, J.S., et al., *Secretion of interleukin-8 following phagocytosis of Mycobacterium tuberculosis by human monocyte cell lines*. Eur J Immunol, 1992. **22**(6): p. 1373-8.
167. Shaw, T.C., L.H. Thomas, and J.S. Friedland, *Regulation of IL-10 secretion after phagocytosis of Mycobacterium tuberculosis by human monocytic cells*. Cytokine, 2000. **12**(5): p. 483-6.
168. Ken S. Rosenthal, M.J.T., *Rapid Review Microbiology and Immunology*. 3rd ed. 2011, United States of America: Elsevier.
169. Alan Stevens, J.L., *Human histology 2005*, Spain Elsevier.
170. Wolbers, F., et al., *Apoptotic cell death kinetics in vitro depend on the cell types and the inducers used*. Apoptosis, 2004. **9**(3): p. 385-92.
171. Schmitz-Valckenberg, S., et al., *[In vivo imaging of retinal cell apoptosis following acute light exposure]*. Ophthalmologe, 2010. **107**(1): p. 22-9.
172. Chiamonte, R., et al., *Oxidative stress signalling in the apoptosis of Jurkat T-lymphocytes*. J Cell Biochem, 2001. **82**(3): p. 437-44.
173. *Wheater's Basic Pathology: A Text, Atlas and Review of Histopathology*. 5 edition ed. 2009: Churchill Livingstone.
174. McCracken, J.M. and L.A. Allen, *Regulation of human neutrophil apoptosis and lifespan in health and disease*. J Cell Death, 2014. **7**: p. 15-23.
175. Bocchino, M., et al., *Role of mycobacteria-induced monocyte/macrophage apoptosis in the pathogenesis of human tuberculosis*. Int J Tuberc Lung Dis, 2005. **9**(4): p. 375-83.
176. Micheal H.Ross, W.P., *Histology with correlated cell and molecular biology*. 2011, China Wolters Kluwer/ Liiincott Williams and Wilkins.
177. Yang, C.T., et al., *Neutrophils exert protection in the early tuberculous granuloma by oxidative killing of mycobacteria phagocytosed from infected macrophages*. Cell Host Microbe, 2012. **12**(3): p. 301-12.
178. Bogdan, C., M. Rollinghoff, and A. Diefenbach, *Reactive oxygen and reactive nitrogen intermediates in innate and specific immunity*. Curr Opin Immunol, 2000. **12**(1): p. 64-76.
179. Winterbourn, C.C., *Reconciling the chemistry and biology of reactive oxygen species*. Nat Chem Biol, 2008. **4**(5): p. 278-86.
180. Amulic, B., et al., *Neutrophil function: from mechanisms to disease*. Annu Rev Immunol, 2012. **30**: p. 459-89.
181. Jones, G.S., H.J. Amirault, and B.R. Andersen, *Killing of Mycobacterium tuberculosis by neutrophils: a nonoxidative process*. J Infect Dis, 1990. **162**(3): p. 700-4.
182. Kisich, K.O., et al., *Tumor necrosis factor alpha stimulates killing of Mycobacterium tuberculosis by human neutrophils*. Infect Immun, 2002. **70**(8): p. 4591-9.
183. Martineau, A.R., et al., *Neutrophil-mediated innate immune resistance to mycobacteria*. J Clin Invest, 2007. **117**(7): p. 1988-94.
184. Majeed, M., et al., *Roles of calcium and annexins in phagocytosis and elimination of an attenuated strain of Mycobacterium tuberculosis in human neutrophils*. Microb Pathog, 1998. **24**(5): p. 309-20.
185. Da Silva, R.P., et al., *CR1, the C3b receptor, mediates binding of infective Leishmania major metacyclic promastigotes to human macrophages*. J Immunol, 1989. **143**(2): p. 617-22.
186. Stead, W.W., et al., *Racial differences in susceptibility to infection by Mycobacterium tuberculosis*. N Engl J Med, 1990. **322**(7): p. 422-7.
187. Eum, S.Y., et al., *Neutrophils are the predominant infected phagocytic cells in the airways of patients with active pulmonary TB*. Chest, 2010. **137**(1): p. 122-8.
188. Kawamoto, H., et al., *[A case of cervical-mediastinal lymph node tuberculosis progressed to pulmonary lesion through a bronchial fistula]*. Nihon Kokyuki Gakkai Zasshi, 1998. **36**(12): p. 1053-7.
189. Berry, M.P., et al., *An interferon-inducible neutrophil-driven blood transcriptional signature in human tuberculosis*. Nature, 2010. **466**(7309): p. 973-7.
190. Denis, M., *Human neutrophils, activated with cytokines or not, do not kill virulent Mycobacterium tuberculosis*. J Infect Dis, 1991. **163**(4): p. 919-20.
191. Hedges, J.C., C.A. Singer, and W.T. Gerthoffer, *Mitogen-Activated Protein Kinases Regulate Cytokine Gene Expression in Human Airway Myocytes*. American Journal of Respiratory Cell and Molecular Biology, 2000. **23**(1): p. 86-94.

192. Wickremasinghe, M.I., L.H. Thomas, and J.S. Friedland, *Pulmonary epithelial cells are a source of IL-8 in the response to Mycobacterium tuberculosis: essential role of IL-1 from infected monocytes in a NF-kappa B-dependent network*. J Immunol, 1999. **163**(7): p. 3936-47.
193. Kurashima, K., et al., *Elevated chemokine levels in bronchoalveolar lavage fluid of tuberculosis patients*. Am J Respir Crit Care Med, 1997. **155**(4): p. 1474-7.
194. Friedland, J.S., et al., *Inhibition of ex vivo proinflammatory cytokine secretion in fatal Mycobacterium tuberculosis infection*. Clin Exp Immunol, 1995. **100**(2): p. 233-8.
195. Ronald G. Crystal, W., Weibel *Lung: Scientific Foundations*. Vol. 1-2. 1997: Lippincott Williams & Wilkins.
196. Shepard, C.C., *Phagocytosis by HeLa cells and their susceptibility to infection by human tubercle bacilli*. Proc Soc Exp Biol Med, 1955. **90**(2): p. 392-6.
197. Chen, J., et al., *Isolation of highly pure alveolar epithelial type I and type II cells from rat lungs*. Lab Invest, 2004. **84**(6): p. 727-35.
198. Sato, K., et al., *Type II alveolar cells play roles in macrophage-mediated host innate resistance to pulmonary mycobacterial infections by producing proinflammatory cytokines*. J Infect Dis, 2002. **185**(8): p. 1139-47.
199. van Crevel, R., T.H. Ottenhoff, and J.W. van der Meer, *Innate immunity to Mycobacterium tuberculosis*. Clin Microbiol Rev, 2002. **15**(2): p. 294-309.
200. Edwards, Y.S., *Stretch stimulation: its effects on alveolar type II cell function in the lung*. Comp Biochem Physiol A Mol Integr Physiol, 2001. **129**(1): p. 245-60.
201. Shannon, J.M., R.J. Mason, and S.D. Jennings, *Functional differentiation of alveolar type II epithelial cells in vitro: effects of cell shape, cell-matrix interactions and cell-cell interactions*. Biochim Biophys Acta, 1987. **931**(2): p. 143-56.
202. Shannon, J.M., et al., *Effect of a reconstituted basement membrane on expression of surfactant apoproteins in cultured adult rat alveolar type II cells*. Am J Respir Cell Mol Biol, 1990. **2**(2): p. 183-92.
203. Dobos, K.M., et al., *Necrosis of lung epithelial cells during infection with Mycobacterium tuberculosis is preceded by cell permeation*. Infect Immun, 2000. **68**(11): p. 6300-10.
204. Fehrenbach, H., *Alveolar epithelial type II cell: defender of the alveolus revisited*. Respir Res, 2001. **2**(1): p. 33-46.
205. B.E. Garcia-Perez, N.S.C.-J.a.J.L.-H., *The Role of Non-Phagocytic Cells in Mycobacterial Infections*. Understanding Tuberculosis - Analyzing the Origin of Mycobacterium Tuberculosis Pathogenicity, 2012.
206. Khechinashvili, G.N. and N.G. Khvitiya, *Protective characteristics of platelets in tuberculosis*. Bull Exp Biol Med, 2004. **138**(5): p. 513-4.
207. Hall, G., *Textbook of Medical Physiology*. 12th edition ed. 2011: Saunders.
208. Novitskii, V.V., et al., *[Immune pathology in pulmonary tuberculosis]*. Patol Fiziol Eksp Ter, 2008(1): p. 15-8.
209. Driss, V., et al., *[Eosinophil: a new effector of innate immunity?]*. Med Sci (Paris), 2010. **26**(6-7): p. 621-6.
210. Hernandez-Pando, R., et al., *Persistence of DNA from Mycobacterium tuberculosis in superficially normal lung tissue during latent infection*. Lancet, 2000. **356**(9248): p. 2133-8.
211. De Laurenzi, V., et al., *Cell death by oxidative stress and ascorbic acid regeneration in human neuroectodermal cell lines*. Eur J Cancer, 1995. **31a**(4): p. 463-6.
212. Okayasu, H., et al., *Cytotoxic activity of vitamins K1, K2 and K3 against human oral tumor cell lines*. Anticancer Res, 2001. **21**(4a): p. 2387-92.
213. Gilloteaux, J., et al., *Scanning electron microscopy and transmission electron microscopy aspects of synergistic antitumor activity of vitamin C - vitamin K3 combinations against human prostatic carcinoma cells*. Scanning Microsc, 1995. **9**(1): p. 159-73.
214. Gilloteaux, J., et al., *Cancer cell necrosis by autophagy: synergism of antitumor activity of vitamin C: vitamin K3 on human bladder carcinoma T24 cells*. Scanning, 1998. **20**(8): p. 564-75.
215. Jamison, J.M., et al., *Flow cytometric and ultrastructural aspects of the synergistic antitumor activity of vitamin C-vitamin K3 combinations against human prostatic carcinoma cells*. Tissue Cell, 1996. **28**(6): p. 687-701.
216. Gilloteaux, J., et al., *Autophagy: another cell death for cancer cells induced by oxidative stress*. Ital J Anat Embryol, 2001. **106**(2 Suppl 1): p. 79-92.
217. Gilloteaux, J., et al., *Ultrastructural aspects of autophagy: a new cancer cell death induced by the synergistic action of ascorbate/menadione on human bladder carcinoma cells*. Ultrastruct Pathol, 2001. **25**(3): p. 183-92.

218. Pais, V., L. Danaila, and E. Pais, *A comparative ultrastructural study of a new type of autoschizis versus a survival cellular mechanism that involves cell membranes of cerebral arteries in humans*. *Ultrastruct Pathol*, 2012. **36**(3): p. 166-70.
219. Bram, S., et al., *Vitamin C preferential toxicity for malignant melanoma cells*. *Nature*, 1980. **284**(5757): p. 629-31.
220. Prasad, K.N., et al., *Sodium ascorbate potentiates the growth inhibitory effect of certain agents on neuroblastoma cells in culture*. *Proc Natl Acad Sci U S A*, 1979. **76**(2): p. 829-32.
221. Gilloteaux, J., et al., *Autoschizis of human ovarian carcinoma cells: scanning electron and light microscopy of a new cell death induced by sodium ascorbate: menadione treatment*. *Scanning*, 2003. **25**(3): p. 137-49.
222. Mirabelli, F., et al., *Cytoskeletal alterations in human platelets exposed to oxidative stress are mediated by oxidative and Ca²⁺-dependent mechanisms*. *Arch Biochem Biophys*, 1989. **270**(2): p. 478-88.
223. Sata, N., et al., *Menadione induces both necrosis and apoptosis in rat pancreatic acinar AR4-2J cells*. *Free Radic Biol Med*, 1997. **23**(6): p. 844-50.
224. Sun, Y., N.H. Colburn, and L.W. Oberley, *Decreased expression of manganese superoxide dismutase mRNA and protein after immortalization and transformation of mouse liver cells*. *Oncol Res*, 1993. **5**(3): p. 127-32.
225. Park, C.H., et al., *Growth suppression of human leukemic cells in vitro by L-ascorbic acid*. *Cancer Res*, 1980. **40**(4): p. 1062-5.
226. Jana, M., R. Rajaram, and A. Rajaram, *Autoschizis of T-cells is induced by the nutritional supplement, Cr(III)picolinate*. *Toxicol In Vitro*, 2010. **24**(2): p. 586-96.
227. Pais, V., L. Danaila, and E. Pais, *Ultrastructural patterns of the activated cell death programs in the human brain*. *Ultrastruct Pathol*, 2013. **37**(2): p. 110-20.
228. Park, S., *The effects of high concentrations of vitamin C on cancer cells*. *Nutrients*, 2013. **5**(9): p. 3496-505.
229. Taper, H.S. and M. Roberfroid, *Non-toxic sensitization of cancer chemotherapy by combined vitamin C and K3 pretreatment in a mouse tumor resistant to oncovin*. *Anticancer Res*, 1992. **12**(5): p. 1651-4.
230. Castro, L. and B.A. Freeman, *Reactive oxygen species in human health and disease*. *Nutrition*, 2001. **17**(2): p. 161, 163-5.
231. Pohanka, M., *Role of oxidative stress in infectious diseases. A review*. *Folia Microbiol (Praha)*, 2013. **58**(6): p. 503-13.
232. Granados-Oliveros, G., et al., *Photoproduction of H₂O₂ and hydroxyl radicals catalysed by natural and super acid-modified montmorillonite and its oxidative role in the peroxidation of lipids*. *RSC Advances*, 2013. **3**(3): p. 937-944.
233. Khan, M.U., et al., *Mitochondria play a central role in nonischemic cardiomyocyte necrosis: common to acute and chronic stressor states*. *Pflugers Arch*, 2012. **464**(1): p. 123-31.
234. Ramalingam, M. and S.J. Kim, *Reactive oxygen/nitrogen species and their functional correlations in neurodegenerative diseases*. *J Neural Transm*, 2012. **119**(8): p. 891-910.
235. Sung, H.J., et al., *Increased expression of interleukin-1beta in triglyceride-induced macrophage cell death is mediated by p38 MAP kinase*. *BMB Rep*, 2012. **45**(7): p. 414-8.
236. Fukui, M., H.J. Choi, and B.T. Zhu, *Rapid generation of mitochondrial superoxide induces mitochondrion-dependent but caspase-independent cell death in hippocampal neuronal cells that morphologically resembles necroptosis*. *Toxicol Appl Pharmacol*, 2012. **262**(2): p. 156-66.
237. Armstrong, J.A. and P.D. Hart, *Phagosome-lysosome interactions in cultured macrophages infected with virulent tubercle bacilli. Reversal of the usual nonfusion pattern and observations on bacterial survival*. *J Exp Med*, 1975. **142**(1): p. 1-16.
238. Lee, J., et al., *Mycobacterium tuberculosis induces an atypical cell death mode to escape from infected macrophages*. *PLoS One*, 2011. **6**(3): p. e18367.
239. Jamison, J.M., et al., *Autoschizis: a novel cell death*. *Biochemical Pharmacology*, 2002. **63**(10): p. 1773-1783.
240. Ervin, E., et al., *Characterization of the early events in vitamin C and K3-induced death of human bladder tumor cells*. *Scanning*, 1998. **20**(3): p. 210-1.
241. Esquivel-Solis, H., et al., *Nitric oxide not apoptosis mediates differential killing of Mycobacterium bovis in bovine macrophages*. *PLoS One*, 2013. **8**(5): p. e63464.
242. Mendoza-Aguilar, M.D., et al., *Fate of Mycobacterium tuberculosis in peroxidase-loaded resting murine macrophages*. *International Journal of Mycobacteriology*, 2013. **2**(1): p. 3-13.
243. Chan, J., et al., *Killing of virulent Mycobacterium tuberculosis by reactive nitrogen intermediates produced by activated murine macrophages*. *J Exp Med*, 1992. **175**(4): p. 1111-22.

244. de Bruijne, J., et al., *Antiviral activity of narlaprevir combined with ritonavir and pegylated interferon in chronic hepatitis C patients*. *Hepatology*, 2010. **52**(5): p. 1590-9.
245. Deshmane, S.L., et al., *Activation of the oxidative stress pathway by HIV-1 Vpr leads to induction of hypoxia-inducible factor 1alpha expression*. *J Biol Chem*, 2009. **284**(17): p. 11364-73.
246. Nickel, D., et al., *Hypoxia triggers the expression of human beta defensin 2 and antimicrobial activity against Mycobacterium tuberculosis in human macrophages*. *J Immunol*, 2012. **188**(8): p. 4001-7.
247. Sever, J.L. and G.P. Youmans, *The relation of oxygen tension to virulence of tubercle bacilli and to acquired resistance in tuberculosis*. *J Infect Dis*, 1957. **101**(2): p. 193-202.
248. Olender, S., et al., *Low prevalence and increased household clustering of Mycobacterium tuberculosis infection in high altitude villages in Peru*. *Am J Trop Med Hyg*, 2003. **68**(6): p. 721-7.
249. Sanchez-Lopez, F., et al., *Oxidative stress and inflammation biomarkers in the blood of patients with Huntington's disease*. *Neurol Res*, 2012. **34**(7): p. 721-4.
250. Ishizakai, M., et al., *[Urinary 8-hydroxy-2'-deoxyguanosin (8-OHdG) in patients with chronic liver diseases]*. *Rinsho Byori*, 2004. **52**(9): p. 732-6.
251. Capone, F., et al., *Characterization of metalloproteinases, oxidative status and inflammation levels in the different stages of fibrosis in HCV patients*. *Clin Biochem*, 2012. **45**(7-8): p. 525-9.
252. Qiagen "Sample & Assay Technologies". Protocol: DNA isolation Available from: <http://www.qiagen.com/search.aspx?q=QIAamp%20DNA%20Mini%20Kit%2C%20Qiagen%2C%20Germany#&&p=1>.
253. Scientific, T.F., *NanoDrop 2000/2000c Spectrophotometer V1.0 User Manual*. 2009: USA.
254. Qiagen "Sample & Assay Technologies". Protocol: RNA isolation Available from: <http://www.qiagen.com/search.aspx?q=RNeasy%20Mini%20kit#&&p=1>.
255. Technologies, A., *Agilent 2100 Bioanalyzer 2100 Expert User's Guide*. 2003: Germany

Appendices

Appendix-I

Table 1. Reagents and tools for incubation of tissue culture

Reagents	Tools
<ul style="list-style-type: none"> • 10mM Sodium pyruvate, Cat.No: L0473, Lot: 0502A (Biochrom, Germany), • 10% Fetal calf serum (PPA, Austria), • 1M HEPES buffer solution (4-(2-hydroxyethyl)-1piperazineethane sulfonic acid) ref: 15630-056, Lot: 1222418 (Invitrogen, Germany), • BBL™ MGIT™ PANTA™ antibiotic mixture Lot: 0426068, MD21152 • RPMI Medium 1640 (1x)+ GlutaMAX™-I ref: 61870-010, Lot: 1209058 (Invitrogen, Germany) 	<ul style="list-style-type: none"> • 2°C fridge • Costar 3513 cell culture cluster, 12 well, flat bottom with lid (lifesciences, USA). • Gloves, nitril blue S, ref: 74210 (MaiMed, Germany) • Ice box, ice • Text markers • Pathological knife and cutting board • Pipetus 240 V pipetting controller, manufacturer No: 9907200 (Hirschmann, Germany) • Serological pipet-10 mL (Costar, USA) • Transfer pipettes, Lot: 032822005 (Sarstedt, Germany)

Table 2. Reagents and tools used for collecting supernatants and tissue processing steps

Reagents	Tools and equipments
<ul style="list-style-type: none"> • HOPE I solution • Low melting paraffin for HOPE fixation, Cat.No PL003S2K (DCS labLine, Germany) • Pure acetone • Pursept-A Xpress disinfection, reg-No: N-44915 	<ul style="list-style-type: none"> • Box of microcentrifuge tube • Discard canisters for solutions • Discarding tube, sac, safety box • Filter paper • Filtropur S 0.2 (Sarstedt, Germany) • Gloves, nitril blue S, ref: 74210 (MaiMed, Germany) • Heat shelf or block maker TM-1, manufacturer No: 065 (Kunz instruments aps, Danmark) • Heraeus D-6450 Hanau incubator, manufacturer No: 93114723 • Ice box • Paraffin melter, Medax Nagel PW43, manufacturer No: 40592 (GmbH, Germany) • Forceps • Refrigerators (-20°C, 4°C) • Safe seal micro tube 2ml, PP, ref: 72.695.500 (Sarstedt, Germany) • Safety cabinet • Standard cassette (Edermuende, Germany) • Sterile syringe 10ml (Becton Dickinson, Spain) • Text marker • Transfer pipettes Lot: 032822005 (Sarstedt, Germany) • Tube 50 ml, ref: 62.547.254 (Sarstedt, Germany) • Tube rack

Table 3. Reagents and tools used for sectioning, deparaffinization and rehydration of HOPE-fixed, paraffin-embedded tissue

Reagents	Tools and equipments
<ul style="list-style-type: none"> • 70% acetone, cat No: 100034 (VWR, ES) • Aq.dest • 70% Isopropanol, company Cat.No. K31354834 (Merck, Germany) 	<ul style="list-style-type: none"> • Automatic microtome –Leica RM 2255, manufacturer No: 1941/07.2007 (GmbH, Germany) • Brush • Heating plate I (~55°C) – leica HI1220, manufacturer No: 6043/05/06 (GmbH, Germany) • Heating plate II (~37°C)– Madex SP-13, manufacturer No: 10708 (GmbH, Germany) • Manual microtome – Leica SM2000R, manufacturer No:

	3742/09.2007 (GmbH, Germany) <ul style="list-style-type: none"> • Microscope slides are ZN staining, microscope slides Superfrost Plus are for IHC staining. • Slide rack • Gloves, nitril blue S, ref: 74210 (MaiMed, Germany) • Cuvette and handle
--	--

Table 4. Histochemical stainings	
Reagents	Tools and equipments
<ul style="list-style-type: none"> • 0.05% NH₃-Water • 0.5 % H₂O₂ • Antibody diluent , Ref/Cat.No: ZUC025-500 (ZytoMed, Germany) • Aq.dest • Auramine-Rhodamin solution, Lot.181825 (Waldeck, Germany) • 0.2% eosin, ref: FN1123235036 (Merck, Germany) • EtOH 70 %, 80%, 96%, 100% • Gabett, ref: 55 531, (bioMérieux SA, France) • Gram-s crystal violet solution, ref: HX817114 (Merck, Germany) • 37% HCL • Mayer's hemalum solution, ref: HX376911 (Merck, Germany) • Iodine-potassium iodide solution, Art.-Nr.N052.1 (Roth, Germany) • 0.2% Potassium acetate, ref: Art.-Nr.T0874.2 (Roth, Germany) • Kinyoun carbol fuchsin, ref: 55 521, (bioMérieux SA, France) • Aq.dest • Permanent AEC kit, Ref/Cat.No: ZUC054-200 (ZytoMed Systems, Germany) • Pertex mounting medium, ref: 41-4012-00, 1000 ml (Medite GmbH, Germany) • 0.6% Safranin O solution in 20% ethyl alcohol, Art.-Nr.CN01.1 (Roth, Germany) • Tris wash buffer B (20x) TBS 200ml, ref: ZUC066-500 (Medac diagnostika, Germany) • Tween 20, Lot: SZBC0470V (Sigma Aldrich, France) • ZytoChem –Plus HRP Polymer Kit, Ref/Cat.No: POLHRP-006 (ZytoMed Systems, Germany) • Kaiser's glycerol gelatine Los/lot HX252144 (Merck, Germany) 	<ul style="list-style-type: none"> • Cover slips (24x32, 24x40, 24x50, thickness 0.13-0.16) (R.Langenbrick, Germany) • Cuvette and handle • Cuvette carriage • Cylinders with measurements • Eppendorf tubes • Filter paper • Filter tips, Ref: 70.1116.210 (Spectrum, USA) • Forceps • Funnel • Gloves, nitril blue S, ref: 74210 (MaiMed, Germany) • Heraeus D-6450 Hanau incubator, manufacturer No: 93114723 • Humidified chamber • Extractorhood (Koettermann, Gemrany) • Magnetic mixer IKA labortechnik • Microscope slides are ZN staining, microscope slides Superfrost Plus are for IHC staining. • Microscopy Nikon E 200 • Safe seal micro tube 2ml and 1,5 ml PP, Ref: 72.695.500 (Sarstedt, Germany) • Timer C5079 (Roth, Germany) • Tissue auto-stainer TST 46 • Tube racks • Vortex mixer VM-300, Ser.-Nr: 001051 (neoLab, Germany) • Costar stripette 5 ml-4487, 10 ml-4488 (Corning, USA) • Parafilm "M" laboratory film (Bemis, USA) • Pipetus 240 V pipetting controller, manufacturer No: 9907200 (Hirschmann, Germany)

Table 4.1. Histochemical staining	
Hematoxilin and Eosin staining:	
1.	Stain in Hematoxylin Mayer (10 minutes)
2.	Rinse in distilled water
3.	Immerse in 0.2% Potassium acetate (1 minutes)
4.	Rinse in water
5.	Counterstain in 0.2% eosin (2 minutes)
6.	Dehydrate
	a. EtOH 70 % (10 seconds)
	b. EtOH 80% (10 seconds)
	c. EtOH 96 % (10 seconds)
	d. 2 x EtOH 100 % (10 seconds)
7.	Clear in Xylol I and II (10 seconds)
8.	Mount with Pertex mounting medium and cover slip

Table 4.2. Histochemical staining	
Cold Ziehl-Neelsen technique/Kinyoun staining:	

1.	Flood slides in Kinyoun carbol fuchsin	(5 minutes)
2.	Rinse gently with water until the water flows off clear	
3.	Flood slides with acid-alcohol (3% HCl in ethanol)	(3~5 seconds)
4.	Rinse gently with water until the water flows off clear	
5.	Counterstain with Gabett solution	(2 minutes)
6.	Optimization:	
7.	Stain in Hematoxylin Mayer	(20 seconds)
8.	Rinse in Aq.dest I	(10 seconds)
9.	Rinse in Aq.dest II	(10 seconds)
10.	Rinse in Aq.dest III	(10 seconds)
11.	0.05% NH ₃ -Watter	(20 seconds)
12.	Rinse in Aq.dest	(10 seconds)
13.	Dehydrate	
	a. EtOH 70 %	(10 seconds)
	b. EtOH 80%	(10 seconds)
	c. EtOH 96 %	(10 seconds)
	d. 2 x EtOH 100 %	(10 seconds)
14.	Clear in Xylol I and II	(10 seconds)
15.	Mount with Pertex mounting medium and cover slip.	
	Preparation of 3% acid alcohol:	
16.	475 ml EtOH 100 %	
17.	10 ml dH ₂ O	
18.	15 ml HCL 37%	

Table 4.3. Histochemical staining		
Gram staining:		
1.	Flood in Gram-s crystal violet solution	(3-5 minutes)
2.	Rinse off the crystal violet with distilled water.	
3.	Flood the slide with iodine solution (#2)	(2-3 minutes)
4.	Rinse off the iodine-potassium iodide solution with distilled water.	
5.	Dry the slide on bibulous paper	
6.	Flood the slide with EtOH 100 % until the alcohol flows off clear	
7.	Rinse off the alcohol with distilled water.	
8.	Flood the slide with Safranin O solution	(1 minute)
9.	Dry the slide on bibulous paper	
10.	Rinse off the safranin with EtOH 100 %	(3 seconds)
11.	Clear in Xylol	(10 seconds)
12.	Mount with Pertex mounting medium and cover slip.	

Table 4.4 Histochemical staining	
Immunohistochemical staining:	
Preparation of Chromogen	A permanent AEC kit was performed according to manufacturer's instruction.
Deparaffinization	Isopropanol 60° C (10 minutes) Isopropanol 60° C (2 minutes) Dry slides in air at room temperature Aceton 70% (4° C) (10 minutes) A. dest (4°C) (10 minutes) A. dest (room temperature) (wash shortly)
Detection of target antigen	To block endogenous peroxidases, deparaffinized and rehydrated tissue sections were placed for 10 minutes in a cuvette with 0.5 % H ₂ O ₂ (in aqua dest.). After blocking, slides were transferred immediately into a new cuvette with wash buffer T-TBS pH 7.6 with 0.05% Tween 20 (Tween-Tris buffered saline). Diluted primary antibodies were applied for an hour at room temperature in humid chamber. Afterwards the detection system (Zytochem-Plus HRP Polymer Kit) was applied by following steps. For all applied reagents a volume of 200 µl was used: <ul style="list-style-type: none"> • Wash buffer in a cuvette (3 times) • Postblock (not needed if rabbit primary antibody is used) (15 minutes) • Wash buffer in a cuvette (3 times) • Polymer (20 minutes) • Wash buffer in a cuvette (3 times) • Chromogen (200 µl)
Counter staining	Color reaction was stopped with aq. dest and slides transferred into cuvette carriage:: <ul style="list-style-type: none"> • Stain in Hematoxylin Mayer (20 seconds)

Dehydration and mounting	<ul style="list-style-type: none"> • Rinse in Aq.dest I (10 seconds) • Rinse in Aq.dest II (10 seconds) • Rinse in Aq.dest III (10 seconds) • 0.05% NH₃-water (20 seconds) • Immerse in 0.2% kaliumacetat (1 minute) • Rinse in Aq.dest (10 seconds) • Dehydrate <ul style="list-style-type: none"> a. EtOH 70 % (10 seconds) b. EtOH 80% (10 seconds) c. EtOH 96 % I (10 seconds) d. EtOH 96 % I (10 seconds) e. 2 x EtOH 100 % (10 seconds) • Clear in Xylol I and II (10 seconds) • Mount with Pertex mounting medium and cover slip
---------------------------------	---

Table 4.5. Histochemical stainings

IHC with Auramin- Rhodamin- Fluorescence double staining:

Preparation of Chromogen	Preparation of DAB chromogen is: 1ml Imidazol- Puffer + 1 drop H ₂ O ₂ + 1 drop DAB, afterwards mix them well.
Deparaffinazation	<ul style="list-style-type: none"> Isopropanol 60°C (10 minutes) Isopropanol 60°C (2 minutes) Dry slides in air at room temperature Acetone 70% (4°C) (10 minutes) Aq.dest (4°C) (10 minutes) Aq.dest (room temperature) (wash shortly)
Detection of target antigen	To block endogenous peroxidases, deparaffinized and rehydrated tissue sections were placed for 10 minutes in a cuvette with 0.5 % H ₂ O ₂ (in aqua dest.). After blocking, slides were transferred immediately into a new cuvette with wash buffer T-TBS pH 7.6 with 0.05% Tween 20 (Tween-Tris buffered saline). Diluted primary antibodies were applied for an hour at room temperature in humid chamber. Afterwards the detection system (Zytochem-Plus HRP Polymer Kit) was applied by following steps. For all applied reagents a volume of 200 µl was used: <ul style="list-style-type: none"> • Wash buffer in a cuvette (3 times) • Postblock (not needed if rabbit primary antibody is used) (15 minutes) • Wash buffer in a cuvette (3 times) • Polymer (20 minutes) • Wash buffer in a cuvette (3 times) • Chromogen (200 µl)
Auramin-Rhodamin-Staining	Color reaction was stopped with wash buffer and slides transferred into cuvette carriage. Protect slides from light. <ul style="list-style-type: none"> • 15 minutes Auramin- Rhodamin • Rinse off tap water • 2 minutes HCL- Alcohol 70% • Rinse off tap water • 2 minutes 30 seconds 0.5% Kaliumpermanganat • Rinse off tap water • Rinse in Aq.dest
Counter staining	<ul style="list-style-type: none"> • Stain in Hematoxylin Mayer (20 seconds) • Rinse in Aq.dest I (10 seconds) • Rinse in Aq.dest II (10 seconds) • Rinse in Aq.dest III (10 seconds) • 0.05% NH₃-water (20 seconds)
Mounting	Mount with Kaiser's glycerol gelantine and cover slip

Table 4.6. Histochemical stains

Pappenheim staining:

Cover the smear with 1 ml of May-Grünwald's solution	(3 minutes)
Add 1 ml buffer solution, mix and stain	(~ 3-5 minutes)
Cover with diluted Giemsa's solution and stain	(~ 15-20 minutes)
Rinse with buffer solution and dry	

Table 5. Purification of DNA from formalin-fixed, paraffin-embedded tissues. Protocol obtained and adapted from [252].		
Preparation	Reagents & other preparation	Tools
	<ul style="list-style-type: none"> • QIAamp DNA Mini Kit • Xylene • EtOH (100%) • Nitrogen • Distilled water 	<ul style="list-style-type: none"> • Manual microtome– Leica SM2000R, manufacturer No: 3742/09.2007 (GmbH, Germany) • Forceps, Gloves, nitril blue S, ref: 74210 (MaiMed, Germany) • Filter tips, Ref: 70.1116.210 (Spectrum, USA) • Eppendorf and microcentrifuge tube (1,5 ml) • Tube racks • Extrator hood (Koettermann, Germany) • Microscope slides are ZN staining, microscope slides Superfrost Plus are for IHC staining. • Vortex mixer VM-300, Ser-Nr: 001051 (neoLab, Germany) • Centrifuge • Silver paper • Water bath (70°C) • Shaking water bath (56°C) • Vacuum centrifuge
Deparaffinization	<ol style="list-style-type: none"> 1. Add 1ml Xylene to the paraffin sections and rotate (ca.30 U/minutes) for 10 minutes. 2. Centrifuge tube for 5 minutes at 13000 x g and remove the supernatant carefully. 3. Repeat steps 2 times. In case of residual paraffin: Repeat again one step of Xylene 4. Add 1 ml of EtOH (100%) and rotate for 10 minutes. 5. Centrifuge tube for 5 minutes at 13000 x g and remove the supernatant carefully. 6. Repeat step 2 times and turn vacuum centrifuge on meanwhile. 7. Remove residual EtOH by use of vacuum centrifuge (2-5 minutes) 	
Isolation	<ol style="list-style-type: none"> 1. Place in a 1.5 ml micro-centrifuge tube and add 180 µl of Buffer ATL 2. 3 repetitions of temperature shock (from liquid nitrogen into water bath with 37°C) 3. Add 20 µl proteinase K and incubate at 56°C until the tissue is completely lysed in shaking water bath for overnight 4. Next day, temperature shock was repeated (see 3) 5. 200 µl Buffer AL were added to the sample, mix by pulse-vortexing for 15 second, and incubate at 70°C for 10 minutes 6. Add 200 µl ethanol 100% to the sample 7. Briefly centrifuge the 1.5 ml micro-centrifuge tube to remove drops from the inside of the lid for 1 minute at 6000 x g. 8. Transfer 600µl from mixture to QIAamp Mini spin column (in a 2 ml collection tube) and centrifuge for 1 minute at 8000x g and discard the tube containing the filtrate. If the solution has not completely passed through the membrane, centrifuge again at a higher speed until all the solution has passed through. 9. Carefully open the QIAamp Mini spin column and add 500 µl Buffer AW1 without wetting the rim. Close the cap, and centrifuge at 6000 x g (8000 rpm) for 1 minute. Place the QIAamp Mini spin column in a clean 2 ml collection tube 10. Discard the collection tube containing the filtrate. 11. Carefully open the QIAamp Mini spin column and add 500 µl Buffer AW2 without wetting the rim. Close the cap and centrifuge at full speed (20000 x g; 14000 rpm) for 3 minutes. 12. Place the QIAamp Mini spin column in a clean 1.5 ml microcentrifuge tube (not provided), and discard the collection tube containing the filtrate. Carefully open the QIAamp Mini spin column and add 200 µl distilled water. Incubate at room temperature for 1 minute, and then centrifuge at 6000 x g (8000 rpm) for 1 minute. 	

Table 6. Quantification of DNA and RNA. Protocol obtained and adapted from [253]		
Preparation	Reagents & other preparation	Tools
	<ul style="list-style-type: none"> • RNase free water Lot.No 1450173344 (Qiagen GmbH, Germany) 	<ul style="list-style-type: none"> • Gloves, nitril blue S, ref: 74210 (MaiMed, Germany) • Tube racks • Biosphere® Filter Tips (DNA-free, ATP-free, RNase free) • Waste box • Precision wipes 11.8x11.8 in./po (30x30 cm) (Kimberly-Clark professional, UK)
Making Nucleic	Sample Retention Pedestal Measurements A 1 - 2 µL sample is pipetted onto a measurement pedestal. A smaller, 0.5 µL volume sample,	

Acid Measurements	<p>may be used for concentrated nucleic acid and protein A280 samples. A fiber optic cable (the receiving fiber) is embedded within this pedestal.</p> <p>Pedestal Basic Use</p> <ol style="list-style-type: none"> 1. Raise the sampling arm and pipette the sample onto the lower measurement pedestal. 2. Lower the sampling arm and initiate a spectral measurement using the software on the PC. The sample column is automatically drawn between the upper and lower pedestals and the measurement is made. 3. When the measurement is complete, raise the sampling arm and wipe the sample from both the upper and lower pedestals using a dry, lint-free laboratory wipe. Simple wiping prevents sample carryover in subsequent measurements for samples varying by more than 1000 fold in concentration.
--------------------------	---

Table 7. DNA agarose gel electrophoresis		
Preparation	Reagents & other preparation	Tools
	<ul style="list-style-type: none"> • RNase free water Lot.No 1450173344 (Qiagen GmbH, Germany) • Ethidium bromide • DNA molecular weight ladder 	<ul style="list-style-type: none"> • Gloves, nitril blue S, ref: 74210 (MaiMed, Germany) • Tube racks • Biosphere ® Filter Tips (DNA-free, ATP-free, RNase free) • Waste box • Precision wipes 11.8x11.8 in./po (30x30 cm) (Kimberly-Clark professional, UK) • Erlenmeyer flask • Microwave • Electrophoresis power supply • UV box • Digital camera • Refrigerator • Fume hood • Gel tray and comb • Vortexer

Table 8. Total RNA extraction from HOPE-fixed, paraffin-embedded tissue blocks. Protocol obtained and adapted from [254]		
Preparation	Reagents & other preparation	Tools
	<ul style="list-style-type: none"> • Qiagen RNeasy Kit • Remove as much paraffin as possible around the tissue piece from the block • Cut sections from the block and transfer the rolls to a fresh 1.5 ml Eppendorf tube. • Only use fresh cut paraffin-material. Do not store paraffin sections longer than 2 days at 4⁰c before use. • Prepare solution of 70% EtOH with DEPC-treated water • Preapre and label 3 eppendorf tubes per sample: 1. 98 µl DEPC water for quantification, 2. Empty for elution of RNA, 3. 600µl 70EtOH • Prepare fresh Lysis buffer with beta-Mercaptoethanol (BME) under the hood. • Add 10µl BME per 1 ml RLT Lysis buffer. • Xylene • EtOH (100%) 	<ul style="list-style-type: none"> • Manual microtome – Leica SM2000R, manufacturer No: 3742/09.2007 (GmbH, Germany) • Forceps, Gloves, nitril blue S, ref: 74210 (MaiMed, Germany) • Filter tips, Ref: 70.1116.210 (Spectrum, USA) • Eppendorf and microcentrifuge tube (1.5 ml) • Tube racks • Extrator hood (Koettermann, Germany) • Microscope slides are for ZN staining, microscope slides Superfrost Plus are for IHC staining. • Vortex mixer VM-300, Ser.-Nr: 001051 (neoLab, Germany) • Centrifuge • Silver paper • Water bath (70°C) and shaking water bath (56°C) • Vacuum centrifuge • Box with ice
Deparaffinization	<ul style="list-style-type: none"> • Cut up to 25 mg of tissue into small pieces and determine the amount of tissue. Do not use more than 25 mg. Weighing tissue is the most accurate way to determine the amount. • Add 1ml Xylene to the paraffin sections and rotate (ca.30 U/min) for 10 minutes. • Centrifuge tube for 5 minutes at 13.000 x g and remove the supernatant carefully. • Repeat steps 2 times. In case of residual paraffin: Repeat again one step of Xylene • Add 1 ml of EtOH (100%) and rotate for 10 minutes. • Centrifuge tube for 5 minutes at 13.000 x g and remove the supernatant carefully. 	

	<ul style="list-style-type: none"> • Repeat step 2 times and turn vacuum centrifuge on meanwhile. • Remove residual EtOH by use of vacuum centrifuge (2-5 minutes)
Isolation	<ul style="list-style-type: none"> • Place in a 1.5 ml micro-centrifuge tube and add 600 µl Lysis buffer per sample. • Homogenize and use fresh pistil for every sample! • Centrifuge tubes for 5 minutes at 14.000 x g and to spin down cellular debris. • Transfer supernatant in the prepared tube with 600 µl EtOH mix well and resuspend • Add 700 µl of supernatant/ethanol solution to Qiagen column • Centrifuge tubes for 2 minutes at 8000 x g and trash eluted liquid • Add 700 µl RW1 buffer and centrifuge for 2 minutes at 8000 x g and trash eluted liquid • Transfer column to fresh collection tube • Add 500 µl RPE buffer and centrifuge for 1 minute at 8000 x g and trash eluted liquid • Add 500 µl RPE buffer and centrifuge for 1 minute at 14.000 x g and trash eluted liquid • Transfer tube to fresh 1.5 ml tube and add 30 µl DEPC water. • Incubate room temperature for 1 minute • Elute for 1 minute at 14.000 x g • Put samples on ice

Table 9. Determining RNA integrity number via bioanalyzer.
Protocol obtained and adapted from [255]

Preparation	Reagent	Tools
	<ul style="list-style-type: none"> • RNase-free water • RNaseZAP • RNA 6000 Nano dye • RNA Nano gel matrix • RNA 6000 Nano marker 	<ul style="list-style-type: none"> • Chip priming station • IKA vortex mixer IKA - Model MS2-S8/MS2-S9 • 16-pin bayonet electrode cartridge • RNaseZAP® recommended for electrode decontamination (Ambion, Inc. Cat. No. 9780) • Pipettes (10 µl and 1000 µl) with compatible tips (RNase-free, no filter tips, no autoclaved tips) • 1.5 ml microcentrifuge tubes (RNase-free) • Microcentrifuge (≥1300 g) • Heating block
Preparing the RNA ladder after arrival	<ol style="list-style-type: none"> 1 After reagent kit arrival, pipette the ladder in RNase-free vial. 2 Heat denature it for 2 minutes at 70 °C 3 Immediately cool down the vial on ice 4 Prepare aliquots in RNase-free vials with the required amount for a typical daily use. 5 Store aliquots at -70°C 6 Before use, thaw ladder aliquots and keep them on ice 	
Decontaminating the electrodes	<ol style="list-style-type: none"> 1 Slowly fill one of the wells of an electrode cleaner with 350 µl RNaseZAP. 2 Open the lid and place electrode cleaner in the Agilent 2100 bioanalyzer. 3 Close the lid and leave it closed for about 1 minute. 4 Open the lid and remove the electrode cleaner. 5 Slowly fill one of the wells of another electrode cleaner with 350 µl RNase-free water. 6 Place electrode cleaner in the Agilent 2100 bioanalyzer. 7 Close the lid and leave it closed for about 10 seconds. 8 Open the lid and remove the electrode cleaner. Label it and keep it for further use. 9 Wait another 10 seconds for the water on the electrodes to evaporate before closing the lid. 	
Preparing the gel	<ol style="list-style-type: none"> 1 Allow all reagents to equilibrate to room temperature for 30 minutes before use. 2 Place 550 µl of Agilent RNA 6000 Nano gel matrix (red) into the top receptacle of a spin filter. 3 Place the spin filter in a microcentrifuge and spin for 10 minutes at 1500 g ± 20 % 4 Aliquot 65 µl filtered gel into 0.5 ml RNase-free microfuge tubes that are included in the kit. 	
Preparing the gel-dye mix	<ol style="list-style-type: none"> 1 Allow all reagents to equilibrate to room temperature for 30 minutes before use. Protect the dye concentrate from light while bringing it to room temperature. 2 Vortex RNA 6000 Nano dye concentrate (blue) for 10 seconds and spin down. 3 Add 1 µl of RNA 6000 Nano dye concentrate (blue) to a 65 µl aliquot of filtered gel 4 Cap the tube, vortex thoroughly and visually inspect proper mixing of gel and dye. Store the dye concentrate at 4°C in the dark again. 5 Spin tube for 10 minutes at room temperature at 13000 x g 	
Loading the gel-dye mix	<ol style="list-style-type: none"> 1 Allow the gel-dye mix to equilibrate to room temperature for 30 minutes before use and protect the gel-dye mix from light during this time. 2 Take a new RNA Nano chip out of its sealed bag. 3 Place the chip on the chip priming station. 	

<p>Loading the RNA 6000 nano marker</p>	<p>4 Pipette 9.0 µl of the gel-dye mix at the bottom of the well marked and dispense the gel-dye mix. 5 Set the timer to 30 seconds, make sure that the plunger is positioned at 1 ml and then close the chip priming station. The lock of the latch will click when the Priming Station is closed correctly. 6 Press the plunger of the syringe down until it is held by the clip. 7 Wait for exactly 30 seconds and then release the plunger with the clip release mechanism. 8 Visually inspect that the plunger moves back at least to the 0.3 ml mark. 9 Wait for 5 seconds, then slowly pull back the plunger to the 1 ml position. 10 Open the chip priming station. 11 Pipette 9.0 µl of the gel-dye mix in each of the wells marked.</p> <p>1 Pipette 5 µl of the RNA 6000 Nano marker (green) into the well marked with the ladder symbol and each of the 12 sample wells.</p>
<p>Loading the ladder and samples</p>	<p>1 Before use, thaw ladder aliquots and keep them on ice 2 To minimize secondary structure, heat denature (70 °C, 2 minutes) the samples before loading on the chip. 3 Pipette 1 µl of the RNA ladder into the well marked with the ladder symbol. 4 Pipette 1 µl of each sample into each of the 12 sample wells. 5 Set the timer to 60 seconds. 6 Place the chip horizontally in the adapter of the IKA vortex mixer and make sure not to damage the buldge that fixes the chip during vortexing. 7 Vortex for 60 seconds at 2400 x g. 8 Refer to the next topic on how to insert the chip in the Agilent 2100 bioanalyzer. Make sure that the run is started within 5 minutes.</p>
<p>Inserting a chip in the Agilent 2100 Bioanalyzer</p>	<p>1 Open the lid of the Agilent 2100 bioanalyzer. 2 Check that the electrode cartridge is inserted properly and the chip selector is in position (1). Refer to “Setting up the Bioanalyzer” on page 8 for details. 3 Place the chip carefully into the receptacle. The chip fits only one way. 4 Carefully close the lid. The electrodes in the cartridge fit into the wells of the chip. 5 The 2100 expert software screen shows that you have inserted a chip and closed the lid by displaying the chip icon at the top left of the <i>Instrument</i> context.</p>
<p>Starting the chip run</p>	<p>1 In the <i>Instrument</i> context, select the appropriate assay from the <i>Assay</i> menu. 2 Accept the current <i>File Prefix</i> or modify it. 3 Click the <i>Start</i> button in the upper right of the window to start the chip run. The incoming raw signals are displayed in the <i>Instrument</i> context. 4 To enter sample information like sample names and comments, select the <i>Data File</i> link that is highlighted in blue or go to the <i>Assay</i> context and select the <i>Chip Summary</i> tab. Complete the sample name table. 5 To review the raw signal trace, return to the <i>Instrument</i> context. 6 After the chip run is finished, remove the chip from the receptacle of the bioanalyzer and dispose it according to good laboratory practices.</p>
<p>Cleaning up after a RNA 6000 nano chip run</p>	<p>1 Slowly fill one of the wells of the electrode cleaner with 350 µl RNase-free water. 2 Open the lid and place the electrode cleaner in the Agilent 2100 bioanalyzer. 3 Close the lid and leave it closed for about 10 seconds. 4 Open the lid and remove the electrode cleaner. 5 Wait another 10 seconds to allow the water on the electrodes to evaporate before closing the lid.</p>

Table 2-10. TUNEL assay

Preparation	Reagents	Tools
	<ul style="list-style-type: none"> • In Situ Cell death detection kit, TMR red • Enzyme solution • Label solution • Xylene and ethanol • Washing buffer : PBS • Proteinase K • Working solution [10-20µg/ml in 10mM Tris/HCl, pH 7.4-8] • Permeabilisation solution : (0.1% Triton X-100, 0.1% sodium citrate) • Pepsin (0.25%-0.5% in HCl, pH 2) • 0.1 M citrate buffer 	<ul style="list-style-type: none"> • Humidified chamber • Coverslip • Diamond writing pen • Marker • Incubator
Deparaffinization	Isopropanol 60° C (10 minutes)	

	<p>Isopropanol 60° C (2 minutes) Dry slides in air at room temperature Aceton 70% (4° C) (10 minutes) A. dest. (4° C) (10 minutes) A. dest. (room temperature) (Wash shortly)</p>
Preparation of controls	Negative control: incubate fixed and permeabilized slides in 50 µl Label solution (without terminal transferase) instead of TUNEL reaction mixture
Protease treatment	Positive control: Incubate fixed and permeabilized slides in DNAase I recombinant for 10 minutes at room temperature to induce DNA strand breaks, prior to labeling procedures.
Permeabilisation	<ul style="list-style-type: none"> • Incubate tissue section for 15-30 minutes at +37⁰C with Proteinase K working solution • Rinse slides twice with PBS • Dry area around sample
Labeling reaction with TUNEL reaction mixture	<ul style="list-style-type: none"> • Add 50 µl TUNEL reaction mixture on samples • Incubate slides in a humidified atmosphere for 60 minutes at +37⁰C in the dark place • Rinse slides 3 x with PBS buffer
Analyse by fluorescence microscope	Samples can directly be analysed under a fluorescence microscopy with an excitation wavelength in the range of 520-560 nm and detection in the range of 570-620 nm.

Appendix II

Decision rules for these normality tests:

The null hypothesis for this test of normality is that the data are normally distributed.

- If p value is above 0.05, the H_0 cannot be rejected,
- If p value is below 0.05, the H_0 is rejected.

Decision rules for non-parametric Levene's test:

The null hypothesis is that there is an equality of variance.

- If p value is above 0.05, the H_0 cannot be rejected,
- If p value is below 0.05, the H_0 is rejected.

Decision rules for Kruskal-Wallis test:

In our case, $\alpha=0.05$, $df_1(k-1)=5$, $df_2(k-1)=2$, Z_1 value (χ^2 distribution)=11.07, Z_2 value (χ^2 distribution)=5.99. To find to Z values, the percentage points of the Chi square distribution table was used.

The null hypothesis is that there is no difference between groups.

- If χ^2 is higher than critical value, the H_0 is rejected.

Decision rules for median test:

In our case, $\alpha=0.05$, $df_1(k-1)=5$, $df_2(k-1)=2$, Z_1 value (χ^2 distribution)=11.07, Z_2 value (χ^2 distribution)=5.99. To find to Z values, the percentage points of the Chi square distribution table was used and attached in Appendix-II.

The null hypothesis is that there is no difference between groups.

If χ^2 is higher than critical value, the H_0 is rejected.

Decision rules for Mann-Whitney U test:

The null hypothesis is that there is no difference between the ranks of the 2 group.

In our case, state $\alpha=0.05$, 2 tailed,

- If Z value is less than -1.96 or higher than 1.96, reject the null hypothesis

Decision rule for Chi square test:

The null hypothesis: The observed frequencies in each category are equal to the expected frequencies.

Decision rules for correlation analysis:

The null hypothesis for the test of correlation is that, there is no statistically significant relationship between variables.

- If p value is above 0.05, the H_0 cannot be rejected,
- If p value is below 0.05, the H_0 is rejected

Decision rules for linear regression:

The null hypothesis for the test of correlation is that, there is no supported relationship between 2 variables.

At α level=0.05

- If regression coefficient is zero ($H_0:\beta=0$), the H_0 cannot be rejected,
- If regression coefficient differs from zero, the H_0 is rejected

3.1.1.b. Results of MTT assay

Descriptive statistics associated with MTT assay

	N	Minimum	Maximum	Mean		Std. Deviation	Skewness		Kurtosis	
					Std. Error			Std. Error		Std. Error
positive control (1 piece)	5	.09500	.09800	.0963200	.00048311	.00108028	.796	.913	2.108	2.000
incubation-2ml (1 piece)	5	.05900	.06800	.0640000	.00144914	.00324037	-.735	.913	2.000	2.000
incubation-3ml (1 piece)	5	.06000	.06500	.0632000	.00086023	.00192354	-1.517	.913	2.608	2.000
negative control (1 piece)	5	.00561	.00651	.0059100	.00015811	.00035355	1.697	.913	3.152	2.000
positive control (2 pieces)	5	.19700	.20000	.1983200	.00048311	.00108028	.796	.913	2.108	2.000
incubation-2ml (2 pieces)	5	.05600	.06700	.0620000	.00176068	.00393700	-.615	.913	2.000	2.000
incubation-3ml (2 pieces)	5	.11300	.13300	.1226000	.00317175	.00709225	.280	.913	1.976	2.000
negative control (2 pieces)	5	.00527	.00667	.0057780	.00025664	.00057386	1.134	.913	.439	2.000
positive control (3 pieces)	5	.34400	.36400	.3540000	.00316228	.00707107	.000	.913	2.000	2.000
incubation-2ml (3 pieces)	5	.06800	.07200	.0708000	.00073485	.00164317	-1.736	.913	3.251	2.000
incubation-3ml (3 pieces)	5	.12700	.14400	.1354000	.00304302	.00680441	.073	.913	-1.428	2.000
negative control (3 pieces)	5	.00537	.01540	.0077700	.00192556	.00430568	2.136	.913	4.615	2.000

Test assumptions associated with MTT assay

Tests of Normality							Test of Homogeneity of Variances				
pieces	Kolmogorov-Smirnov				Shapiro-Wilk			Levene Statistic	df1	df2	Sig.
	Statistic	df	Sig.		Statistic	df	Sig.				
positive control	1	.307	5	.138	.915	5	.496	1.775	2	12	.211
	2	.307	5	.138	.915	5	.496				
	3	.300	5	.161	.883	5	.325				
negative control	1	.300	5	.161	.836	5	.154	5.240	2	12	.073
	2	.241	5	.200 [*]	.894	5	.376				
	3	.388	5	.113	.663	5	.204				
incubation-2ml	1	.300	5	.161	.922	5	.543	.431	2	12	.660
	2	.300	5	.161	.920	5	.530				
	3	.348	5	.067	.779	5	.054				
incubation-3ml	1	.261	5	.200 [*]	.859	5	.223	1.573	2	12	.247
	2	.278	5	.200 [*]	.910	5	.470				
	3	.150	5	.200 [*]	.980	5	.934				

Inferential statistics associated with MTT assay

Multiple Comparisons

Dependent Variable: all samples

Tukey HSD

(I) group name	(J) group name	Mean Difference (I-J)	Std. Error	Sig.	95% Confidence Interval	
					Lower Bound	Upper Bound
positive control	negative control	.20972733 [*]	.02094590	.000	.1542649	.2651897
	incubation-2ml	.15061333 [*]	.02094590	.000	.0951509	.2060757
	incubation-3ml	.10914667 [*]	.02094590	.000	.0536843	.1646091
negative control	positive control	-.20972733 [*]	.02094590	.000	-.2651897	-.1542649
	incubation-2ml	-.05911400 [*]	.02094590	.032	-.1145764	-.0036516
	incubation-3ml	-.10058067 [*]	.02094590	.000	-.1560431	-.0451183
incubation-2ml	positive control	-.15061333 [*]	.02094590	.000	-.2060757	-.0951509
	negative control	.05911400 [*]	.02094590	.032	.0036516	.1145764
	incubation-3ml	-.04146667	.02094590	.208	-.0969291	.0139957
incubation-3ml	positive control	-.10914667 [*]	.02094590	.000	-.1646091	-.0536843
	negative control	.10058067 [*]	.02094590	.000	.0451183	.1560431
	incubation-2ml	.04146667	.02094590	.208	-.0139957	.0969291

*. The mean difference is significant at the 0.05 level.

3.1.2.b. Histopathological overview

Descriptive statistics and test assumptions associated with numbers of infected cells in different layers of block

Descriptive Statistics

	N	Minimum	Maximum	Mean	Std. Deviation	Skewness		Kurtosis	
	Statistic	Statistic	Statistic	Statistic	Statistic	Statistic	Std. Error	Statistic	Std. Error
1-25th slides	25	3	127	47.84	38.908	.602	.464	-1.017	.902
51-75th slides	25	11	286	126.92	59.466	.582	.464	.814	.902
Valid N (listwise)	25								

Tests of Normality

group	Kolmogorov-Smirnov ^a			Shapiro-Wilk		
	Statistic	df	Sig.	Statistic	df	Sig.
slides 1-25th slides	.187	25	.024	.890	25	.011
51-75th slides	.106	25	.200*	.967	25	.570

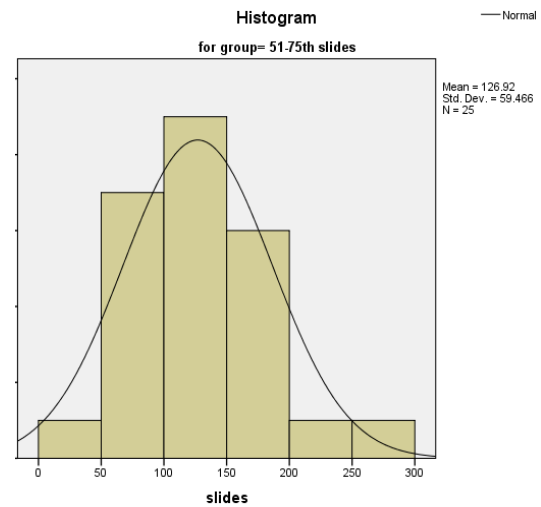
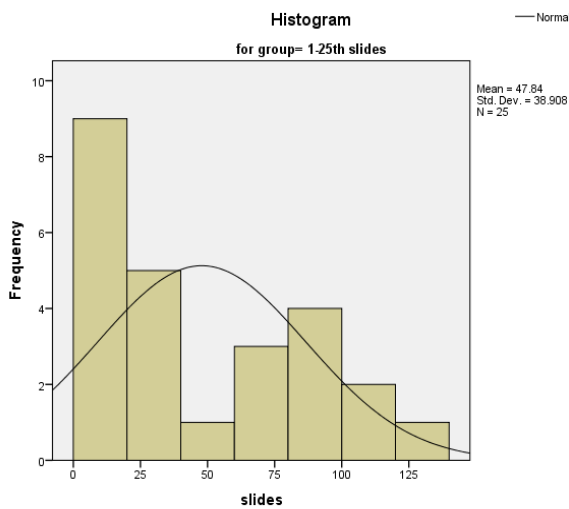
*. This is a lower bound of the true significance.

a. Lilliefors Significance Correction

Test of Homogeneity of Variances

slides1

	Sum of Squares	df	Mean Square	F	Sig.
Between Groups	1.708	1	1.708	.044	.835
Within Groups	1869.844	48	38.955		
Total	1871.551	49			



Ranks

group	N	Mean Rank	Sum of Ranks
slides 1-25th slides	25	16.38	409.50
51-75th slides	25	34.62	865.50
Total	50		

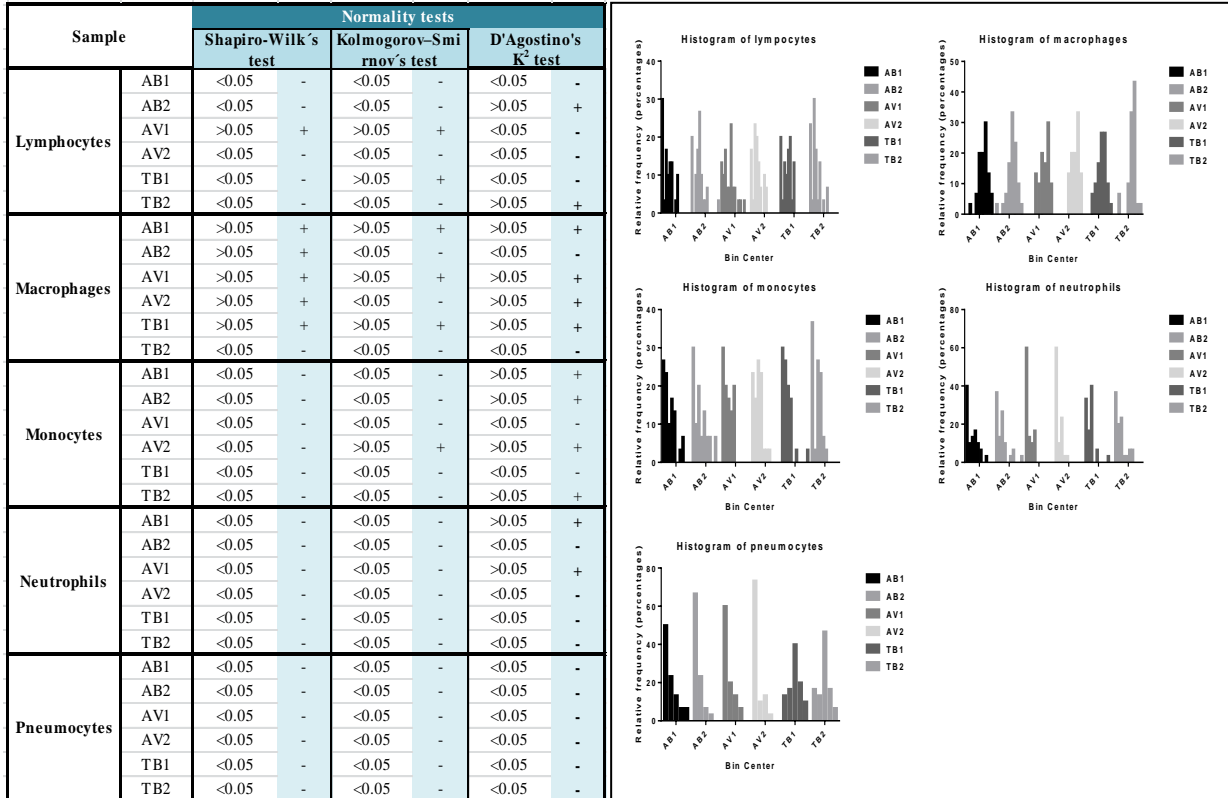
Test Statistics^a

	slides
Mann-Whitney U	84.500
Wilcoxon W	409.500
Z	-4.424
Asymp. Sig. (2-tailed)	.000

a. Grouping Variable: group

3.2.1. Infected cell types

Descriptive statistics and test assumptions associated with cell count



*We evaluated H_0 via critical value and the summaries are referred as (+) or (-).

Test of Homogeneity of Variances

		Sum of Squares	df	Mean Square	F	Sig.
monocyte	Between Groups	3263.194	5	652.639	1.108	.358
	Within Groups	102488.131	174	589.012		
	Total	105751.325	179			
macrophages	Between Groups	3870.178	5	774.036	1.177	.322
	Within Groups	114385.574	174	657.388		
	Total	118255.752	179			
pneumocyte	Between Groups	3275.830	5	655.166	1.397	.228
	Within Groups	81593.735	174	468.930		
	Total	84869.564	179			
neutrophil	Between Groups	3009.303	5	601.861	1.380	.234
	Within Groups	75880.247	174	436.093		
	Total	78889.550	179			
lymphocyte	Between Groups	2554.359	5	510.872	.763	.577
	Within Groups	116455.273	174	669.283		
	Total	119009.633	179			

3.2.2. *In vitro* infection of primary cells

Descriptive statistics and test assumptions associated with initial invasion

Descriptive Statistics

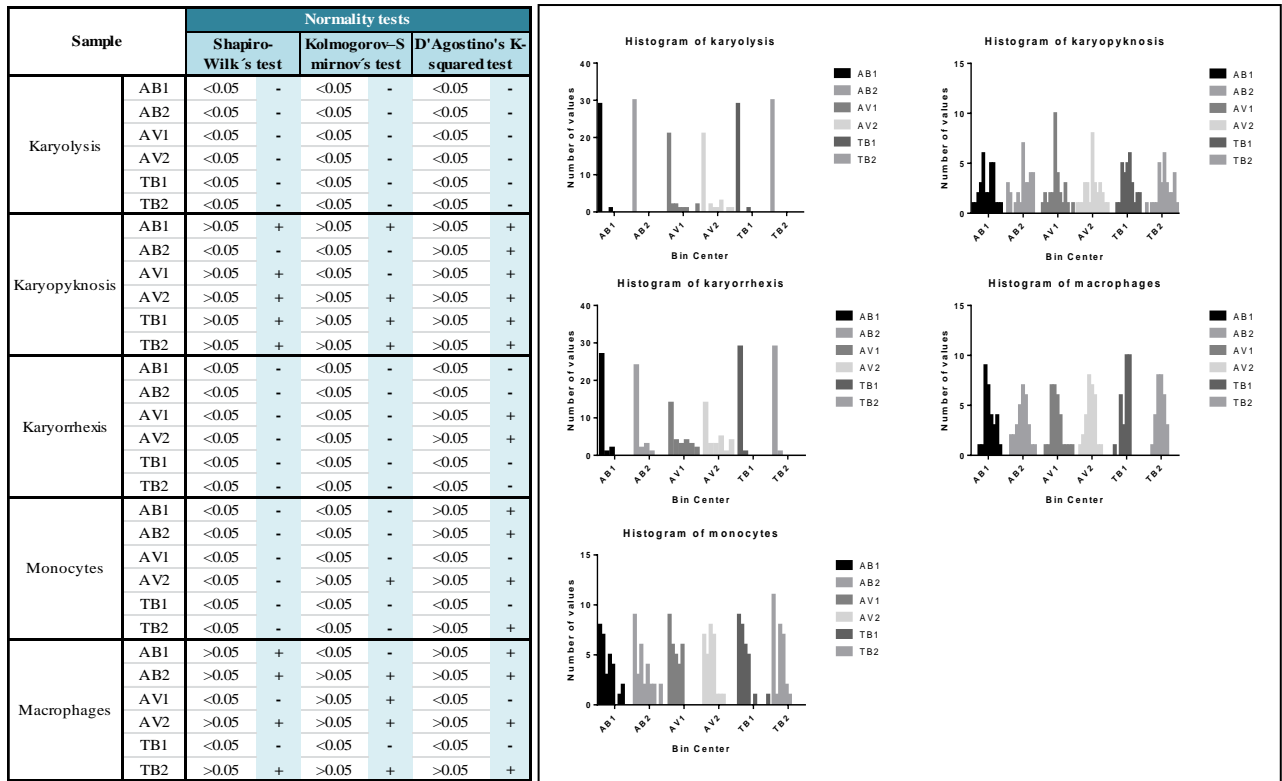
Cell types		N	Minimum	Maximum	Mean		Std. Deviation	Skewness		Kurtosis	
		Statistic	Statistic	Statistic	Statistic	Std. Error	Statistic	Statistic	Std. Error	Statistic	Std. Error
Pneumocytes-II	Initial invasion (MOI of 1:1)	4	.27	2.78	1.2875	.56979	1.13957	.844	1.014	-.946	2.619
	Initial invasion (MOI of 3:1)	4	.22	6.02	2.3130	1.33545	2.67090	1.257	1.014	.815	2.619
	Initial invasion (MOI of 10:1)	4	.12	2.66	1.4025	.68196	1.36393	-.009	1.014	-5.814	2.619
Macrophages	Initial invasion (MOI of 1:1)	4	4.00	17.73	9.0150	3.04837	6.09675	1.481	1.014	2.192	2.619
	Initial invasion (MOI of 3:1)	4	2.67	36.36	13.4725	7.90311	15.80623	1.627	1.014	2.479	2.619
	Initial invasion (MOI of 10:1)	4	1.52	4.00	2.2825	.57646	1.15292	1.916	1.014	3.751	2.619

Cell types		Data characteristic	Tests of Normality			Z value		Levene's Test for Equality of Variances		Nonparametric Levene's Test for Equality of Variances	
			Shapiro-Wilk			skewness	kurtosis	F	Sig.	F	Sig.
			Statistic	df	Sig.						
Initial invasion (MOI of 1:1)	Pneumocytes-II	0.92	4	0.545	0.832	-0.361	3.987	0.092			
	Macrophages	0.87	4	0.319	1.46	0.836					
Initial invasion (MOI of 3:1)	Pneumocytes-II	0.87	4	0.300	1.239	0.311	4.666	0.074			
	Macrophages	0.80	4	0.111	1.604	0.946					
Initial invasion (MOI of 10:1)	Pneumocytes-II	0.79	4	0.093	-8.875	-2.219			2.000	0.207	
	Macrophages	0.73	4	0.026	1.889	1.432					

Test of Homogeneity of Variances					
		Nonparametric Levene's test for macrophages		Levene's test for pneumocytes-II	
	df	F	Sig.	F	Sig.
Between Groups	2	3.180	0.090	1.541	0.265
Within Groups	9				

3.2.3.a. Types of cellular changes-1

Descriptive statistics associated with cell morphology



*We evaluated H_0 via critical value and the summaries are referred as (+) or (-).

Test of Homogeneity of Variances

		Sum of Squares	df	Mean Square	F	Sig.
macrophage	Between Groups	2654.479	5	530.896	.827	.532
	Within Groups	111766.526	174	642.336		
	Total	114421.005	179			
monocyte	Between Groups	3263.194	5	652.639	1.108	.358
	Within Groups	102488.131	174	589.012		
	Total	105751.325	179			
karyolysis	Between Groups	50145.572	5	10029.114	58.049	.000
	Within Groups	30062.078	174	172.771		
	Total	80207.650	179			
karyopyknosis	Between Groups	1657.042	5	331.408	.465	.802
	Within Groups	124016.821	174	712.740		
	Total	125673.862	179			
karyorrhexis	Between Groups	54531.007	5	10906.201	48.857	.000
	Within Groups	38841.153	174	223.225		
	Total	93372.161	179			

3.2.3.a. Types of cellular changes-2
Factorial ANOVA for TUNEL assay

Descriptive Statistics

Dependent Variable: occurrence

type	group	Mean	Std. Deviation	N
alive cells	PC	388.35	105.012	17
	MED	310.08	203.127	12
	AB	314.41	102.676	17
	AV	431.86	158.423	7
	TB	358.83	107.008	18
	NC	385.63	88.379	8
	Total	357.41	130.024	79
apoptotic cells	PC	12.65	11.000	17
	MED	51.67	66.812	12
	AB	29.59	28.881	17
	AV	51.14	35.083	7
	TB	20.94	22.193	18
	NC	207.13	60.706	8
	Total	47.22	66.879	79
Total	PC	200.50	204.361	34
	MED	180.88	198.214	24
	AB	172.00	162.516	34
	AV	241.50	226.219	14
	TB	189.89	187.506	36
	NC	296.37	117.735	16
	Total	202.31	186.626	158

Tests of Between-Subjects Effects

Dependent Variable: occurrence

Source	Type III Sum of Squares	df	Mean Square	F	Sig.	Partial Eta Squared
Corrected Model	4163322.31 ^a	11	378483.847	42.349	.000	.761
Intercept	6259872.154	1	6259872.154	700.421	.000	.828
type	3144620.847	1	3144620.847	351.854	.000	.707
group	211001.873	5	42200.375	4.722	.001	.139
type * group	151719.014	5	30343.803	3.395	.006	.104
Error	1304845.492	146	8937.298			
Total	11935011.00	158				
Corrected Total	5468167.804	157				

a. R Squared = .761 (Adjusted R Squared = .743)

Levene's Test of Equality of Error Variances^a

Dependent Variable: occurrence

F	df1	df2	Sig.
10.175	11	146	.000

Tests the null hypothesis that the error variance of the dependent variable is equal across groups.

a. Design: Intercept + type + group + type * group

Estimates

Dependent Variable: occurrence

group	Mean	Std. Error	95% Confidence Interval	
			Lower Bound	Upper Bound
PC	200.500	16.213	168.457	232.543
MED	180.875	19.297	142.737	219.013
AB	172.000	16.213	139.957	204.043
AV	241.500	25.266	191.565	291.435
TB	189.889	15.756	158.749	221.029
NC	296.375	23.634	249.665	343.085

Univariate Tests

Dependent Variable: occurrence

	Sum of Squares	df	Mean Square	F	Sig.	Partial Eta Squared
Contrast	211001.873	5	42200.375	4.722	.001	.139
Error	1304845.492	146	8937.298			

The F tests the effect of group. This test is based on the linearly independent pairwise comparisons among the estimated marginal means.

Estimates

Dependent Variable: occurrence

type	Mean	Std. Error	95% Confidence Interval	
			Lower Bound	Upper Bound
alive cells	364.861	11.410	342.311	387.410
apoptotic cells	62.186	11.410	39.636	84.736

Pairwise Comparisons

Dependent Variable: occurrence

(I) type	(J) type	Mean Difference (I-J)	Std. Error	Sig. ^b	95% Confidence Interval for Difference ^b	
					Lower Bound	Upper Bound
alive cells	apoptotic cells	302.675*	16.136	.000	270.785	334.565
apoptotic cells	alive cells	-302.675*	16.136	.000	-334.565	-270.785

Based on estimated marginal means

*. The mean difference is significant at the ,05 level.

b. Adjustment for multiple comparisons: Least Significant Difference (equivalent to no adjustments).

Pairwise Comparisons

Dependent Variable: occurrence

(I) group	(J) group	Mean Difference (I-J)	Std. Error	Sig. ^b	95% Confidence Interval for Difference ^b	
					Lower Bound	Upper Bound
PC	MED	19.625	25.204	.437	-30.187	69.437
	AB	28.500	22.929	.216	-16.815	73.815
	AV	-41.000	30.021	.174	-100.331	18.331
	TB	10.611	22.608	.640	-34.070	55.292
	NC	-95.875*	28.661	.001	-152.519	-39.231
MED	PC	-19.625	25.204	.437	-69.437	30.187
	AB	8.875	25.204	.725	-40.937	58.687
	AV	-60.625	31.793	.058	-123.458	2.208
	TB	-9.014	24.913	.718	-58.250	40.222
	NC	-115.500*	30.512	.000	-175.802	-55.198
AB	PC	-28.500	22.929	.216	-73.815	16.815
	MED	-8.875	25.204	.725	-58.687	40.937
	AV	-69.500*	30.021	.022	-128.831	-10.169
	TB	-17.889	22.608	.430	-62.570	26.792
	NC	-124.375*	28.661	.000	-181.019	-67.731
AV	PC	41.000	30.021	.174	-18.331	100.331
	MED	60.625	31.793	.058	-2.208	123.458
	AB	69.500*	30.021	.022	10.169	128.831
	TB	51.611	29.776	.085	-7.237	110.460
	NC	-54.875	34.597	.115	-123.251	13.501
TB	PC	-10.611	22.608	.640	-55.292	34.070
	MED	9.014	24.913	.718	-40.222	58.250
	AB	17.889	22.608	.430	-26.792	62.570
	AV	-51.611	29.776	.085	-110.460	7.237
	NC	-106.486*	28.405	.000	-162.624	-50.348
NC	PC	95.875*	28.661	.001	39.231	152.519
	MED	115.500*	30.512	.000	55.198	175.802
	AB	124.375*	28.661	.000	67.731	181.019
	AV	54.875	34.597	.115	-13.501	123.251
	TB	106.486*	28.405	.000	50.348	162.624

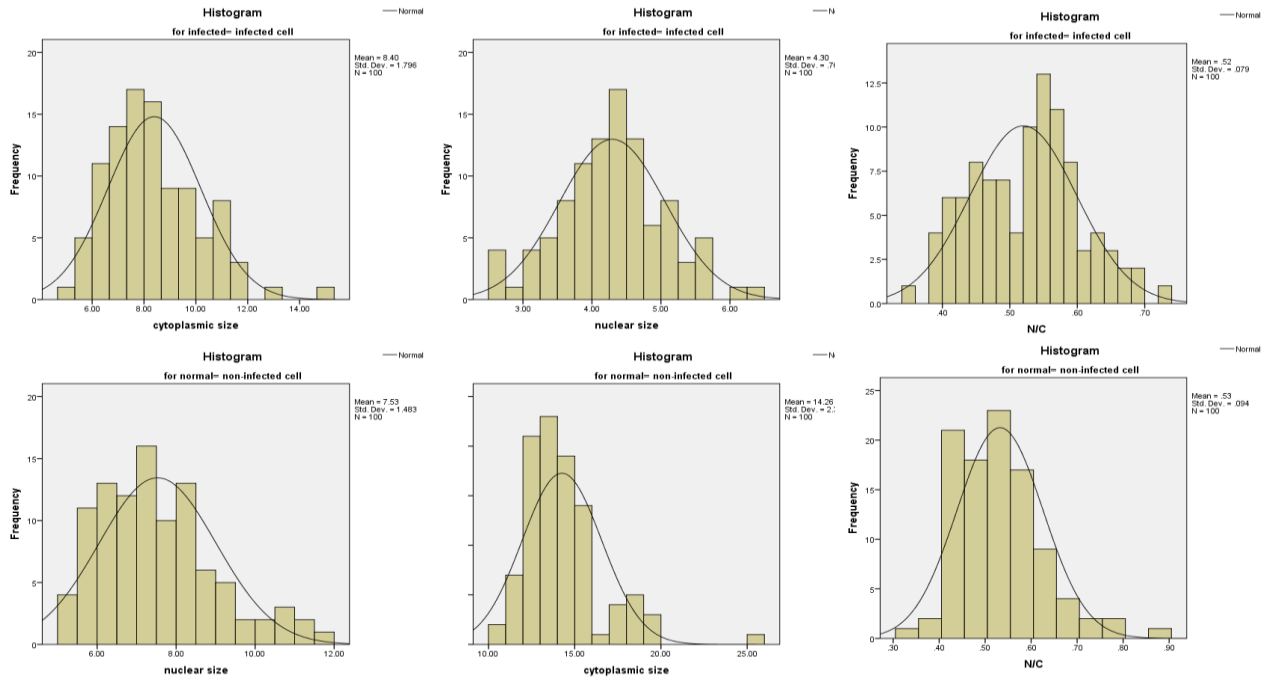
Based on estimated marginal means

*. The mean difference is significant at the ,05 level.

b. Adjustment for multiple comparisons: Least Significant Difference (equivalent to no adjustments).

3.2.3.b. Cellular measurements-1

Measurements of cytoplasmic and nuclear sizes



Sample		Normality tests					
		Shapiro-Wilk's test		Kolmogorov-Smirnov's test		D'Agostino's K-squared test	
Infected cells	cytoplasmic size	0.0056	-	0.0149	-	0.0064	-
	nuclear size	0.8079	+	>0.1	+	0.9378	+
	N/C	0.3105	+	>0.1	+	0.5406	+
Non-infected cells	cytoplasmic size	<0.0001	-	0.0005	-	<0.0001	-
	nuclear size	0.0017	-	0.0554	+	0.0093	-
	N/C	0.0015	-	0.0299	-	0.0002	-

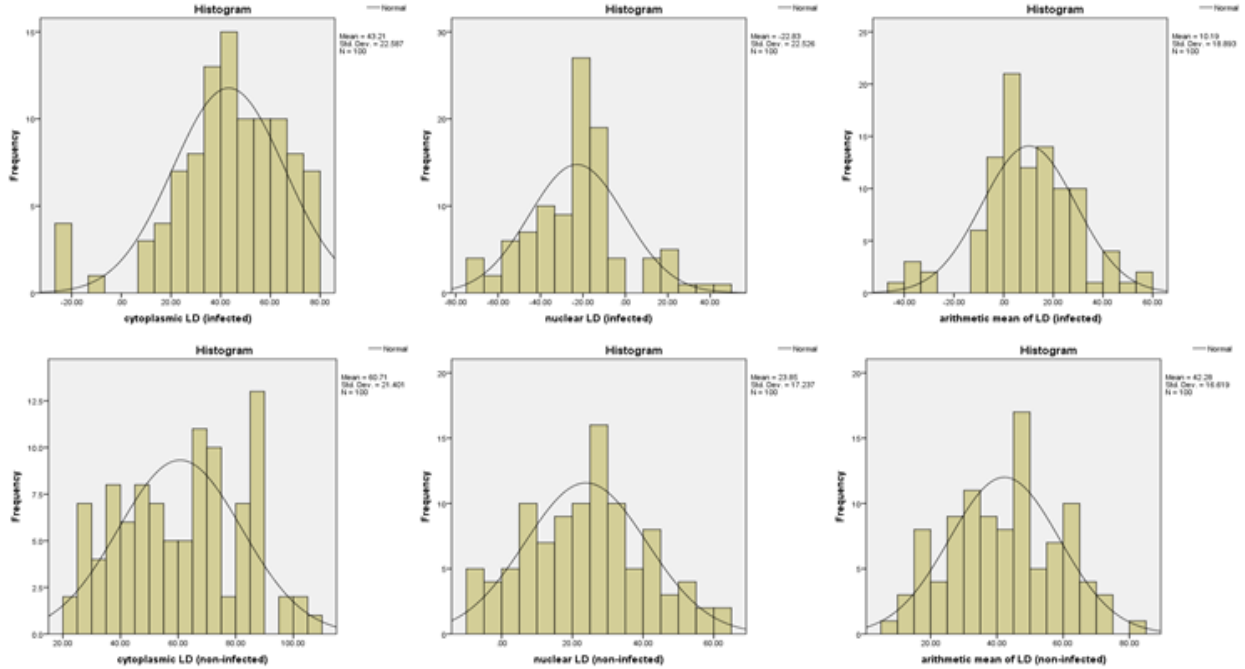
*: we evaluated H_0 via critical value and the summaries are referred as (+) or (-).

Sample		Homogeneity in variance	
		Non-parametric Levene's test	
Infected cells	cytoplasmic size	1	+
Non-infected cells		1	+
Infected cells	nuclear size	1	+
Non-infected cells		1	+
Infected cells		0.981	+
Non-infected cells	N/C	0.981	+

*: we evaluated H_0 via critical value and the summaries are referred as (+) or (-).

3.2.3.b. Cellular measurements-2

Measurements of cytoplasmic and nuclear light density (LD) of the atypical pyknotic cells



Sample		Normality tests					
		Shapiro-Wilk's test		Kolmogorov-Smirnov's test		D'Agostino's K-squared test	
Infected cells	cytoplasmic LD	<0.05	-	<0.05	-	<0.05	-
	nuclear LD	<0.05	-	<0.05	-	>0.05	+
Non-infected cells	cytoplasmic LD	<0.05	-	>0.05	+	<0.05	-
	nuclear LD	>0.05	+	>0.05	+	>0.05	+

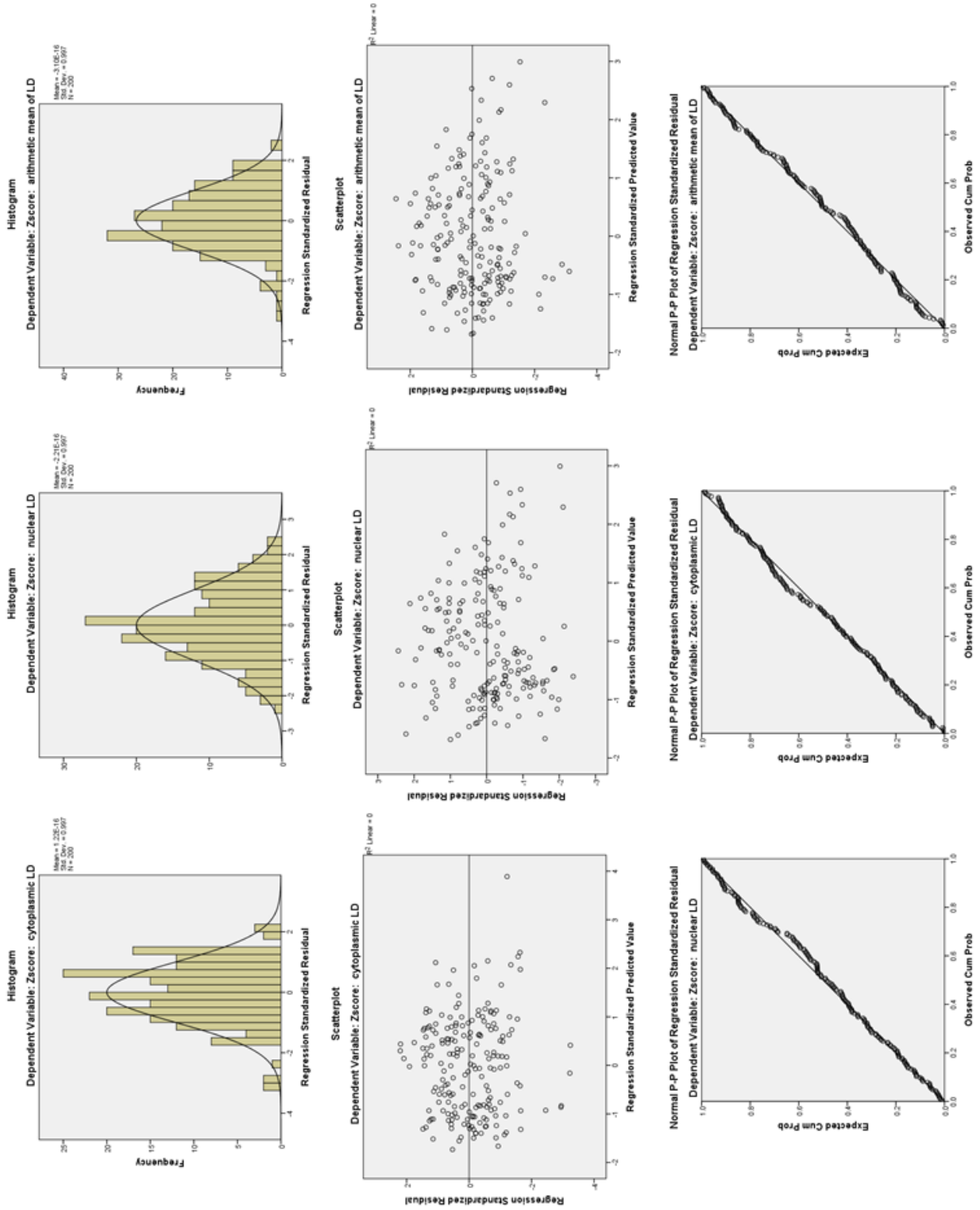
*: we evaluated H_0 via critical value and the summaries are referred as (+) or (-).

Test of homogeneity of variances

		df	F	Sig.
cytoplasmic LD	Between Groups	1	.000	.996
	Within Groups	198		
	Total	199		
nuclear LD	Between Groups	1	.000	1.000
	Within Groups	198		
	Total	199		

3.2.3.b. Cellular measurements-3

Relationship between cell sizes and light density (LD) of the atypical pyknotic cells



Declaration

- The thesis has been written without the help of others and that no other than the stated auxiliaries have been used
- For establishing *ex vivo* STST model, fresh human tissue samples were obtained from Lungen Clinic Grosshansdorf
- Helps for stimulating tissues were received from the division of National Reference Center (NRC) for Mycobacteria. Particularly, preparation of suspension was being done by Anne-Kathrin Witt, performances of real time PCR and sequencing were done by technician Daniela Sievert.
- Isolation of primary cells was done by Bettina Baron-Lühr and Patricia Prilla from the the department of Clinical and Experimental Pathology at the Research Center Borstel.
- *In vitro* infection of primary cells was done by Lisa Niwinski from the division of Microbial Interface Biology at the Research Center Borstel.
- The procedure of transcriptomics was done by Jasmin Tiebach and Maria Lammers from the department of Clinical and Experimental Pathology at the Research Center Borstel.
- Helps for multivariable analysis were received from Dr. Kurt Fellenberg (correspondence analysis), and Dr. Sebastian Marwitz (GeneSpring analysis).
- The thesis has not been presented anywhere else and that no other application for admission has been placed

PhD student: **Dariimaa Ganbat (MD, M.Sc)**

Acknowledgements

First of all, I am very grateful to Mongolian government for supporting my PhD study. I would like to express my heartfelt gratitude to my supervisors Prof. Dr. rer. nat. Torsten Goldmann, PD Dr. rer. nat. Elvira Richter, and Prof. Dr. med. Dr. med. vet. Dr. h.c. Ekkehard Vollmer to whom I am indebted for excellent, enthusiastic, support and for being an invaluable and constant source of inspiring ideas.

I owe sincere gratitude to all my colleagues at Clin. & Exp. Pathology for all helps for my entire study, not only the scientific way, but also to being a family; Dr. S.Martiwz, Dr. S.Seehase, Dr. D.Lang, Dr. I.Watermann, Dr. B.Schmith, J.Tiebach, M.Lammers, S.Fox, K.Wiczowski, A.Shiller, B.Baron-Lühr, and P.Prilla. I am deeply indebted to the technicians for their excellent technical support, advice and for always being willing to lend an extra hand when needed.

Thanks are also due to PD Dr. Norbert Reiling and his technician Lisa Niwinski supporting me *in vitro* experiment, Dr. Kurt Fellenberg for multivariable analysis. I am extremely thankful to A.Witt and K.Ott for helps in stimulating tissues and D.Sievert for performances of real time PCR and sequencing at the division of National Reference Center (NRC) for Mycobacteria.

Curriculum vitae

Personal Data

Full Name : Dariimaa Ganbat

Nationality: Mongolian

Date and place of birth: 02.11.1985 / Moscow, Russia

Languages: Mongolian, English



Education

1993-2003: Primary & secondary education at School #1, Ulaanbaatar, Mongolia

2003-2009: School of Medicine in Health Science University of Mongolia (HSUM),

2009-2014: Postgraduate continuing medical education

- *M.Sc of human histology & pathology (2009-2011) at HSUM*
- *Resident of pathology and forensic medicine (2010-2011) at department of Pathology and Forensic medicine, HSUM, Mongolia*
- *PhD student (since 2012) at department of Clinical and Experimental Pathology, Research Center Borstel, Germany*

Qualifications

- Degree of Medical Bachelor (2009)
- Master of Science in Medicine (2011)

Workshops and courses attended

- English for scientific purposes and German course (2012-2013)
- 3rd BBRs Retreat 2012, Ammersbek, Germany (15-16.08.2012)-talk
- Annual meeting of the DGP, Münster, Germany (16-17.11.2012)-talk
- Workshop: the art of writing a manuscript (06.06.2013)
- 4th BBRs Retreat 2012, Ammersbek, Germany (06-07.08.2013)-talk
- 36th Symposium of the North-German Immunologists, Borstel, Germany (23.11.2013)-poster
- Systems Biology Symposium, Egmond aan Zee, The Netherlands (25-26.11.2013)-poster
- Department Retreat 2013, Amsterdam, The Netherlands (10-12.06.2013)-talk
- Research visit of CAVAREM at department of Pathology and Medical Biology, Medical University of Groningen, The Netherlands (13.06.2012)

Published abstracts

- Dariimaa G, Goldmann T, Richter E, Vollmer E, A novel human short term *ex vivo* model for the initial phase of mycobacterial infection, Annual meeting of the DGP, 2012

- Dariimaa G, Goldmann T, Richter E, Vollmer E, Functional studies on the initial phase of mycobacterial infection in human lung tissues, System biology symposium booklet, 2013
- Dariimaa G, Goldmann T, Richter E, Vollmer E, Functional studies on the initial phase of mycobacterial infection in human lung tissues, 36th symposium of NDI abstract book, 2013